A New Model for Thin Film Solar Cells Using Photon Cycling

by

Abdulrahman Aloraynan

A thesis

presented to the University of Waterloo

in fulfillment of the

thesis requirement for the degree of

Master of Applied Science

in

Electrical and Computer Engineering

Waterloo, Ontario, Canada, 2018

© Abdulrahman Aloraynan 2018

AUTHOR'S DECLARATION

I hereby declare that I am the sole author of this thesis. This is a true copy of the thesis, including any required final revisions, as accepted by my examiners.

I understand that my thesis may be made electronically available to the public.

Abstract

The solar energy has emerged as one of the most promising and reliable renewable energy resources attracting much attention to the study of photovoltaics. A principal aim of solar cells is to maximize the absorption of light to increase the generation of electron-hole pairs and harnessing it to increase the power generated. An attractive approach of increasing the generation rate in a thin PV cell by employing photon cycling. In this thesis, I report the results of my study using the updated solar irradiance, and a new model for calculating the generation rate in thin film solar cells.

I develop a multiple light path model to arrive at a generation rate using my approximation of absorption coefficient and other physical structures at the back and front contacts. By increasing the path lengths, the generation of photocarriers at each level results in enhanced photocurrent. In calculating this, I have used a new approximation of the absorption coefficient as a function of wavelength. The consequence of the bandgap narrowing effect on the absorption coefficient has been studied using an existing model to show its impact on the generation rate. Furthermore, an optimized design for thin film solar cells is introduced to examine the photon cycling effect on the generation rate. It shows that considering the impact of photon cycling efficiently leads to enhancing the total generation rate by 144%. This permits reducing the thickness of the solar cell, which eventually reduces the cost of the cell. A novel model for accurate computation of the photon cycling effect has been developed, applicable

to different semiconductor PVs. Finally, the photon recycling and the luminescent coupling effect are investigated to show an improvement up to 65% for the GaAs generation rate.

Acknowledgements

In the name of Allah, the most merciful, and the most compassionate, all praises are due to Allah for his favours abundantly on us. All acknowledgements from the beginning to the end is due to Allah who eases every difficulty in the way of accomplishing this mission.

I would like to express my sincere gratitude and appreciation to my supervisor Professor. Chettypalayam Selvakumar, for his precious guidance, encouragement and continuous support throughout the entire period of my master study.

I would like to thank Professor Omar Ramahi and Professor Bo Cui to be part of my MASc committees and thesis readers.

I would like to show my genuine acknowledge everyone in my entire family individually, especially my beloved parents for their continuous devotion, care, generosity and support on everything since I was born. Also, my countless appreciation is for my wife for her patience and love throughout my journey. Special thanks is for my grandmothers for their sustenance prayers and love. Another appreciation is for my sisters and brothers for their support and motivation during my study. Lastly, my sweet thanks is for the sweetest person on this earth, my daughter Deem who is the source of happiness in my life!

Unlimited recognitions is for my friends and colleagues for their support and assistance to successfully accomplish this work. An exclusive acknowledge is for Hassan Alsiraji, for his motivation and cooperation during the master journey. Further gratefulness is toward my closest colleagues Ahmad AlQurashi, Dawood Alsaedi, AbdulAziz Almutairi, and Thamer Almoneaf.

Also, I would like to express my gratitude to the administrative staff at the Electrical and Computer Engineering at the University of Waterloo for their assistance.

Finally, I would like to thank University of Umm AlQura and Saudi Arabian Cultural Bureau for their full sponsorship.

Dedication

To my parents, my wife, my daughter, my sisters, my brothers

and my grandmother who passed away before I graduate.

Table of Contents

AUTHOR'S DECLARATION iii
Abstract iv
Acknowledgements vi
Dedication viii
Table of Contents ix
List of Figures xi
List of Tables xv
Chapter 1 Introduction 1
1.1 Preface 1
1.2 Solar Irradiance 3
1.3 Optical Properties of Silicon 5
1.4 Thesis Objectives 6
1.5 Thesis Outline 7
Chapter 2 Basic Principles of Photocarriers Generation Rate in PV and Fundamentals Theory of Optical Properties of Semiconductors 9
2.1 Introduction 9
2.2 Generation and Recombination Process in Semiconductors 11
2.2.1 Transport Equations in Semiconductors 13
2.2.2 Carrier Generation Rate 14
2.2.3 Fermi's Golden Rule 16
2.2.4 Photogeneration Rate 17
2.3 Principle Measurements of Absorption Coefficient 21
2.3.1 Spectroscopic Ellipsometry Measurement 21
2.3.2 Reflectance and Transmittance Measurement 22
2.3.3 Spectral Responsivity Measurement 23
2.3.4 Spectrally Resolved Luminescence Measurements 24
2.4 Absorption Coefficient of Intrinsic Silicon 25

2.5 Analytical Models of Silicon Absorption Coefficient 29
2.6 Doping Effects on Absorption Coefficient 33
2.7 Analytical Models of Silicon Generation Rate 35
2.8 Photon Cycling 38
2.9 Photon Recycling 40
Chapter 3 45
3.1 Introduction 45
3.2 A New Approximation for Silicon Absorption Coefficient 45
3.3 Modelling the Carrier Generation rate for Si Solar Cells 51
3.4 Photon Cycling Approximations for Carrier Generation Rate of Si 55
3.5 A Novel Modelling of Carrier Generation Rate Including Photon Cycling Effect 65
3.6 The Effect of Doping Concentration on Carriers Generation Rate 83
3.7 Optimizing a GaAs/Si tandem solar cell by introducing Photon cycling, Photon Recycling, and Luminescent Coupling Effects. 85
Chapter 4 Conclusion and Future Work 95
References 98
Appendix A Generation Rate Calculation 107

List of Figures

Figure 1.1. Solar PV global capacity and annual additions between 2006 and 2016.............. 1

Figure 1.2 The solar spectrum radiation for AM0 and AM1.5G.. 4

Figure 1.3 Silicon band structure where different direct and indirect bandgaps are illustrated. 5

Figure 1.4 Silicon complex refractive index, including the real part refraction index (*n*) and the imaginary part the extinction coefficient (*k*)... 6

Figure 2.1 Recombination mechanisms in semiconductors 20

Figure 2.2 The attenuation of light intensity in a sample of solar cells with thickness t, considering the light reflections. The remaining intensity decaying exponentially with the distance as shown in the orange line... 26

Figure 2.3 The photons wavelength contribution for the silicon solar cell at different junction depths based on equation (2.21)... 26

Figure 2.4 Silicon absorption coefficient as Dash and Newman presented at 300 K in 1955. 33

Figure 2.5 Absorption coefficient comparison done by Schinke *et al.*, of several most widely data of papers at room temperature... 35

Figure 2.6 A comparison between Rajkanan *et al.,* 1979 and Green, 2008 data for Si absorption coefficient at 300 K.. 37

Figure 2.7 Silicon absorption coefficient according to Palmer expression 39

Figure 2.8 Silicon absorption coefficient according to Geist et al. analytical expression at 289 K.. 39

Figure 2.9 Absorption coefficient as a function of doping concentration for n-type Si, applying equation 2.17 42

Figure 2.10 A comparison between Forlan and Amon approximation with a recent actual data for the generation rate of silicon at AM0. 44

Figure 2.11 The principle of the critical angle of the semiconductor-air interface. 47

Figure 2.12 Different scenarios for photon recycling effect, where a photon is emitted in a junction with a perfect rear reflector.. 51

Figure 3.1 Results of the exponential approximation using equation 3.3, the polynomial approximation using equation 3.2, and finally compare the results with the experimental data of Green for Si absorption coefficients. 56
Figure 3.2 The percentage error of the exponential and polynomial approximations comparing to the Green's data 56
Figure 3.3 Results of the approximation using equation (3.1) and compare the results with the experimental data of Green for Si absorption coefficients 57
Figure 3.4 The percentage error of the exponential approximations (3.1) comparing to the Green's data 57
Figure 3.5 The scheme of the silicon junction used in the calculation of carrier generation rate 58
Figure 3.6 Calculating the carrier generation rate using model (3.4) comparing to the actual generation rate for Si junction assuming no external light reflection. 61
Figure 3.7 The percentage error of the approximations model (3.4) comparing to the actual data of generation rate of Si junction. 61
Figure 3.8 The enhancement of the photon cycling to the generation rate. 63
Figure 3.9 The initial approach of the silicon solar cell design to determine the photon cycling effect on generation rate. 63
Figure 3.10 The generation rate of the first pass, first cycle, second cycle, and third cycle for 50 μm silicon solar cell. 64
Figure 3.11 The design principle for the total generation rate of solar cells including the photon cycling effect 66
Figure 3.12 The modified pattern for the total generation rate of solar cells based on previous model, including the photon cycling effect 68
Figure 3.13 A comparison between the actual cycling carrier generation and the approximation cycling generation rate using (3.10) for a 50 μm Si junction assuming no light losses. 69
Figure 3.14 The final approach of the solar cell design which is selected to determine the total carrier generation rate including the photon cycling effect. 75

Figure 3.15 An example for the final approach of the solar cell design which is selected to determine the total carrier generation rate including the photon cycling effect, assuming all *R=0%.* 78
Figure 3.16 The outcome of the current actual model for the carrier generation rate, including three photon cycles and comparing the results with the previous model 79
Figure 3.17 A comparison between the current model and Sarkar's model for the generation rate of the first cycle 80
Figure 3.18 A comparison between the current model and Sarkar's model for the generation rate of the second cycle 80
Figure 3.19 A comparison between the current model and Sarkar's model for the generation rate of the third cycle 81
Figure 3.20 The contribution percentage of the photon cycling generation rate to the total generation rate based on the number of the cycle $\theta o=0$ *and* $\theta 1,2,3=30$........ 82
Figure 3.21 The effect of the reflection angle on the generation rate of the cycle incident rays. 83
*Figure 3.22 T*he effect of thickness on the total generation rate of a solar cell. The generation rate is showed up to 30 μm. 84
*Figure 3.23 T*he effect of thickness on the generation rate of the cycle rays only 85
Figure 3.24 The actual data of the first cycle generation rate comparing to the results of the approximation using equation (3.31). 88
Figure 3.25 The actual data of the second cycle generation rate comparing to the results of the approximation using equation (3.31). 88
Figure 3.26 The actual data of the third cycle generation rate comparing to the results of the approximation using equation (3.31). 89
Figure 3.27 The effect of increasing the absorption coefficient on the normalized generation rate........ 91
Figure 3.28 The effect of the doping concentration on the n-type silicon generation rate using Jellison *et al.* data........ 92
Figure 3.29 The luminescent coupling effect in tandem solar cells. 93

Figure 3.30 The tandem solar cell structure of Ren *et al.* for the GaAs/Si double-junction.. 94
Figure 3.31 The optimized tandem solar cell structure of Ren *et al.* for the GaAs/Si double-junction, applying the photon cycling effect on the rear texturing surface. 95
Figure 3.32 The generation rate of the bottom junction (Si) of optimized tandem solar cell structure of Ren *et al.* [95] for the GaAs/Si double-junction, including three photon cycles 96
Figure 3.33 The generation rate of the top junction (GaAs) of tandem solar cell structure of Ren *et al.* [95] for the GaAs/Si double-junction with and without the photon recycling effect. 97
Figure 3.34 The contribution of the photon recycling generation rate to the total generation rate in the GaAs junction. 97
Figure 3.35 The reabsorption and absorption probability in the GaAs and Si, for the radiative emission of the GaAs at *Rb*=0. 100
Figure 3.36 The generation rate of Silicon without LC and the generation rate of the LC effect of the Si junction for different coupling factors at *Rb*=0. 100

List of Tables

Table 1.1 Semiconducting materials 2
Table 3.1 Coefficients ai and bi for silicon absorption range between 300 to 360 *nm* using equation 3.3. 55
Table 3.2 Coefficients ai and bi for silicon absorption range between 300 to 360 *nm* using equation 3.2. 55
Table 3.3 Coefficients ai, bi, ci and di for silicon absorption range between 370 to 1100 *nm* using equation 3.1. 55
Table 3.4 Coefficients ai and bi for the silicon carrier generation rate approximation of the 50 μm junction thickness under AM1.5G with no reflection at front surface. 60
Table 3.5Coefficients ai and bi for the silicon cycling carrier generation rate approximation of the 50 μm junction thickness under AM1.5G assuming no net light losses, 10% losses at back surface, and 20% losses at front surface, using Sarkar's model 70
Table 3.6 Coefficients ai and bi for the silicon cycling carrier generation rate approximation of the 50 μm junction thickness under AM1.5G assuming no net light losses, 10% losses at back surface, and 20% losses at front surface, using Sarkar's model 71
Table 3.7 Coefficients ai for the silicon cycling carrier generation rate approximations for a 50 μm Si junction thickness under AM1.5G assuming no net light losses at the front surface or back surface, using the new model. The approximation form is $gn{-}cyc(x){=}\Sigma aixi(\mu m)$. 87

Chapter 1

Introduction

1.1 Preface

Several accumulating deleterious effect of non-renewable energy sources, and the rapid energy expenditure around the world motivate scientists to develop the renewable energy resources. The solar energy has emerged as one of the most promising and reliable renewable energy resources which attracts much attention to the study the photovoltaic (PV) effects. In 1941, Russell Ohl invented the first silicon solar cells that worked in 1% efficiency [1]. The developing of PV started to grow up ever since. Figure 1.1 shows the global growth rate of the PV capacity around the world between 2005 and 2015. From another perspective, despite the fact that PV capacity accelerates over the years, the consumption of the solar energy compared to the total world energy consumption is less than 1% [2].

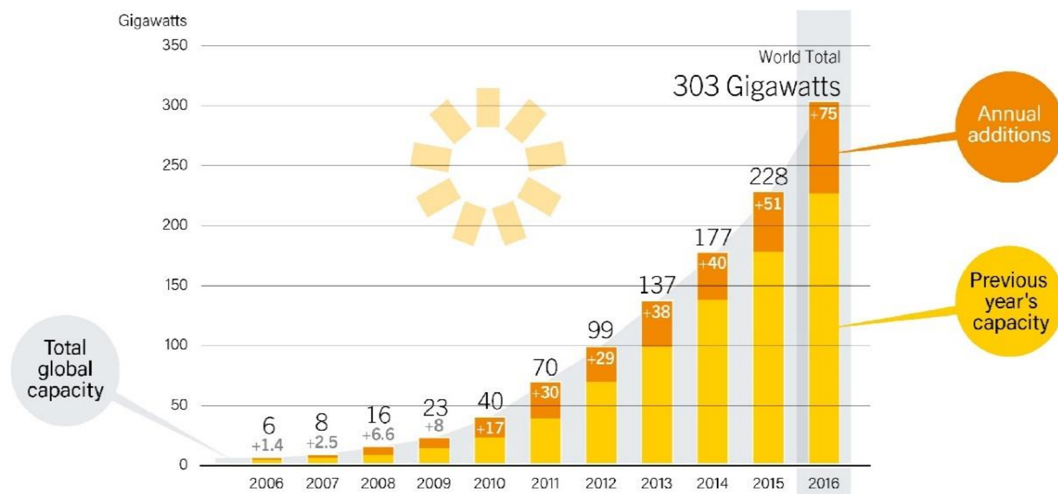

Figure 1.1. Solar PV global capacity and annual additions between 2006 and 2016 [2].

Table 1.1 Semiconducting materials

Group II	Group III	Group IV	Group V	Group VI
	B **Boron** 5	**C** **Carbon** 14	**N** **Nitrogen** 14	**O** **Oxygen** 14
Mg **Magnesium** 12	**AL** **Aluminium** 13	**Si** **Silicon** 14	**P** **Phosphorus** 15	**S** **Sulphur** 16
Zn **Zinc** 30	**Ga** **Gallium** 31	**Ge** **Germanium** 32	**As** **Arsenic** 33	**Se** **Selenium** 34
Cd **Cadmuim** 48	**In** **Indium** 49	**Sn** **Tin** 50	**Sb** **Antimony** 51	**Te** **Tellurium** 52
Hg **Mercury** 80	**TI** **Thallium** 81			

PV depends on the interaction between the sunlight and semiconducting materials, which directly generate the electricity by exploiting the photovoltaic effect. The semiconductors which are in group IV of the periodic table, or a combination of group III-V, or a combination of group II-VI are viable for PV. Table 1 shows the list of semiconducting materials that contain one or more elements. Silicon is the most developed and well-understood semiconductor; for a long time, and still, the silicon (Si) dominates the industrial of the PV due to its economic large scale manufacturability and its proven field stability. Recent publications show that 85% of the solar cells in the markets are based on the silicon-wafer which is the first generation of photovoltaic [3]. However, Si-based solar cells confront some challenges in the fabrication process in addition to the theoretical efficiency limitation that is found to be 29.8% under AM1.5 (terrestrial air mass) [4]. Although an efficiency of 24.7% has been recorded by a silicon structure with passivated emitter, rear locally-diffused (PERL) solar cell and 13.44% has been achieved using a thin silicon film, the mass production of these cells is still too expensive [5]. Another approach that has emerged is employing heterojunction PV or tandem

solar cells which demonstrate a high efficiency; nevertheless, the financial constraint remains the main obstacle for fabrication the tandem PV.

The second generation of solar cells aims to reduce the thickness of the cells and produce a thin-film solar cell. Amorphous silicon (a-Si) is one of the popular material used in solar cells; it provides a thin layer that lower the manufacturing cost and enhances the advantage of flexibility. On the other hand, the concern of efficiency is a crucial part of obstacle the a-Si development for PV; moreover, the a-Si efficiency is significantly lower than poly and monocrystalline Si (c-Si) [6].

Based on what has been discussed above, it can be said that Si-based solar cells currently dominate the PV industry. Hence, providing a comprehensive review of Si properties and how these properties impact the solar cell operation is required. The relevant properties of Si that need to be studied are, for example, Optical, thermal, chemical and electrical properties. In this review, the absorption coefficient of crystalline Si (c-Si) is considered to be discussed due to its key impact on the performance and the efficiency of the optical properties of the cells. First, some fundamentals of the c-Si optical properties are briefly discussed, and then Si absorption coefficient in the literature is reviewed.

1.2 Solar Irradiance

The sun provides energy, by means of electromagnetic radiation, to the earth. The sunlight covers a wide range of wavelengths from around 250 nm, which locate in the ultraviolet (UV),

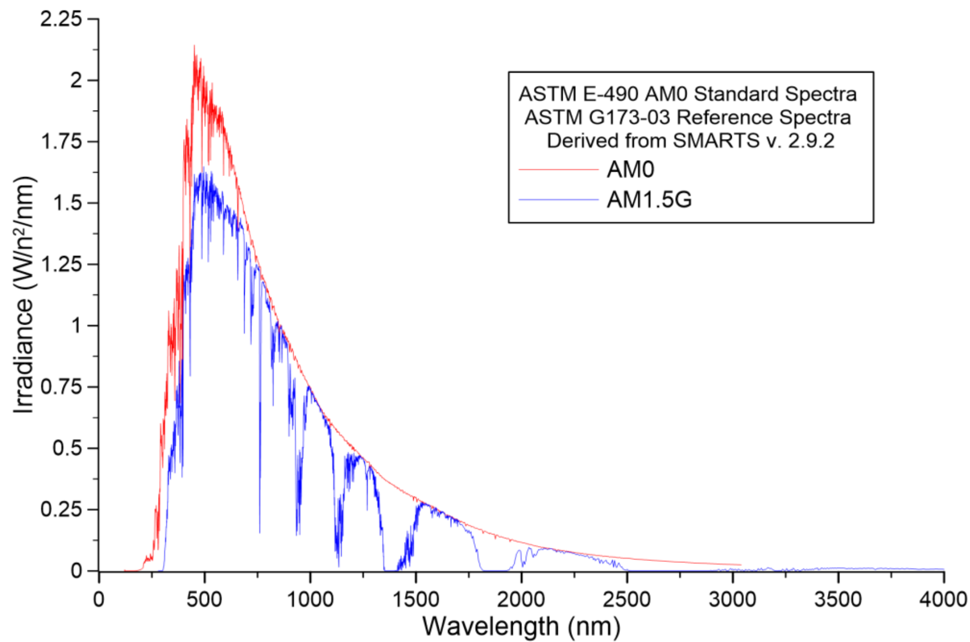

Figure 1.2 The solar spectrum radiation for AM0 and AM1.5G [7, 8].

and passing through the visible spectrum (400-700 nm) up to a few thousands of nm wavelengths, which span into infrared (IR). The flux of sun energy at an average distance of the earth is 1366 W/m2 that called the solar constant. However, some of the photon energies are absorbed by the Ozone layer, water vapour and carbon dioxide. As a result, the irradiation density of the sun varies from place to place. The light is a group of photons; each photon has an energy, the wave that has a high length has a low energy while the wave that has a small length has a high energy. Figure 1.2 shows the solar spectrum radiation at two common of air mass ratio; outside of atmosphere AM0 and terrestrial AM1.5, which are the standard air mass ratio for PVs [7, 8].

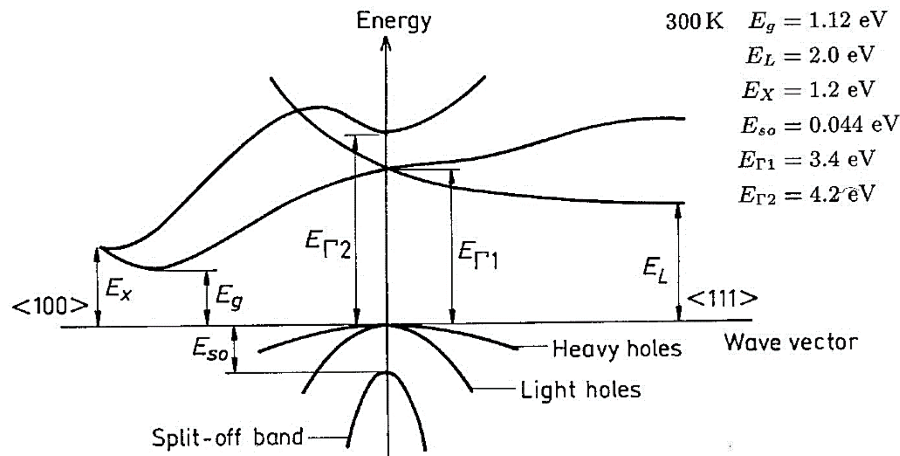

Figure 1.3 Silicon band structure where different direct and indirect bandgaps are illustrated [9].

1.3 Optical Properties of Silicon

Optical properties and light absorption play a critical role in both photovoltaics and optoelectronic devices in general. Silicon is an indirect band semiconductor material from group IV that has a diamond structure. It is important to understand the band structure of Si to realise the interaction between the conduction band (CB) and the valence band (VB). Figure 1.3 shows the band structure of Si [9]. When the minima of CB and maxima of VB are not at the same wave vector (k, $k_{min} \neq k_{max}$), it is called an indirect semiconductor. It shows that Si has an indirect bandgap (E_g) that equals to 1.12 eV, while it has a direct bandgap at $E_{gd} = E_{\Gamma1} = 3.4$ eV and $E_{\Gamma2}= 4.2$ eV. Also, Si has two indirect gap at $E_x = 1.2$ eV and $E_L = 2.0$ eV. However, different references may show slightly different results for the direct and indirect bandgap. For a typical sample of c-Si, the refractive index and extinction coefficient at 632.8 nm are 3.882 and 0.019, respectively. Nonetheless, these numbers are variable based on the wavelength of the light (λ), see figure 1.4 for complete refractive index and extinction

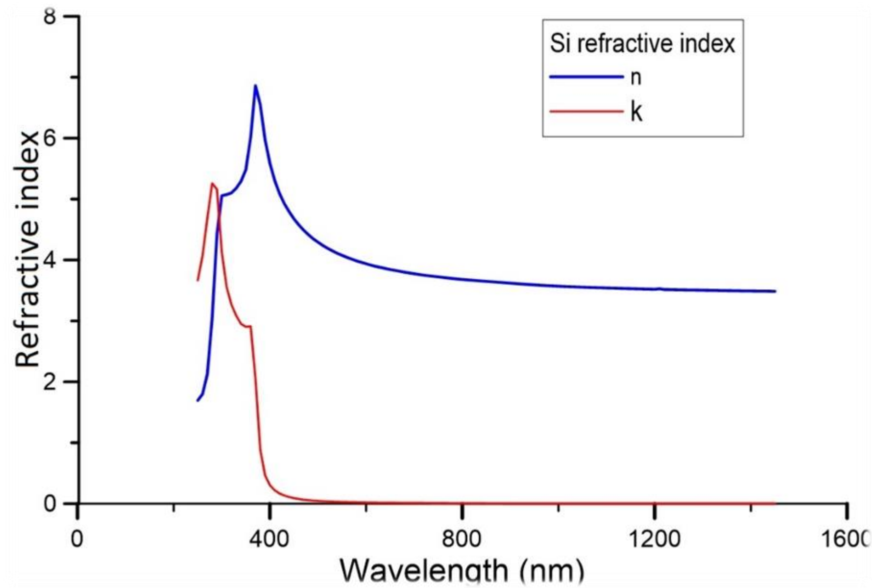

Figure 1.4 Silicon complex refractive index, including the real part refraction index (n) and the imaginary part the extinction coefficient (k).

coefficients [10]. The complex refractive index is n^* is commonly used to describe the optical properties of the material, which may be written as a complex number is equal to $n^* = (n - ik)$, where k is the extinction coefficient. The optical properties depend on a few other parameters such as temperature and doping level. Discussing all factors that impacting is not in the scope of this review, however it will be mentioned in the next sections how they do affect the absorption coefficient which is one of the main aspects of the review.

1.4 Thesis Objectives

The photocarrier generation rate is one of the most significant parameters which plays a key role in determining and constraining the efficiency of the semiconductor devices such as in photodetectors. Therefore, optimizing the generation rate lead to enhance the short circuit current which eventually precedes to raise the efficiency in semiconductor devices. The generation rate in photodetectors mainly depends on the source of light which is exposed to the device, the optical properties of the photodetector material, and the optical confinement in

the junction. In this thesis, an analysis for the optical properties and optical confinement are considered to be studied to optimize the photocarrier generation rate. Furthermore, several different aspect of effects which may influence the productivity of the generation rate have been investigated such as the BGN, photon recycling and photon cycling effects. The photon recycling is the reabsorbing of the photon which is emitted in the radiative recombination, while the photon cycling is the reflecting of light in the cell. One more aim of this work is to establish novel models and approximations to provide an exact computation for the generation rate, in addition to minimize the time-consuming during the calculations. These models and approximations are intended to be applicable to any semiconductor materials. However, due to the volume restriction of the thesis, the results and application are limited to for silicon devices, in addition to consider the gallium Arsenide when reassessing and measuring the photon recycling and luminescent coupling effects.

1.5 Thesis Outline

In order to achieve the thesis objectives that have been discussed above wide-ranging topics have to be covered. Therefore, Chapter 2 provides an intense literature review for different aspects of topics which are related directly or non-directly to the photocarrier generation rate of solar cells. Since the generation rate mainly depends on the optical properties of the material, silicon optical properties have been reviewed including various parameters to observe the most accurate result. Indeed, the absorption coefficient of the silicon has been investigated from different points of view theoretically and experimentally. One of the thesis objects is to establish new models for both absorption coefficient and generation rate, thereby investigating the current models of both of them is important to develop new models.

Eventually, the effects of photon recycling and photon cycling are addressed in order to be considered in the new models and approximations.

Chapter 3 is the main chapter of this thesis where most parts of the work have been demonstrated. After reassessing the applicability of the current models of silicon absorption coefficient in Chapter 2, a new precise model is introduced in Chapter 3. The new model shows high accuracy comparing to the actual data with error less than 1% for the wavelength range between 300 to 950 *nm*. This approximation relates the silicon absorption coefficient to the wavelength of photons directly. One advantage of this approximation is to abbreviate the equation of the absorption coefficient to relay only on the photon wavelength to simplify the calculation the time consuming. After developing an approximation for silicon absorption coefficient, the effect of photon cycling on generation rate has been estimated using a current proposed model which is not been evaluated yet. Nevertheless, it shows that the assumptions which had been stated for the proposed model are not applicable for real semiconductor devices. Thus, a novel model has been developed to assess the actual effect of photon cycling on the carriers generation rate which can be applied for all semiconductor materials. Furthermore, the effect of the angle reflection and junction thickness have been evaluated to optimize the design of solar cells. Finally, the photon recycling and the luminescent coupling effects have been computed for GaAs/Si tandem solar cell.

As a final point Chapter 4 summarizes the contributions of this work and demonstrates some suggestions for future work.

Chapter 2

Basic Principles of Photocarriers Generation Rate in PV and Fundamentals Theory of Optical Properties of Semiconductors

2.1 Introduction

Absorption of light in semiconductors can be divided into three categories, which are inter-band absorption absorbance, free carrier absorption, and impurity absorption. For c-Si, absorption of light is isotropic, the mode of absorption process depends on the spectral range of light wavelength. The E_g for Si is at 1.12 eV, while the photon energy is equal to

$$E_{ph} = h * \frac{c}{\lambda} = h * v, \tag{2.1}$$

$$E_{ph}(eV) = \frac{1.24}{\lambda(\mu m)}, \tag{2.2}$$

where h is plank constant, c is the speed of light, and v is frequency. It illustrates that the absorption edge for Si is at λ around of 1100 *nm.* Therefore*,* for the $\lambda <$ 1100 *nm* range (ultraviolet, visible, and near-infrared spectral range) the fundamental absorption process is the inter-band absorption. The inter-band absorbance, also referred as band-to-band absorption, is where electrons from the valence band are excited into the conduction band. For $\lambda <$ 365 *nm*, direct transitions are possible since the E_{gd} for Si is equal to 3.4 eV. For lower photon energies, the indirect transitions take place by the phonon absorption or emission. The second situation for absorption is where photons may be absorbed is by free carrier absorption (FCA), also known by intra-band absorption in some references. The FCA is caused by the excitation of a free electron within a conduction band to a higher energy state within the same band. For solar

cells and photodiodes, this absorption process is defined in term of parasitic absorption that may obstruct the efficiency of devices, since it does not generate additional free carriers. The last aspect of absorption mechanism is the band-impurity absorption; it is when an electron excited to an empty state within a band gap induced by an impurity, or from an impurity state to a conduction band as well.

By considering the transitions in which an electron is excited from a valence band to a conduction band with the absorption of a photon of energy equal to the energy of the forbidden gap. This mechanism used to be called the fundamental absorption since it provides free carriers. Here, two types of transitions might be involved; the first one is that where only photons are involved, and this is called direct transition, where k-vector being conserved. The second one is when phonons are involved by lattice vibrations or absorbed photons, and this is called indirect transition, where k-vector not being conserved. For the first class, direct transitions may take place in a semiconductor more likely when the k_{min} has the same value as k_{max}. However, still, the direct transitions are possible in the material that $k_{min} \neq k_{max}$, especially for high photon energy, and this situation is applied for Si when $E_{ph} > 3.4$ eV. The second class is indirect transitions where the electrons are excited from valence band to conduction band for different k, by phonons momentum (phonons absorption or emission), which are the dominated transitions for Si. Nevertheless, this type of transitions also may take place in the direct semiconductors, while the probability for this transitions is much lower than the direct transition for the same material.

2.2 Generation and Recombination Process in Semiconductors

Generation and recombination are a contrary process; the generation process is an electronic excitation event where available free carriers increase the carry charges, while recombination is an electronic relaxation process which the number of free carriers are degraded. To generate free carrier, a source of energy or an input is required, whilst recombination releases energy. The energy input can be provided by several type of sources such as a beam of light (photons), vibrational energy of lattice (phonons), or a kinetic energy of a carrier. Indeed, due to the microscopic reversibility, there is an equivalent recombination process for every generation process.

Generation refers to the electrons movement from a lower state to a higher state in the band structure of the materials. When an electron excites from a valence band to a conduction band, an electron-hole pair is generated and this is the essential form of generation in photovoltaic. Another type of generation is when an electron promotes from a valance band into a localised state in the band gap, where only a hole is created, or from a localised state to a conduction band, which only an electron is created. Finally, a parasitic form of generation is the excitation of an electron from a lower state in the conduction band into a higher state, which increases the heating in the device.

Recombination mechanisms can be divided into three main categories, which are radiative recombination, Auger recombination, and Shockley-Read-Hall (SRH) recombination. The radiative recombination is a direct recombination, band to band recombination, where an electron in a conduction band recombines into an empty state in a valance band, at a single transition. An amount of energy has to be disposed of by some means,

and the simplest process can be done by emitting a photon which has an energy similar to the band gap energy. This emitted photon could be utilized by applying photon recycling effect. The radiative recombination is dominated in direct semiconductors, such as in GaAs and InAs. One example of the radiative process is a light emitting diode. Auger recombination is where three carriers are involved in the process, where an electron and a hole recombine, whereas the disposing of energy transfers to another electron in the conduction band, or a hole in the valence band. Thereby, creating a highly energetic electron or hole charge carrier which be eventually thermalized to the conduction or valence, respectively. It is important to consider this type of recombination at high carrier concentration semiconductors in heavily doped or under concentrated sunlight. For silicon solar cells, carriers life time is limited by the Auger recombination, and as the doping level increases the auger lifetime decreases. Last considered type of recombination is the recombination through defects, which is called SRH recombination. In this type of recombination, an electron in the conduction band is trapped by a defect or by a presence of foreign atom within the band gap energy level, firstly. Then in a second step, the trapped electron recombines into an empty state in the valence band, or the electron and the hole might be recombined at the defect state. Surface recombination can be classified as a type of the SRH recombination, where electrons recombine at semiconductor surfaces due to the significant impact of the interfaces, having large states of defect, on the device behaviour. Figure 2.1 summarises the recombination mechanism of semiconductors [11].

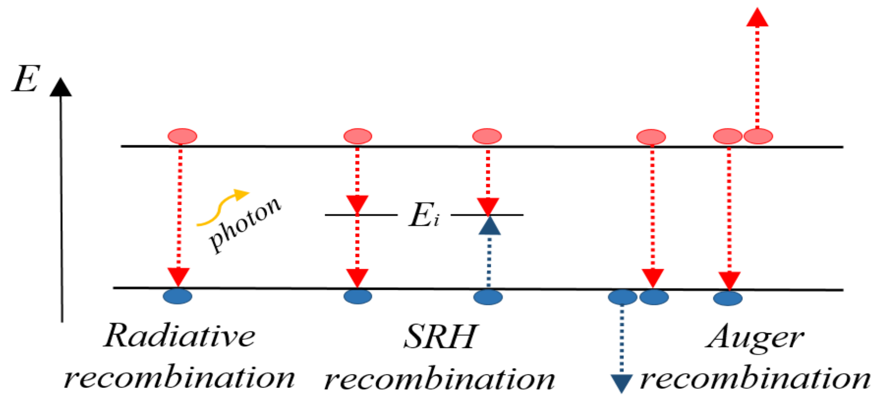

Figure 2.1 Recombination mechanisms in semiconductors.

2.2.1 Transport Equations in Semiconductors

The essential objective of solar cells is absorbing light to generate a photocurrent. The generation and recombination rate depends on the material properties, electronic structure, and operating condition. It is important to drive the generation and recombination equations theoretically, and examine these equations experimentally. The basic fundamental of semiconductor transport equations is based on two simple principles. The first is that the number of carriers of each type must be conserved, and the second one is the electrostatic potential of the carriers charges observes by Poisson's equation. For a semiconductor which contains electrons and holes, the first principle for electron and hole conservation, respectively, requires that

$$\frac{\partial n}{\partial t} = \frac{1}{q} \nabla . J_n + G_n - U_n \tag{2.3}$$

$$\frac{\partial p}{dt} = -\frac{1}{q} \nabla . J_p + G_p - U_p \tag{2.4}$$

where $J_{n,p}$ is the current density, $G_{n,p}$ and $U_{n,p}$ is the generation and recombination rate per unit volume, for electrons and holes. The above equations are general, and once the J, G, and U are identified how they are related to the n, p, and the electrostatic potential ($\emptyset$), coupled with differential equations can be set to be solved for three unknown parameters. For the second principle, Poisson's equation in the differential form is

$$\nabla^2\emptyset = \frac{q}{\varepsilon_s}(-\rho_F + n - p) \tag{2.5}$$

ε_s is the dielectric permittivity of the semiconductor, ρ_F is the local desity of a fixed charge. For the contiutiy equations (2.3) and (2.4) , once the J, G, and U parameters are defined by the dependencies on n, p, and $\emptyset$, and some other material properties or enviroment conditions, a set of couples differental equation can be set and solved for the three unkowns.

2.2.2 Carrier Generation Rate

In the absence of any external bias at zero kelvin, there are no net generation or recombination events. As the temperature is elevated, the lattice obtains a vibrational kinetic energy; a thermal generation starts to take place. Consequently, electrons in excited states start to thermally recombine to a lower energy state. This transition is as any other generation and recombination processes, where band to band transition and transition of localised states are involved. The thermal generation and recombination rate should be correspondingly equivalent at thermal equilibrium.

$$G_{n,p}^{th} = U_{n,p}^{th} \,. \tag{2.6}$$

Since the generation and recombination rate is equal at thermal equilibrium, the excess generation and recombination are only considered in the total rate of transitions of equation 2.3, thereby not considering the thermal generation as contribution to the net generation rate

$$U_n = U_n^{total} - U_n^{th} \tag{2.7}$$

and

$$G_n = G_n^{total} - G_n^{th}. \tag{2.8}$$

For the band to band generation and recombination process

$$U_n = U_p = U \tag{2.9}$$

and

$$G_n = G_p = G. \tag{2.10}$$

In the case of applying an external source such as a steady state light field, the system is not at thermal equilibrium since the light biases the conduction and valence band. The Fermi level splits in this case, and the quasi Fermi level E_{Fn} and E_{Fp} are applied. Assuming that the quasi Fermi level is in thermal equilibrium, the following transitions are possible

- a photon of light can be absorbed and excited from E_v to E_c;
- an electron can be recombined from E_c to E_v while emitting a photon (spontaneous emission);
- a second photon can be stimulated with the emitted photon of the above recombination (stimulated emission).

2.2.3 Fermi's Golden Rule

The Fermi's Golden Rule, 1927 [12], approximation based on first order perturbation theory, describes the quantum mechanical transition rate in many cases of semiconductors. According to Fermi's Golden Rule, the transition probability from the initial state $|i>$ of energy E_i to a final empty state $|f\rangle$ of energy E_f, per unit time under some perturbation Hamiltonian $\mathbf{H'}$ is given by

$$\frac{2\pi}{\hbar}|\langle i|\mathbf{H'}|f\rangle|^2\delta\left(E_f - E_i \mp E\right) \tag{2.11}$$

where the in brackets term $|\langle i|\mathbf{H'}|f\rangle|^2$ is matrix element coupling the initial and final states. The delta function, δ, confirming energy conservation, and if the final state energy is less than the initial one, this indicates for relaxation events, where a quantum E is emitted. For $E_f > E_i$, an excitation events such as absorption are occurred. To obtain the transition rate, a multiplication of probabilities of the occupied initial states and available final states is necessitated. For more details on the Fermi's Golden rule derivation see [13, 14].

The total band to band generation rate is the summation of the transition rate per unit crystal volume over the transition energy, *r(E)*, weighted by the available photon density states $g_{ph}(E)$ of the perturbing field

$$G = \int r(E)g_{ph}(E)dE. \tag{2.12}$$

In the case of optical transitions that involve additional photons, or phonons, it is necessary to expand the quantum mechanical transitions of Fermi's golden rule to a higher order, and not applying the first order approximation.

2.2.4 Photogeneration Rate

The photogeneration is resulted from absorbing the photons in semiconductors, and it is one of the most significant key roles in photovoltaic devices. This term is using in specific for the generation of the free electron-hole pair by absorbing of photons. Trap assisted, and Auger generation are other relevance generation process in photovoltaic. Moreover, for photons which have energy smaller than the bandgap energy might be absorbed to increase the kinetic energy of mobile carriers in high carrier densities semiconductors. This generation is referred to free carrier absorption, where no additional mobile carriers are created, and it is considered as a parasitic absorption for photovoltaic applications. Also, the photon may be absorbed to be scattered, generated phonons, or to promote electrons between localised states. Near to the bandgap edge, band to band transition is dominated, in addition to the transition between localised states and bands. Photon scattering is mostly undesirable for photovoltaics, and it is particularly common by interfaces or by inhomogeneities structures. However, some photon scattering is purposed, in cells designed, to increase the light confinement and amplify the photon field.

The generation rate is as result of the interaction between light and solar cells, and the intensity of light plays a significant role. The microscopic absorption coefficient, α, demonstrates how the light intensity is attenuated while passing through a material. Consider a cell having thickness x, is exposed to a beam of photons of energy E and intensity I_o, counting for surface intensity. A fraction of photon energy will be absorbed and the light intensity $I(x)$ will be decaying by a factor of $e^{-\alpha(E)dx}$, and thus

$$\frac{dI}{dx} = -\alpha I \tag{2.13}$$

By integrating equation (2.13) for a material with depth of x, and non-uniform absorption coefficient, the intensity is given by

$$I(x) = I_s e^{-\int_0^x \alpha(E,x)dx}. \quad (2.14)$$

The I_o is the surface intensity before accounting for reflection. For uniform α, equation (2.14) is reduced to the simple Beer-Lambert law,

$$I(x) = I_s e^{-\alpha x}. \quad (2.15)$$

The reflectivity (R) is determined the fraction of the light incident that would reflect at the front surface of the cells. It is significant to minimise the reflection of light, and different techniques are developed and deposited such as anti-reflection coating, passivation, and texturing into the surface of the cells. By considering the front reflection (R) and the fraction of incident light which escapes from the back surface (1-R_b), angle between the ray direction and normal to the cells surface, in the equation (2.15),

$$I(x) = (1 - R)\,(R_b)\,I_s e^{-\alpha x}. \quad (2.16)$$

By considering the optical interface angle, the above equation becomes

$$I(x) = (1 - R)\,(R_b)\,I_s e^{-\alpha x \sec\theta}. \quad (2.17)$$

The R_b should only be considered in the case of photon cycling, where the incident ray is reflected by the back surface. Figure 2.2 illustrates the process of incident light penetrates and attenuates in a slab of the solar cell, declaring the refractive of light. The angle of the light incidents is assuming to be neglected in the above equations. The internal reflectivity at the back surface can be improved by coating the internal surfaces by reflective material, or to be prepared by metallizing with gold or aluminium. Another choice to reduce the fraction of light which escapes at the rear surface is by designing a cavity containing arrays of cells

(photovoltaic eye) [15]. Alternative choices to increase the intensity of the light is by using concentrator photovoltaics other optical confinement methods.

The rate of the carrier generation depends on the energy and number of photons which penetrate the solar cells. If assuming that for silicon solar cells at room temperature, all photons energy above 1.12 eV are absorbed to generate free carriers, then the rate of carrier generation at depth *x*, per unit volume is given by

$$g(E,x) = (1-R)\, N_{ph}(E,x)\, \alpha(E) e^{-\int_0^t \alpha(E,x) dx} \tag{2.18}$$

where t is the thickness of the junction, and N_{ph} is the photon *flux,* the number of photons per second per unit area which corresponds for the sun to,

$$N(\lambda) = \frac{F(\lambda)\Delta\lambda}{q\, E_{ph}} = \frac{H(\lambda)}{q\, E_{ph}} \tag{2.19}$$

where F is the spectral irradiance (W m^{-2} nm^{-1}) and H is the power density (W m^{-2}). To find the total generation rate at depth *x*, the carrier generation is summed over photon energies

$$G(x) = \int g(E,x)\, dE. \tag{2.20}$$

$$G(x) = \int (1-R)\, N_{ph}\left(E_{ph}, x\right)\, \alpha\left(E_{ph}\right) e^{-\alpha\left(E_{ph}\right)\, x} \tag{2.21}$$

The integral should be extended only over the photon energies which are primarily absorbed and resulted in free electron-hole pairs [11] [16]. Figure 2.3 shows the contribution of each photon wavelength to the generation rate of silicon at different junction depths.

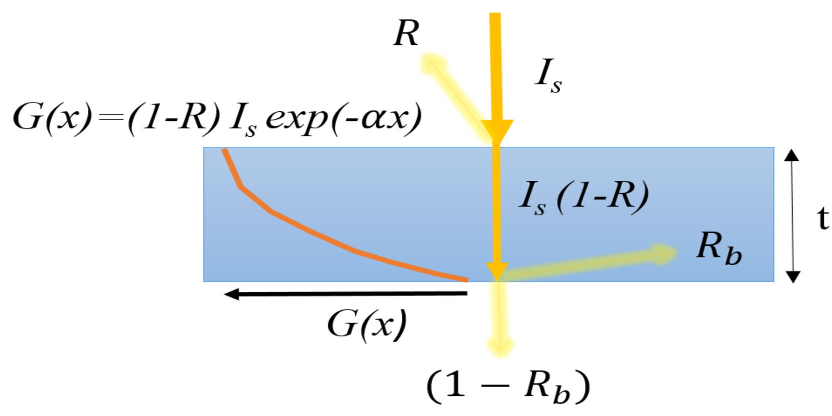

Figure 2.2 The attenuation of light intensity in a sample of solar cells with thickness *t,* considering the light reflections. The remaining intensity decaying exponentially with the distance as shown in the orange line.

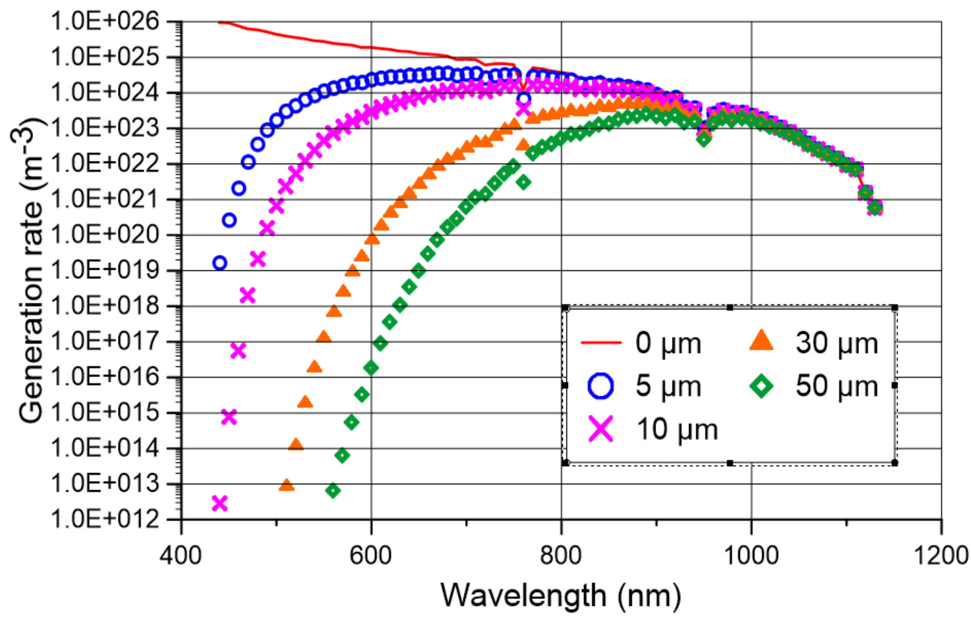

Figure 2.3 The photons wavelength contribution for the silicon solar cell at different junction depths based on equation (2.21)

2.3 Principle Measurements of Absorption Coefficient

Absorption of light in a semiconductor material represents the interaction between light and the semiconductor atomic structure. The absorption coefficient (α) is defined by the relation of the photon flux Φ,

$$-\frac{d}{dz}\Phi(\lambda, z) = \alpha(\lambda)\Phi(\lambda, z), \tag{2.22}$$

where the z-axis is in the same direction of the photon flux. This absorption coefficient includes both band-to-band and free carrier absorption, hence,

$$\alpha = \alpha_{bb} + \alpha_{fca}\,. \tag{2.23}$$

The solution of the equation (2.4) is the standard Lambert-Beer absorption law,

$$\Phi(\lambda, z) = \Phi_o \exp(-\alpha(\lambda)z), \tag{2.24}$$

where Φ_o is the initial photon flux density (number of photons/area^2/sec). Due to the significance of the absorption coefficient, different methods are established for the measurement. In this chapter, a brief review of the theoretical background for different approaches of the applied measurement are investigated. Next sub-sections discuss the following principle measurements which are spectroscopic ellipsometry, reflectance/transmittance, spectral responsivity, and spectrally resolved luminescence [17, 18].

2.3.1 Spectroscopic Ellipsometry Measurement

The Ellipsometric measurement determines the degree of alteration (Δ) for the polarization of the light that reflects at a surface. In this method, the phase difference of the incoming and out-coming light wave is measured between the perpendicular and parallel

components. Also, the ratio of the reflection coefficient (ψ) for the light waves is measured. Using the measured polarization data, the complex indices of the refraction are obtained by fitting them with an appropriate optical model, and then they are carried out individually for each wavelength. In order to obtain consistent data for Kramers-Kroing curves, the discrete values of $\Delta\ and\ \psi$, for each λ, can be fitted by a dispersion relation. The extinction coefficient (k) is related to the absorption coefficient by

$$\alpha(\lambda) = \frac{4\pi k(\lambda)}{\lambda} \tag{2.25}$$

This method is applicable only when the extinction coefficient is large enough to be measured. For Si, this coincides to wavelengths around and below 950 nm. The measurement can be extended or longer wavelengths by taking into account the transmittance and reflectance data. Additional details on the Spectroscopic Ellipsometry measurement are found in reference [19] [20] [21].

2.3.2 Reflectance and Transmittance Measurement

Based on the Kubelka-Munk theory [22], reflectance (R), and transmittance (T) in semiconductors are related to the absorption coefficient for a planar surface by [18]

$$R = R_s\left[1 + \frac{(1 - R_s)^2 \exp(-2\alpha W)}{1 - R_s^2 \exp(-2\alpha W)}\right], \tag{2.26}$$

and

$$T = \left[\frac{(1 - R_s)^2 \exp(-2\alpha W)}{1 - R_s^2 \exp(-2\alpha W)}\right], \tag{2.27}$$

where R_s is the surface reflectance coefficient, and the W denotes the thickness of the planer. Then, the absorption coefficient is given by [18]

$$\alpha = -\frac{1}{W}\ln\left(\frac{C - R + 2R + T^2 - 1}{2T}\right), \tag{2.28}$$

where

$$C = \sqrt{(R^2 - 2R - T^2 - 1)^2}\,. \tag{2.29}$$

It requires collecting all reflected/transmitted data for light that corresponds to the sample to apply this relation. Note that these equations signify only the perpendicular incident of light.

2.3.3 Spectral Responsivity Measurement

For PV or photodiodes, spectral responsivity (SR) at the wavelength λ is defined as a short circuit current per incident intensity of light. The external quantum efficiency (EQE) in term of SR is calculated by [18]

$$EQE(\lambda) = SR(\lambda)\frac{hc}{q\lambda}\,, \tag{2.30}$$

where q is the carrier charge. The EQE and SR are related to the electroluminescence photon flux (Φ_{EL}) of a device by an optical reciprocity theorem [23]

$$\Phi_{EL}(\lambda,\Omega)d\lambda d\Omega = \Phi_{bb}(\lambda,\Omega)\; d\lambda\; d\Omega\; EQE(\lambda,\Omega)\exp\left(\frac{V}{V_T}\right), \tag{2.31}$$

$$\Phi_{bb}(\lambda,\Omega)d\lambda d\Omega = \frac{2c}{\lambda^4}\exp\left(-\frac{hc}{\lambda kT}\right)d\lambda d\Omega \tag{2.32}$$

where Ω is the solid angle which the photons are emitted into, k is the Boltzmann constant, t is the sample temperature, V is the junction voltage, V_T is the thermal voltage which equal to kT/q.

2.3.4 Spectrally Resolved Luminescence Measurements

The Luminescence emission is a result of the radiative recombination, where electrons recombine from a CB to a VB and photons are released. The radiative recombination is generally the dominated mechanism of recombination for direct semiconductors. The emitted photons generate luminescence photon flux Φ for each λ and surface area is determined by [24] [25] [26],

$$\Phi(\lambda) = \int_0^w dz\, G_{ph}(\lambda, z)\, f_{esc}(\lambda, z)\,, \tag{2.33}$$

where G_{ph} is the spectral photon generation rate and f_{esc} is denoted the luminescence photon escape probability. The absorption coefficient and G_{ph} are related to each other by the generalized Planck radiation law [27], and under typical luminescence measurement condition, equation (2.14) can be rewritten by

$$\Phi(\lambda) \approx \alpha_{bb} \frac{8\pi c n^2(\lambda)}{\lambda^4} \int_0^w dz\, f_{esc}(\lambda, z) \exp\left(\frac{\mu_{ph}(z) - E_{ph}}{kT}\right)\,, \tag{2.34}$$

where $\mu_{ph}$is the chemical potential of the photon. The last equation illustrates that α_{bb} is proportional to the luminescence photon flux. The latter equation might be simplified if $\mu_{ph}$is independent of and the carrier concentration is homogenous within the sample. Furthermore, it might be reduced if absorption coefficient is low and $f_{esc}$is independent of z.

The ellipsometric, reflectance and transmittance, responsivity, and luminescence measurement methods of the absorption coefficient have been briefly discussed in the last section. It is significant to understand the process of each method, also, combining results of the measurement enhances the accuracy of the absorption coefficient. Some of the methods have limitations while measuring the absorption coefficient, for example, the Spectroscopic

Ellipsometry is applicable only when the extinction coefficient is large. Moreover, the spectrally resolved luminescence measurement is relevant to materials where the radiative recombination is dominated. Since silicon had been discovered, many papers have been published to deliberate its optical properties. The following chapter discusses some of the papers that have been published on the topic of the absorption coefficient of silicon.

2.4 Absorption Coefficient of Intrinsic Silicon

The absorption coefficient of silicon has received a great attention due to its significant in the determination of the performance characteristics of solar cells [28, 29, 30, 31, 32, 33, 34, 35, 36, 37] [38, 39]. In 1955, Dash and Newman published one of the earliest paper to investigate the intrinsic optical absorption of single-crystal silicon [28]. They measure the intrinsic absorption spectra of high-purity single crystal silicon at 300 K and 77 K, from a range of 0.1 cm^{-1} to 10^5 cm^{-1}. They indicate that the threshold for direct transition is placed at around 2.5 eV, while 1.06 eV and 1.16 eV for indirect transitions at 300 K and 77 K. Previous measurement of the absorption coefficient were limited to the magnitude of 10^3 cm^{-1} because of thickness restriction. [40], but it was possible to measure higher absorption by using evaporated films [28]. The maximum value of the absorption coefficient measured at 300 K is in order of 10^5 cm^{-1}, where the lowest is in order of about 10^{-1} cm^{-1}, for photon energy range of 1.06 to 3.4 eV, see the results in figure 2.4.

Macfarlane and Roberts [31], and Macfarlane et al. [30] published a paper in 1955 and 1958, respectively. In the first paper, Macfarlane and Roberts measure the free carrier absorption of poly-Si at temperatures of 20 K to 3330 K by using reflectance/transmittance method. The results illustrate that the α_{FCA} is well represented by a law of the form

$$\alpha_{FCA} = A\left[\frac{(hv - E_G - k\theta)^2}{1 - \exp\left(-\frac{\theta}{T}\right)} + \frac{(hv - E_G + k\theta)^2}{\exp\left(\frac{\theta}{T}\right) - 1}\right], \tag{2.35}$$

where A is a constant, and $k\theta$ is the phonon energy (E_p), while θ is phonon temperature ($\theta = E_p/k$). The first term in the equation is responsible for the absorption by phonon emission, while the second term is by phonon absorption. This equation will be described in details when reviewing the Rajkanan et al. paper [41]. The temperature decencies of the absorption coefficient of silicon obtained a considerable attention; many other papers have been published to investigate how the temperature affects the absorbance, for example, see [42] [43] [44] [45].

Using the reflectance data and Kramers-Kroing analysis, Philipp and Taft [29] attempted to determine the optical constants of a single crystal silicon in the spectral range of

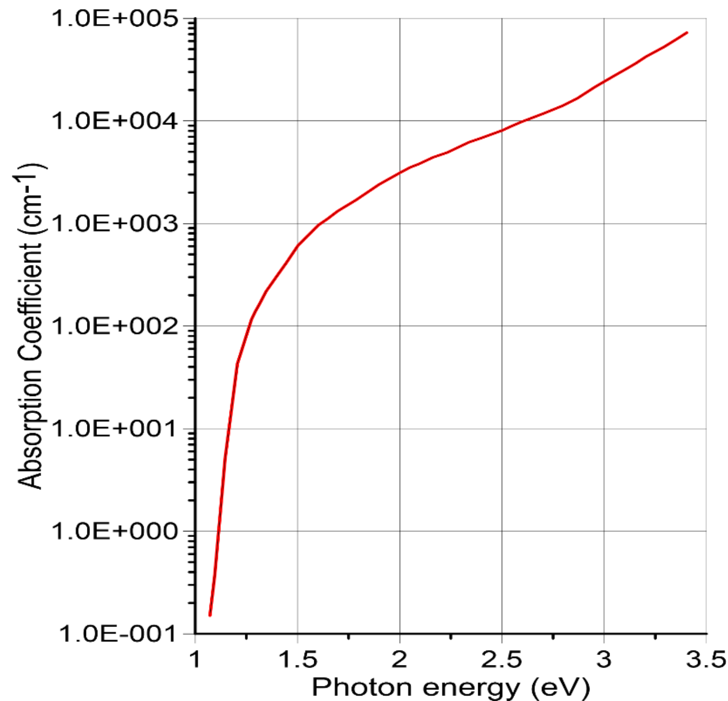

Figure 2.4 Silicon absorption coefficient as Dash and Newman presented at 300 K in 1955 [28].

1 to 10 eV. The Fresnel reflectivity equation then used to derive the optical constants, *n* and *k*. The absorption coefficient values were concluded by using equation (2.25).

One of the highest citation paper in term of the silicon absorbance is the Green's and Keevers's paper in 1995 [38]. An accurate tabulation of intrinsic silicon optical properties was demonstrated over a wavelength range of 250-1450 nm at 10 nm intervals and 300 K, from experimental measurements. For wavelength lower than 460 nm, absorption coefficient was measured using ellipsometric measurements and applying equation (2.25). The transmission measurement was used to extract absorption coefficient for a range of 460 to 1200 nm. Beyond 1200 nm, absorption coefficient was determined by sensitive spectral response measurements. While the table of Green and Keevers (1995) included absorption coefficient, n and k, Green published an updated table for latter parameters in 2008 [39] and in addition he investigated the temperature dependences coefficients for each interval of wavelength. While the minimum absorption data that have been recorded in [28] was in the order of 10^{-1} cm^{-1}, here an order of 10^{-8} cm^{-1} have been achieved.

One of the most recent papers published to examine silicon absorption coefficient is Schinke et al. in 2015 [46] [47]. The uncertainty of the inter-band absorption coefficient of crystalline silicon has been studied, using four different measurement methods, over the wavelength range of 250 to 1450 nm. The measurements where the data have been derived for are spectroscopic ellipsometry, transmittance and reflectance, spectral responsivity measurements, and spectrally resolved luminescence. The objective of the paper was to resolve the inconsistencies of the absorption coefficient data amongst several of published papers. A comparison of various data of absorption coefficient from different papers is shown in figure

2.5, while a 30% ratio of discrepancies has obtained. The data was compared to the Schinke *et al*. paper [18], which had a tabulated record, while some of the old papers the absorption coefficients have been digitized from the figures to obtain the data. The discrepancies of absorption coefficient attributed to an uncertainty accuracy of the combined data, in addition to different measurement conditions such as sample thickness, temperature, doping level, and surface defects. For this paper, the combined data of absorption coefficient was obtained under well-defined sample and laboratory condition from different institutions to avoid any

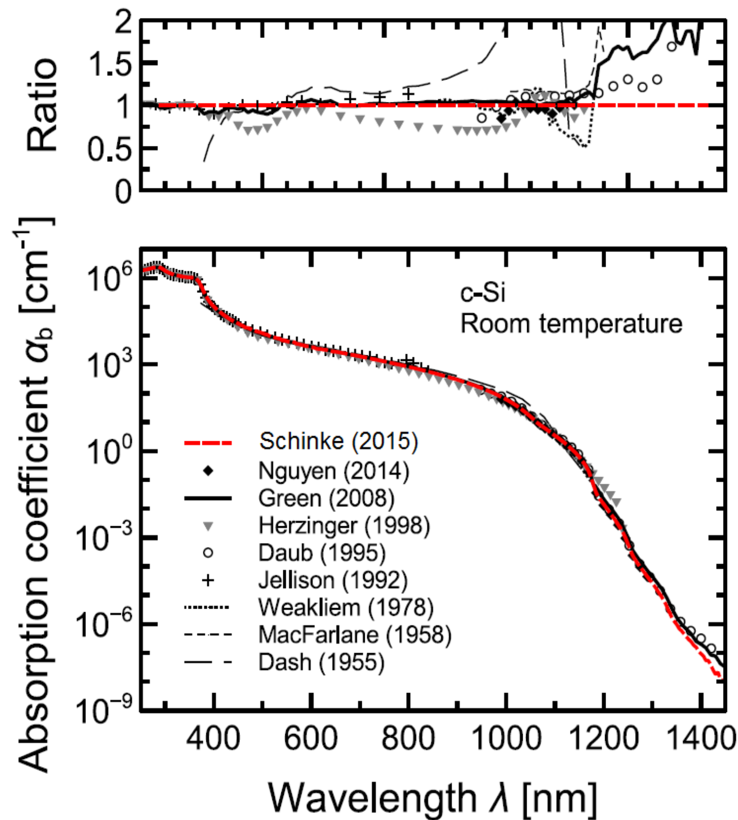

Figure 2.5 Absorption coefficient comparison done by Schinke *et al*., of several most widely data of papers at room temperature [18].

inconsistency. The paper presents a brief review of the theoretical background of the measurements of the absorbance in semiconductors.

2.5 Analytical Models of Silicon Absorption Coefficient

In 1979, an analytical formula was developed by Rajkanan *et al.* [41], for the purpose of calculating the absorption coefficient over a range of 1.1 to 4.0 eV by considering a wide range of temperature. This expression deduced from the available experimental data at that time in term of three bands of silicon, with an accuracy of 20% over 20-500 K of the temperature range. The expression accounts for the direct and indirect inter-band transitions in silicon. The direct transition considered to be at E_{gd}= 3.2 eV, instead of 3.4 eV, since it increases the accuracy of the formula. For a parabolic band approximation, the direct transition (vertical, α_v) is proportional to

$$\alpha_v = \left[hv - E_{gd}(T)\right]^{\frac{3}{2}}. \tag{2.36}$$

While for the indirect transition (non-vertical, α_{nv}); where the phonon are involved by either absorption or emission to conserve electrons momentum, it can be written for a parabolic band as

$$\alpha_{nv} = \sum_{i,j} C_i A_j(T) \left\{ \frac{\left[hv - E_{gj}(T) + E_{pi}\right]^2}{\exp\left(\frac{E_{pi}}{kT}\right) - 1} + p_i \frac{\left[hv - E_{gj}(T) - E_{pi}\right]^2}{1 - \exp\left(\frac{-E_{pi}}{kT}\right)} \right\}. \tag{2.37}$$

The above expression explains various possibilities of indirect transitions, where suffix *i* refers to different of phonon energy E_p, while suffix *j* refers to the indirect bandgaps *Eg*. The factor p_i, depends on the change in the energy of the intermediate and final states, which is slightly more than unity for Si [34]; however, it has been assumed to be unity in this paper [41]. *C* and

A are constants which determined experimentally. Despite the fact that silicon has a direct bandgap at 3.4 eV, Rajkanan *et al.* selected the Egd to be 3.2 eV since it provides more accuracy for the expression. The complete data of the expression is done by adding equation (3.36), multiplying by constant A_d, to equation (2.37). Since the final formula deviates by 20% from the actual value, the expression is purposed for measurement in the devices which not demand high accuracy in the absorption coefficient determination such as photovoltaics. Figure 2.6 shows a compersion between Rajkanan *et al.* [41] and Green data [39] for silicon absorption coefficient at 300 K. Rajkanan *et al.* is not the first group who pursued to develop an expression for silicon absorptance, Bhaumik and Sharan [48] experimentally fitted the

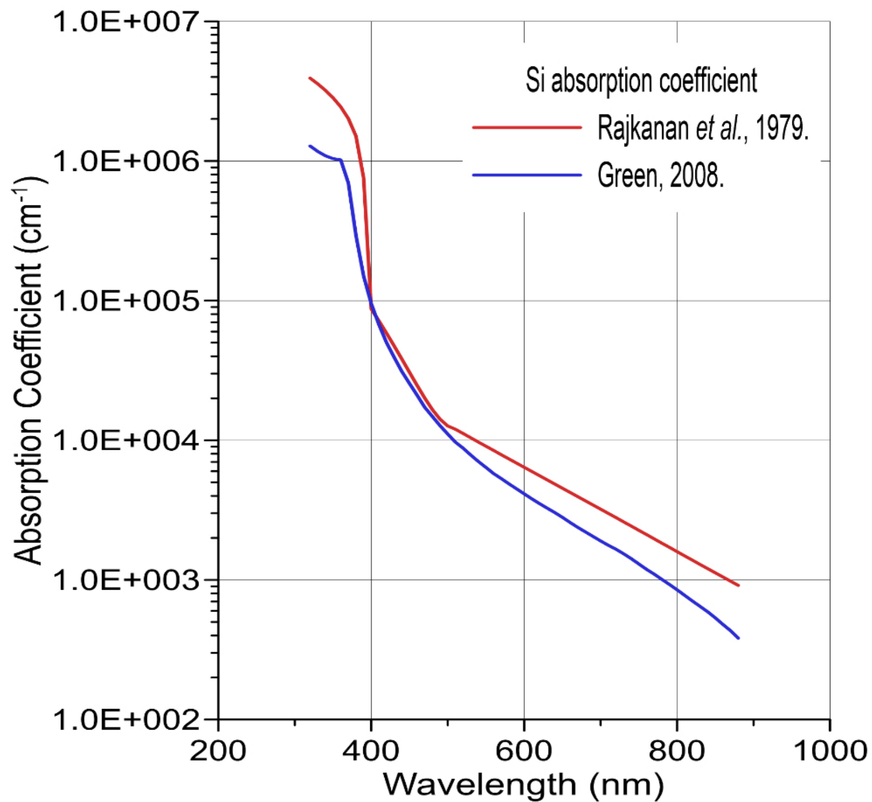

Figure 2.6 A comparison between Rajkanan *et al.,* 1979 [41] and Green, 2008 [39] data for Si absorption coefficient at 300 K.

absorption data over photon energy range of 1.175 to 3.0 eV using a simple form of the Bardeen-Blatt-Hall formula [49] at room temperature.

An appropriate representation of silicon absorption coefficient as a function of wavelength has been done by Palmer, in 1984 for silicon photodetector [50]. The seven-parameter expression demonstrates the absorbance of silicon near to the infrared region from 700-1100 nm, as following,

$$\alpha(\lambda) = 10^{(-25.9601\,\lambda^3 + 54.3882\,\lambda^2 - 40.8028\,\lambda + 14.0886)}, \quad (2.38)$$

where λ is in micrometers. The result of applying the above equation is shown in the figure 2.7

Geist *et al.* [51] published a paper in 1988 to demonstrate an analytic expression for the indirect transitions of the silicon absorption coefficient. The eleven-parameter equation represents the transitions between 1.05 to 2.7 eV at 289 K with maximum error of 10% as following,

$$\alpha(E_{ph})\,\hbar\omega = \sum_{i=i}^{2}\sum_{j=-1}^{1}\left\{C_{i,j}[L(\hbar\omega - \epsilon_1 + jd\epsilon_i]^2\right\} + C_3[2L(\hbar\omega - \epsilon_3)]^{N+dN\hbar\omega}. \quad (2.39)$$

The constants in the above equation are provided in the paper, and the result of the expression is shown in figure 2.8.

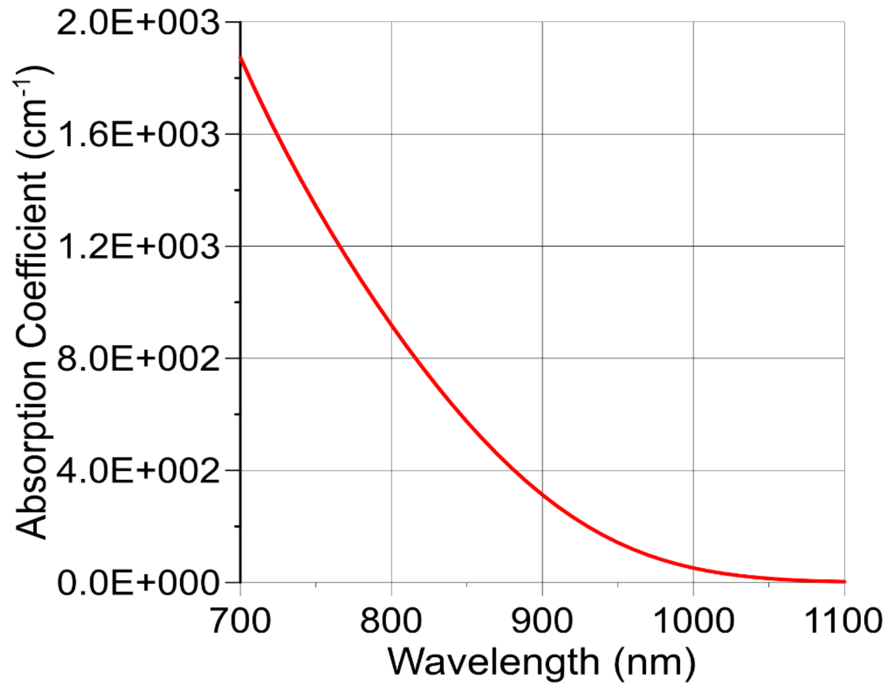

Figure 2.7 Silicon absorption coefficient according to Palmer expression [50].

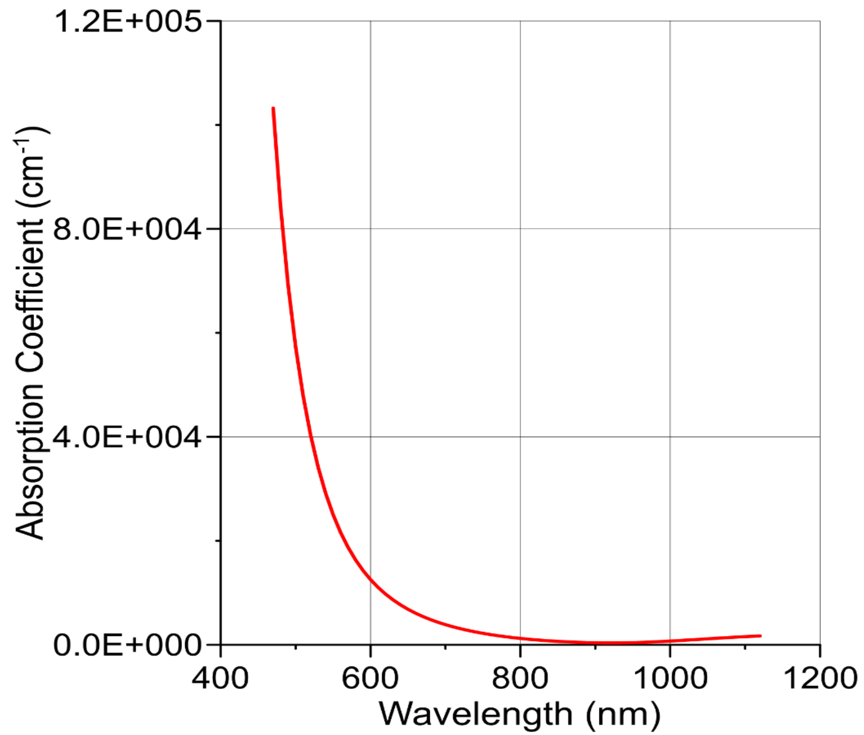

Figure 2.8 Silicon absorption coefficient according to Geist *et al.* [51] analytical expression at 289 K.

2.6 Doping Effects on Absorption Coefficient

The way in which the electronic properties of semiconductors are modified by the heavy doping effect had been described in term of bandgap shrinking and band tailing, where bandgap shrinking characterises the self-energy of different interactions of the charge carriers while band tailing is of the random nature of the impurity distribution. The theoretical assessment of the bandgap narrowing effect in the semiconductor still has much attentions to be well-understood [52, 53, 54]. In the case of heavily-doped semiconductors, the simple exponential equations are no longer valid to determine the carrier concertation, and Fermi-Dirac based derivation is required. The most interest area to be discussed for heavily doped semiconductors is near to the absorption edge, where the free carrier absorption occurs.

While the absorption coefficient which has been reviewed in [28] [31] [30] was for intrinsic silicon, Spitzer and Fan [55] published a paper in 1957 to investigate the absorption of free carriers in n-type silicon. The absorption coefficient of n-type Si has been studied for six different carrier concentrations and impurities samples. The analysis covered the spectral region from 1000 nm to 45000 nm, for donor impurities up to 10^{19} at various temperatures. The donor impurity includes As, P, Sb, and AsSn alloy. The study found that the absorption band height is proportional to the carrier concentration. For the wavelength range of 1500 to 5000 nm, experimental evidence shows that the absorption band is due to electrons excitation from the minima of the conduction band to a higher-lying energy band. Furthermore, the temperature dependence of the absorption is demonstrated for one of the samples. For the same purpose, Balkanski et al. [56] published a paper in 1969 to investigate the free carrier absorption by considering different doping level and various temperature. They used the

transmission measurement in the calculation, while a comprehensive theoretical background was demonstrated.

Jellison *et al.* published a paper in 1981 [57], attempting to determine the optical constants of n and p heavily doped silicon over a range of 1.5 eV to 4.1 eV using the polarization modulation ellipsometry. It has been shown that the absorption coefficient increases dramatically by increasing the doping of the degenerated As-doped sample, while the doping impact is much less for the Boron doped sample. A numerical solution was performed using 2-D analogue Newton's method, to find it is empirically illustrated that for the As sample lower than 3.2×10^{21} cm^{-3}

$$\alpha(hv, N) = \alpha_o(hv) + KN \exp\left(\frac{hv - 3.4\ eV}{E_o}\right), \tag{2.40}$$

where $\alpha_o(hv)$ is the coefficient for undoped-Si, K is equal to 1.8×10^{-15} cm^{-3}, N is the doping concentration, and $E_o = 0.58$ eV. The significant disparities on the impression of the absorption coefficient due to the differences in the n and p-type dopants is adjudicated to the d-electron in the As sample. By applying eqution (2.40) to see the impact of the doping on the absorption coefficinet of the Si as Jellison et al. suggested, it shows that for doping densities above 10^{19} cm^{-3} the absorption coefficient is increased by around an order of magnitude for photon energy below 2.5 eV as shown in figure 2.9. This alteration might be mainly attributed to the effect of the dopant on the bandgap, particularly to the bandgap narrowing effect. However, the effect of doping minimize when approach photon energy of 3.5 eV where the first direct bandgap of Si is pinpointed. This results show how important to study the effect of doping on

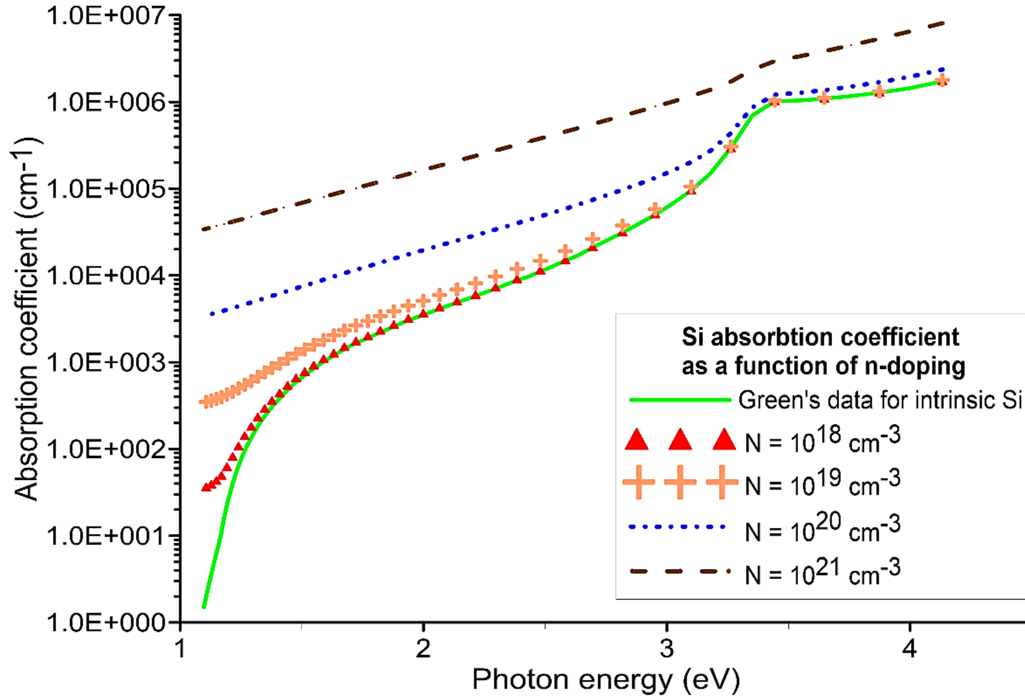

Figure 2.9 Absorption coefficient as a function of doping concentration for n-type Si, applying equation 2.40 [57].

semiconductors, while considering only an intrinsic data measurement, this leads to underestimate the absorption coefficient of a doped material.

2.7 Analytical Models of Silicon Generation Rate

Calculating the total generation rate of photovoltaic devices or a semiconductors material theoretically requires multiple evaluation steps for different elements as demonstrated in equation (2.18). The photon flux in equation (2.19) is calculated by obtaining the power density of the spectral irradiance of the sun which is wavelength dependent. After preparing the photon flux data, equation (2.21) is applied to calculate the generation rate at certain depth of the junction. For example, computing the generation rate at the surface of silicon cell, only, requires more than 80 steps if the segment of the wavelength is assumed to be 10 nm for a

range of 300 to 1100 nm. Moreover, since the generation rate is attenuated with junction depth, it is required to calculate the generation rate at each node of the cells. For a 200 μm junction, calculating the generation rate at each node of 10 μm requires 1600 steps. Hence, obtaining an analytical models to calculate the generation rate of a solar cells is necessary to avoid the time consumption and the extensive process steps.

In 1980, Hsieh *et al.* presented an approximation for the carrier generation rate in silicon [58]. The approximation was under the AM1 and AM2 rates by assuming zero reflecting at the surface. The data of the generation rate which have been used was from [59] and [60] for a junction depth of 1000 μm. The analytical solution was introduced in form of

$$\mathrm{g}(x) = \sum_{i=1}^{n} \frac{\mathrm{g}_i}{x + a_i} \tag{2.41}$$

where g, a are variable parameters and n is the number of terms which can be 1, 2 and 4. The complete details of the parameters, g and a, are tabluted in that paper [58]. Increasing the number of terms in above equation improves the accuracy of the expression. However, the AM0 and AM1.5 are the meanwhile standers for the solar extraterrestrial and terrestrial air masses, not the AM1 and AM2 which have been used in the photon flux calculation.

Another approximation was introduced by Furlan and Amon in term of exponential series to be more convenient than the previous approximation [61]. The generation rate has been calculated for a 100 μm silicon junction for AM0 and AM1 assuming no reflection at the surface. The approximation is presented by

$$g(x) = \sum_{i=1}^{n} a_i \, e^{-b_i x} \tag{2.42}$$

where a and b are variables which have been tabulated in the paper. The series of the exponential was presented in three or five terms and compared to the actual value of the generation rate resulted in an appropriate agreement. The result of the five terms approximation of Forlan and Amon is compared to the recent actual value of the generation rate of silicon for AM0 in figure 2.10. Another series of exponential formula has been proposed by Mohammad [62] using the same scheme of equation (2.42). This solution was for AM1 and AM2 silicon solar using the actual data of [59] and [60] which are not considering the reflectance on the surface.

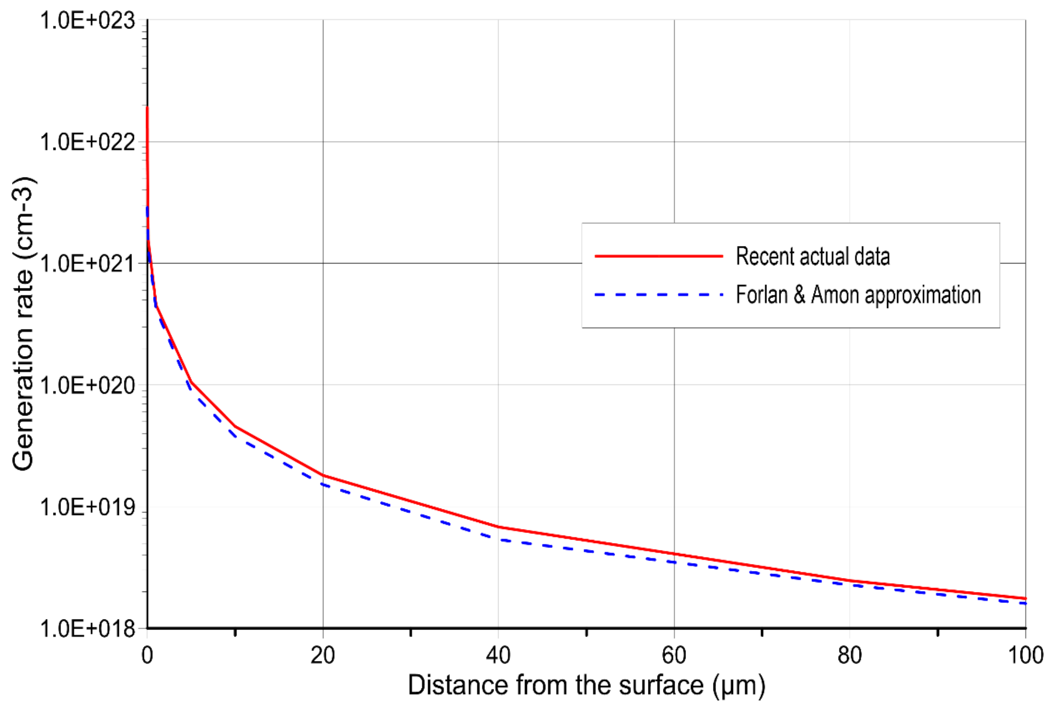

Figure 2.10 A comparison between Forlan and Amon approximation with a recent actual data for the generation rate of silicon at AM0.

Anvar *et al.* [63] and Chowdhury and Debnath [64] published a conference proceedings paper recently to obtain an approximation for the carrier generation rate using the standard air masses AM1.5G, AM1.5D and AM0. Both articles adopted the same scheme of Forlan and Amon [61] solution not only for silicon but also for other semiconductor materials such as CdTe, $CuInSe_2$, GaAs, Ge, InP and $Al_{0.3}Ga_{0.7}As$. Anvar's *et al.* approximation was split into two regions using Prony's method based on the junction thickness to provide more accurate results compared to the previous models. Chowdhury and Debnath exported the actual data of the generation rate stimulatingly from the PC1D software [65]. Nevertheless, both approximations do not account for the reflecting at the surface, doping effect, and photon cycling effect.

As discussed before, obtaining an approximation for the carrier generation rate has not been deeply investigated to achieve an excellent approximation that accounted for surface reflectance. Moreover, all the approximation that has been reviewed do not consider the photon cycling and photon recycling effect which can effectively improve the generation rate of solar cells. Hence, there is a necessity to obtain a new accurate approximation for the carrier generation using recent data for the recent standard air masses. Also, accounting for the photon cycling and photon recycling effects, which have been neglected in the previous approximation, is extensively sinificant.

2.8 Photon Cycling

The internal cycling of the photons is as a result of the optical confinement in the cell, which efficiently enhances the probability of light absorbing by increasing the light path. The reflecting of light at interfaces depends on refractive indices of the two mediums, in addition

to the angle of incident ray. In the plane boundary between two mediums of refractive index n_1 and n_2, the reflecting probability of the incident light at the surface is

$$R = \frac{(n_1 - n_2)^2 + k^2}{(n_1 + n_2)^2 + k^2} \tag{2.43}$$

For semiconductors, the refractive indices are typically in the range of 3 to 4 at visible light. The Snell's law describes the interface of the ray incident at two different mediums for non-polarised light as following,

$$n_1 \, sin(\theta_1) = n_2 \, sin(\theta_2) \tag{2.44}$$

where n, θ are the refractive index and the incident angle of the two mediums. The amount of reflected and transmitted light is described by Fresnel reflection formula depending on the polarization of light. In addition to materials selection for the internal reflector, the critical angle of the interface plays a significant role to determine the probability of escaping or reflecting of the incident ray. When the incident ray passes from a higher refractive index medium to a lower refractive index medium, it may reflect at the interface based on the angle of the ray. The equation of the critical angle is driven from the Snell's law, where the second angle is adjusted to be 90°,

$$n_1 \, sin(\theta_c) = n_2 \, \sin(90°) \tag{2.45}$$

$$\theta_c = \sin^{-1}(\frac{n_2}{n_1}) \tag{2.46}$$

The angle which has been adjusted to 90° is where the incident ray reflects perpendicular to the surface of the junction as shown in figure 2.11. The critical angle (θ_c) is the minimum

angle where the incident ray of light is going to reflect at the surface of the cell. For silicon-air interface with no antireflection coating, the critical angle at 2 eV is 14.8°.

2.9 Photon Recycling

Photon recycling is a phenomenon which is resulted primarily from the radiative recombination in semiconductors. It is the effect of reabsorbing the photons which are emitted in the radiative recombination processes in semiconductors. In 1957, where the effect where first studied, Dumke [66] concluded the emitted photons, of the radiative recombination events, are usually reabsorbed before they passed away from the crystal, for semiconductors which have high absorption constant close to the bandgap edge. This effect was recognised later as photon recycling, which can contribute to the total of generation rate of semiconductors. Since the radiative recombination is particularly unavoidable in non-equilibrium semiconductors, the effect of photon recycling should be considered, particularly in direct semiconductors where the radiative recombination is dominated.

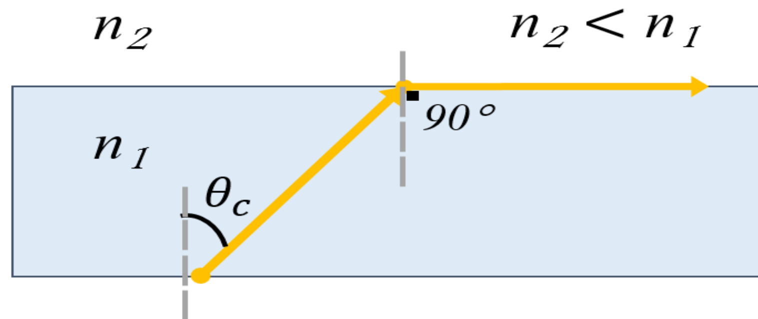

Figure 2.11 The principle of the critical angle of the semiconductor-air interface.

The photon recycling effect was neglected in the Shockley's p-n junction diode theory [67] [68], which is one of the main reasons for the discrepancy with the detailed balance theory for limiting efficiency calculation [69]. Marti *et al.* [68] suggested that neglecting the photon recycling effect could underestimate the limiting efficiency of the solar cells. It is illustrated that the photon reabsorption effect has to be considered for III-V compound semiconductors since the dominance of radiative recombination. However, for silicon solar cells, the efficiency is limited by Auger recombination [70].

Several works published to study the effect of photon recycling in semiconductors [71, 72, 73, 74, 75, 76, 77, 78, 79]. Furthermore, some recent papers examine photon recycling effect numerically and experimentally [80, 81, 82], including electrical models [68] [83, 84] and optical models [85, 86, 87]. Photon recycling effect is not deliberated in most of the physics of semiconductors or physics of solar cells books. However, Nelson's book of solar cells [16], which first published in 2003 and reprinted in 2004-2013, comprises a full subsection to illustrate the effect. Another book which comprehensively demonstrates and addresses the photon recycling effect in the III-V semiconductors is the Ahrenkiel's and Lundstrom's book [88]. When the photon recycling is considered in the generation rate equation, an additional emitted flux (ΔN_e) should be counted into the formula.

$$N_{tot} = N_{ph} + \Delta N_e \tag{2.47}$$

N determines by [89]

$$N(E,x) = \frac{2n_s^2}{h^3c^2}\frac{E^2}{e^{\frac{E-\Delta\mu}{kT}} - 1} \tag{2.48}$$

where $\Delta\mu$ is the splitting of the quasi Fermi level at position x and refractive index of the material n_s. Then, $\Delta N_e$is

$$\Delta N_e(x) = \int_0^x \alpha N_e(x')\, e^{-\alpha(x-x')} dx'. \tag{2.49}$$

When the angle is taking into account, the above equation becomes

$$\Delta N_e(x) = \int_0^x \alpha N_e(x')\, e^{-\alpha(x-x')\sec\theta} \sec\theta\, dx'. \tag{2.50}$$

Above equation shows that the flux which emitted at some points increases the flux at that point. In this particular situation, the carrier generation rate is the summation of the external and internal generation

$$\mathrm{g}(E,x) = \mathrm{g}_{ext}(E,x) + \mathrm{g}_{int}(E,x). \tag{2.51}$$

The photon recycling effect was considered as theoretical objects to optimise solar cells efficiency since all practical photovoltaics are limited by non-radiative recombination process [16]. Nevertheless, recent publications show that achieving higher efficiency by taking the photon recycling effect into account is possible [90, 91, 92, 83].

Ren *et al.* [90] numerically analysis the photon recycling effect on a single-junction (GaAs and tandem (GaAs/Si) solar cells. For multi-junction solar cells, a new expression has to be introduced which is the luminescent coupling (LC), where the emitted photon is reabsorbed by the underlying lower bandgap junction. The luminescent coupling effect utilises the photons, which is emitted during radiative recombination, by the bottom junction of tandem devices since the upper junctions have higher bandgaps. The GaAs and Si are well-investigated materials, and the GaAs/Si tandem are promising devices of photovoltaic [93, 94]. They used

the semiconductor modelling program PC1D [65] to solve the J-V curve numerically. Ren *et al.* [90] define the photon reabsorbing probability as

$$P_{abs}(x,E) = \int_0^{\frac{\pi}{2}} P_{abs}\, d\theta \tag{2.52}$$

where P_{abs} is the reabsorption probability at each node, which can be determined for an L junction thickness using the following equation [83],

$$\begin{aligned} P_{abs} &= \left(1 - e^{\frac{-\alpha x}{cos\theta}}\right) + \frac{e^{\frac{-\alpha x}{cos\theta}} R_f \left(1 + e^{\frac{-\alpha L}{cos\theta}} R_b\right)}{1 - e^{\frac{-2\alpha L}{cos\theta}} R_b R_f} \\ &+ \left(1 - e^{\frac{-\alpha(L-x)}{cos\theta}}\right) \frac{e^{\frac{-\alpha(L-x)}{cos\theta}} R_b \left(1 + e^{\frac{-\alpha L}{cos\theta}} R_b\right)}{1 - e^{\frac{-2\alpha L}{cos\theta}} R_b R_f}. \end{aligned} \tag{2.53}$$

Finally, the generation rate of the photon recycling is the dot product of the following matrices

$$G_{PR}(x,\Delta\mu) = R_{emit}(E,\Delta\mu)\,.\,P_{abs}(x,E). \tag{2.54}$$

The emission of radiative recombination is determined by van Roosbroeck–Shockley equation [89],

$$R_{emit}(E,\Delta\mu) = \int_0^{\infty} \frac{8\pi}{h^3 c^2} \frac{\alpha(E) n_s^2 E^2}{e^{\frac{E-\Delta\mu}{kT}} - 1}\, dE. \tag{2.55}$$

The efficiency achievement for the GaAs/Si tandem solar cells in this work was 0.24% by considering the photon recycling and luminescent coupling effect. Another increasing in the efficiency was up to 0.7%, recording by Ren et al. [91] for InGaP/Si tandem solar cells. The photon cycling inside a slab of solar cells may categorise into three trajectories [16],

a) $\theta < \theta_c$, the incident of light escapes from the front surface with no reflection

b) $\theta_c < \theta < (\pi - \theta_c)$, the ray reflects more than once at front or rear surfaces

c) $(\pi - \theta_c) < \theta < \pi$, the ray reflects once at the rear surface.

The three different scenarios are illustrated in figure 2.12 below.

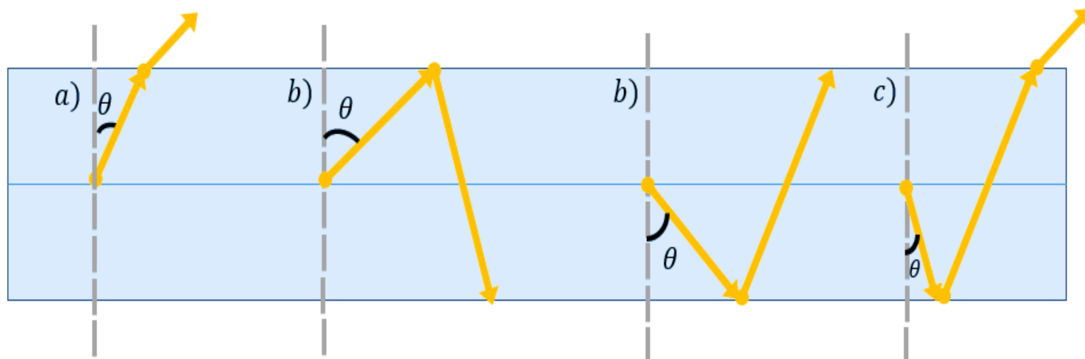

Figure 2.12 Different scenarios for photon recycling effect, where a photon is emitted in a junction with a perfect rear reflector.

Chapter 3

3.1 Introduction

In this chapter an in-depth analysis and investigation for silicon absorption coefficient and carrier generation rate are illustrated which results in new novel models and approximations using recent data.

3.2 A New Approximation for Silicon Absorption Coefficient

The absorption coefficient of silicon has received an inordinate attention due to the extraordinary number of applications that implant silicon in their devices. Silicon is one of most cost-effective semiconductor that is stable at high temperature. The optical properties of semiconductor materials play a key role in the photodetector applications. As seen in the literature review in chapter two, different formulas have been developed to evaluate and determine silicon absorption coefficients theoretically or numerically. However, these approximations did not provide highly accurate results since they vary 20-10% at some points. Consequently, using the tabulated absorption data is still necessary to determine the value of the absorption coefficient at specific wavelength. This process is repeated as the wavelength is changed, which results in time-consuming. To reduce the time-consuming in looking up in the table and to accelerate the process of determining the absorption coefficient, a novel and simple approximation has been developed using this equation form,

$$\alpha(\lambda) = \sum_{i=0}^{n} a_i \, exp(-b_i \lambda) + c_i \, ln(d_i) \,, \tag{3.1}$$

where $a_{i,j}$ and $b_{i,j}$ are variable coefficients. Selecting this scheme of formula refers to the decaying and variation in the absorption coefficient of the semiconductors in addition to the simplicity of differentiation and integration. Otherwise, a series of polynomials can be considered as a pattern for the approximation,

$$\alpha(\lambda) = \sum_{i=0}^{n} a_i \lambda^i (nm) \tag{3.2}$$

For this work, silicon has been to be represented as an example to show the validation of formulating the absorption coefficient of semiconductors for both models. Silicon has an absorption range starting from 300 to 1100 *nm* and a direct bandgap at 3.4 eV (365 *nm*). Considering the latter fact, it is easier to split the silicon absorption coefficient approximate into two regimes due to the sharp slope at 3.4 eV.

The new approximation provides the silicon absorption coefficient depending on the wavelength only. It splits into two regime, the first one starts from 300 to 360 *nm*, while the second one starts from 370 to 1100 *nm*. The new approximation shows high accuracy of fitting along all over the points. The Green's absorption coefficient of silicon [39] is considered the actual data for the approximation. The absorption coefficient of Green is measured at 300 K for an intrinsic silicon as discussed in chapter two. The wavelength interval is 10 *nm* for the whole range.

The approximation of the 300 to 360 nm regime of silicon absorption coefficient can be obtained only by using the first term in equation 3.1, as follows

$$\alpha(\lambda) = \sum_{i=0}^{n} a_i \exp(-b_i). \tag{3.3}$$

The values of a_i and b_i are listed in table 3.1. Another approximation has been obtained using the polynomial model for the same absorption range. The coefficients a_i for equation 3.2 are listed in table 3.2. The results for both approximation in addition to results compared to the actual data shown in figure 3.1. The point to point percentage error value for both approximations is less than 1% over the whole range. The percentage of error at this range is meant to be as small as possible because this region contributes to the generation rate most. Figure 3.2 presents the percentage error value at each point for both approximations comparing to Green's data [39].

For the second regime starting from 370 *nm* to 1100 *nm*, the original pattern of equation 3.1 has been employed. Since the range of the second regime is outspread, the absorption coefficient approximation is expanded. The parameters of the approximation are listed in table 3.3. The approximation exceedingly fits the actual data of Green's [39] with an error of less than 2% for the range between 370 *nm* to 980 *nm*. However, beyond that range the value of the absorption coefficients become extremely small which slightly rises the error of the approximation as shown in figure 3.3. The percentage error value at each point has been plotted in figure 3.4.

Formulating the absorption coefficient of semiconductors is important to determine the absorbance at each wavelength. Generating an approximation of absorption coefficient minimizes the time of tracing the absorption value in tables or searching in references. Indeed, the absorption coefficient approximation of semiconductors eases the further process where the absorbance of the material is embedded such as in generation rate calculation. On the other hand, the weakness of this type of modelling is the absence of the physical meaning. The

concept of obtaining an approximation for absorption coefficients can be simply adapted to all other semiconductors which is not yet ascertained.

Table 3.1 Coefficients a_i and b_i for silicon absorption range between 300 to 360 *nm* using equation 3.3.

a_i	$\times 10^3$ cm^{-1}	b_i	
a_0	9.711×10^2	b_0	0
a_1	1.924×10^2	b_1	$15.08 - 0.0457 * \lambda(nm)$
a_2	1.442×10^{-1}	b_2	$0.05 * \lambda(nm) - 16.5$

Table 3.2 Coefficients a_i and b_i for silicon absorption range between 300 to 360 *nm* using equation 3.2.

a_i	$\times 10^3$ cm^{-1}
a_0	1318.586×10^3
a_1	$- 15.486 \times10^3$
a_2	68.418
a_3	- 0.135
a_4	0.099×10^{-3}

Table 3.3 Coefficients a_i, b_i, c_i and d_i for silicon absorption range between 370 to 1100 *nm* using equation 3.1.

a_i	$\times 10^{10}$ cm^{-1}	b_i		c_i	$\times 10^4$ cm^{-1}	d_i	
a_0	6.064×10^{21}	b_0	0.1598	c_1	2.5486	d_o	$\lambda(nm)$
a_1	$2.676\times10^{-2} * \lambda(nm)$	b_1	0.0361	c_2	-1.693	d_1	$\lambda(nm) - 3.696 \times 10^2$
a_2	2.458×10^{27}	b_2	0.1959	c_3	-6.683	d_2	2.718

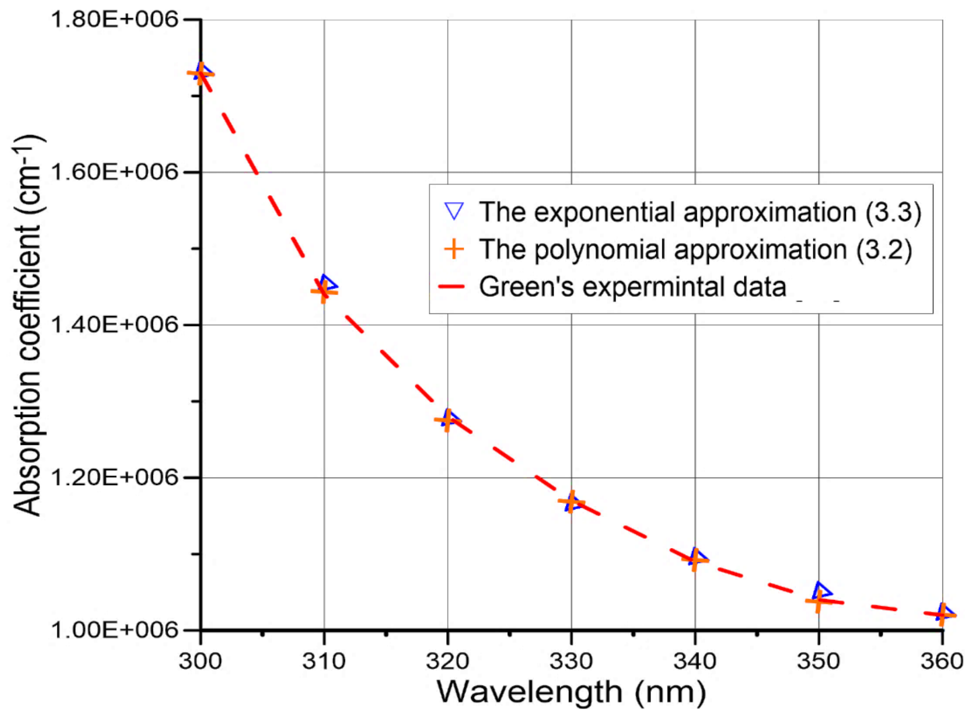

Figure 3.1 Results of the exponential approximation using equation 3.3, the polynomial approximation using equation 3.2, and finally compare the results with the experimental data of Green [39] for Si absorption coefficients.

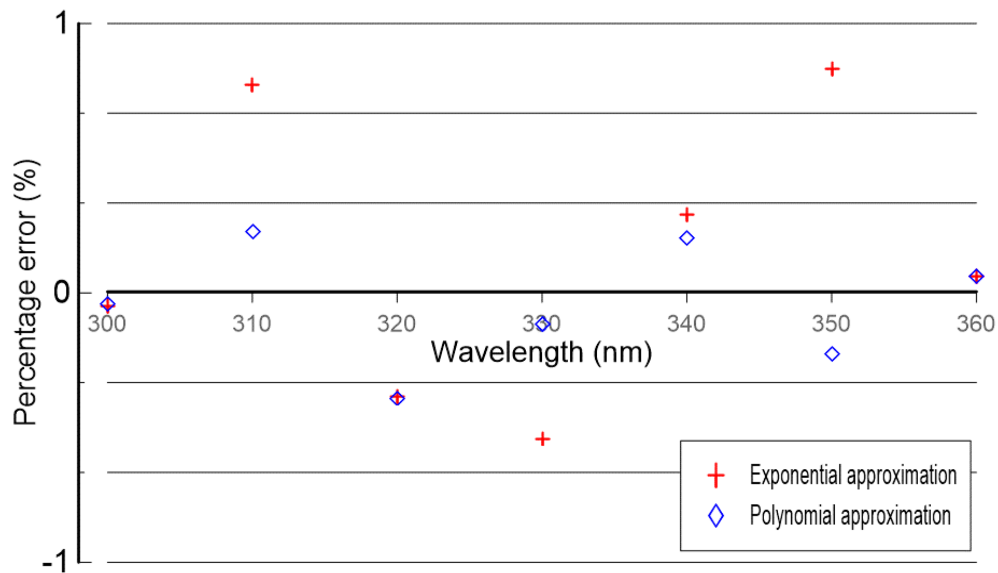

Figure 3.2 The percentage error of the exponential and polynomial approximations comparing to the Green's data.

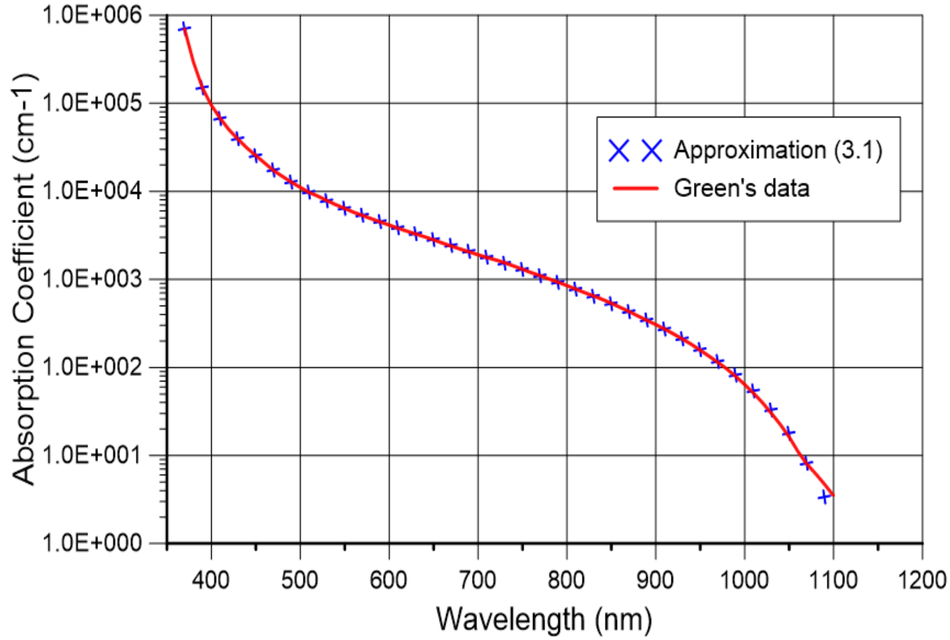

Figure 3.3 Results of the approximation using equation (3.1) and compare the results with the experimental data of Green [39] for Si absorption coefficients.

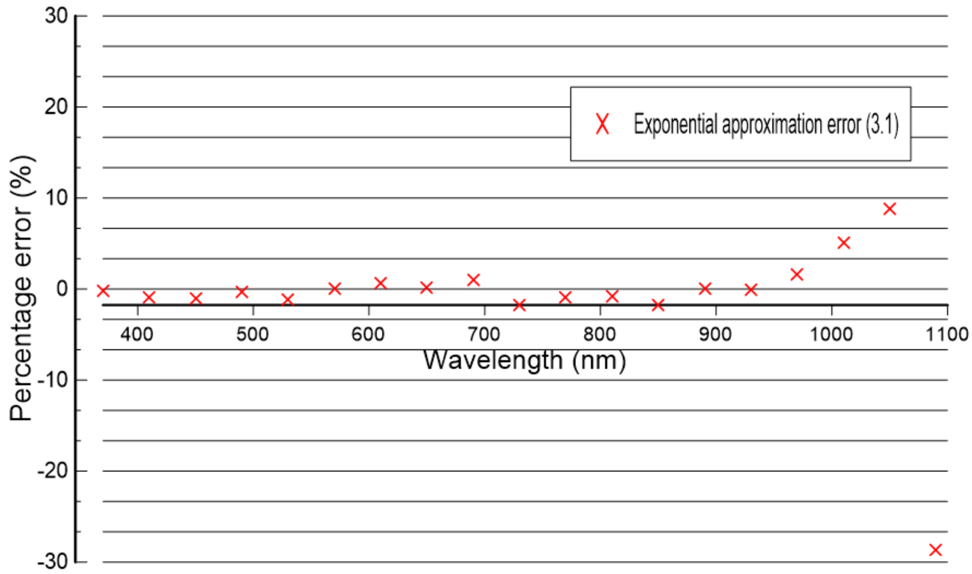

Figure 3.4 The percentage error of the exponential approximations (3.1) comparing to the Green's data.

3.3 Modelling the Carrier Generation rate for Si Solar Cells

The carrier generation rate is one of the most important parameters of PV since it is embedded in the limitation of the efficiency of the solar cells. As illustrated before, the series of processes needed in computation the generating rate in addition to the time consuming derives the necessity to establish an absolute model to simplify the calculation. Indeed, since the air masses are updatable from time to time, revising the approximation of the generation rate is essential. The model established in [61] still endorses an excellent fitting to the actual generation rate. Thus, this model is implemented here,

$$\mathrm{g}(x) = \sum_{i=1}^{n} a_i \, e^{-b_i \, x(\mu m)} \, . \tag{3.4}$$

The optimal thickness for crystalline silicon is in range of 100 to 350 μm [95, 96] or even 30 to 70 μm for an optimal efficiency conversion [97]. For this work, the junction thickness for Si solar cell has been chosen to be 50 μm initially, and then the photon cycling effect applies to increase the ray path to be 200 μm. Another example of a few micron Si thin-film junction is considered also to be studied in this thesis to show the effect of photon cycling on it. Furthermore, an investigation of the effect of photon cycling photon, recycling and luminescent coupling for multi-junction solar cells or tandem solar cells is studied.

The first approximation of the carrier generation rate is assumed for a 50 μm Si junction solar cells under AM1.5G. The internal and external reflectance are set to be zero at the beginning to check the validation of the approximation comparing to the actual value. A Sample for the calculation of the actual data of carrier generation rate of 50 μm Si junction using AM1.5G is listed in appendix A. The scheme of the silicon cell used in the calculation

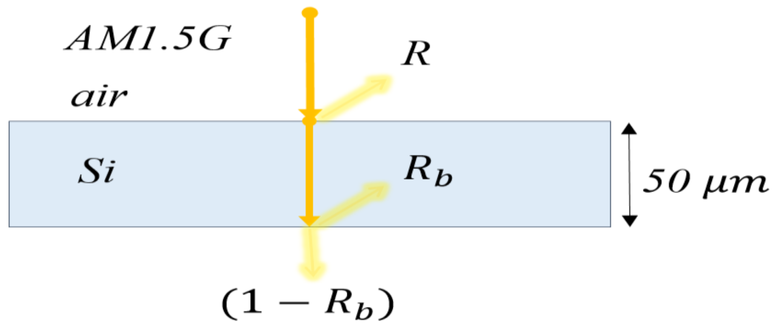

Figure 3.5 The scheme of the silicon junction used in the calculation of carrier generation rate.

is illustrated in figure 3.5. The new approximation of the carrier generation rate shows high accuracy comparing to the actual data. Due to the outsized contribution of generation rate at the surface and at the few nanometers from the surface, the approximation of the generation rate splits into two regions. The first region starts from 0 to 0.028 μm and the second region starts from 0.028 to 50 μm. The coefficients a_i and b_i of the models (3.4) are listed in table 3.4a and 3.5b for both regions. The results of the new approximation comparing to the actual value of the carrier generation rate is shown in figure 3.6 and 3.7.

The neglecting of the external reflection at the front surface leads to an overestimation to the actual carrier generation rate as seen in figure 3.6. Most of the approximations which have been formulated for the carrier generation rate neglect the external and internal reflection. Therefore, it is essential to approach a new approximation by accounting to the reflection based on equation (2.43). Using the same schematic of figure 3.5 and expression (3.4) by including the external reflection at the front surface a new approximation has been approached. The coefficients a_i and b_i for the new approximation of carrier generation rate that includes the external reflection under AM1.5G are listed in table 3.4c and 3.4d.

Table 3.4 Coefficients a_i and b_i for the silicon carrier generation rate approximation of the 50 μm junction thickness under AM1.5G with no reflection at front surface.

a) Generation rate of the first region [0, 0.028 μm] no external reflection.			
a_i	$\times 10^{27}$ m^{-3}	b_i	
a_0	5.260	b_0	0
a_1	40.297	b_1	1.960
a_2	7.764	b_2	86.337
a_3	-21.746	b_3	12.789
a_4	-24.026	b_4	3.988
b) Generation rate of the second region (0.028, 50 μm] no external reflection.			
a_i	$\times 10^{25}$ m^{-3}	b_i	
a_0	1.297	b_0	0
a_1	73.033	b_1	10.742
a_2	59.082	b_2	2.410
a_3	47.764	b_3	0.497
a_4	2.197	b_4	0.216
a_5	$0.0178 * x\ \mu m$	b_5	0
c) Generation rate of [0, 0.028 μm] with the external reflection (R).			
a_i	$\times 10^{27}$ m^{-3}	b_i	
a_0	3.491	b_0	0
a_1	$-2.203\times 10^{2} * x\ \mu m$	b_1	33.904
d) Generation rate of (0.028, 50 μm] with the external reflection (R).			
a_i	$\times 10^{25}$ m^{-3}	b_i	
a_0	2.220	b_0	0
a_1	$-7.698\times 10^{-2} * x\ \mu m$	b_1	0
a_2	$7.630\times 10^{-4} * x^2\ \mu m$	b_2	0
a_3	$1.084\times 10^{-1} * x^3\ \mu m$	b_3	0.488
a_4	5.289×10^{1}	b_4	3.946
a_5	3.371×10^{1}	b_5	0.488

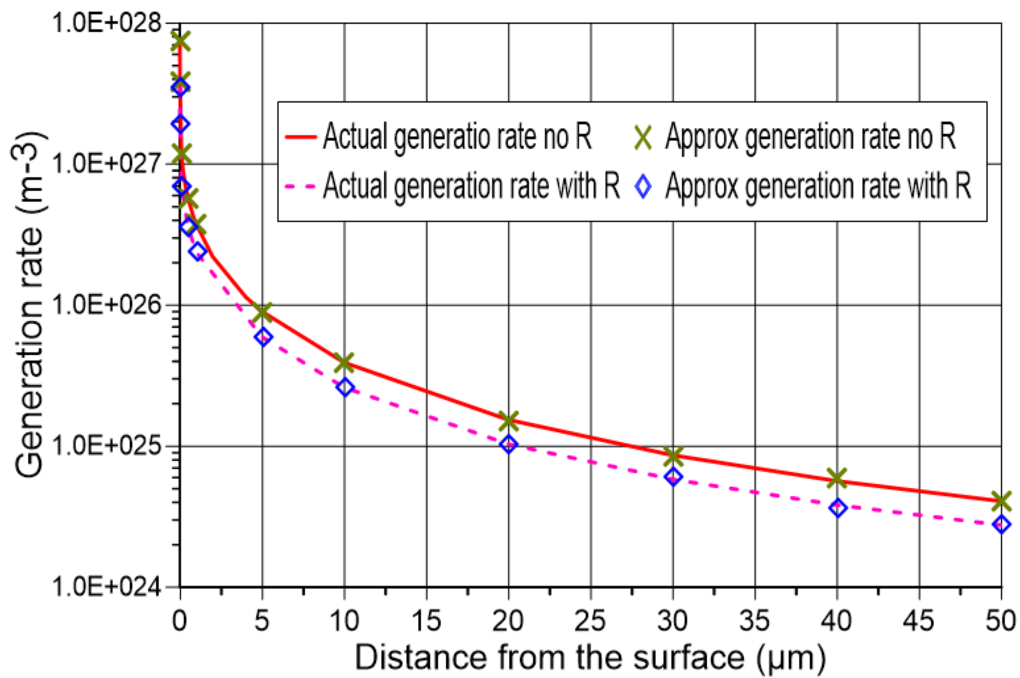

Figure 3.6 Calculating the carrier generation rate using model (3.4) comparing to the actual generation rate for Si junction assuming no external light reflection.

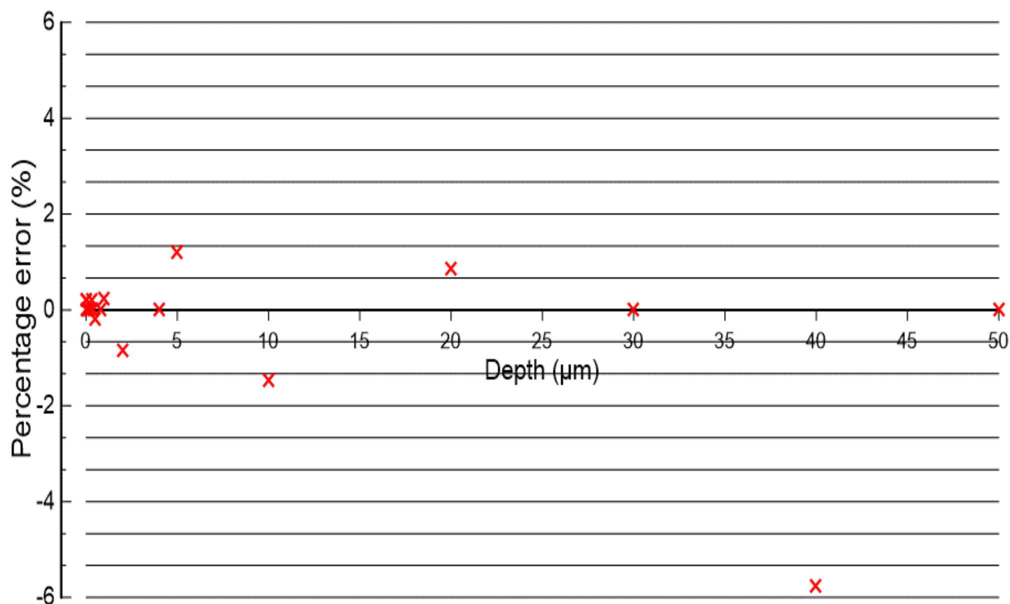

Figure 3.7 The percentage error of the new approximation models (3.4) comparing to the actual data of generation rate of Si junction.

3.4 Photon Cycling Approximations for Carrier Generation Rate of Si

The phenomena of photon recycling increases the length of the incident ray efficiently in present of an excellent reflector at the internal back and front surface. For example, the ray path of the previous 50 μm silicon solar cell improves three times by implanting three cycles only to reach to 200 μm for the total length. This increasing in the path of the light efficiently enhances generating of the free carriers of the solar cells especially at the bottom area as shown in figure 3.8. The generation rate of the cycle rays effectively enhances the generation rate near to the back surface not the front surface because the generation rate near to the front surface has much higher magnitude. Increasing the number of cycling, which is highly possible, leads to much more improvement in in magnitude of the generation rate. This results in enhancing to the *I-V* characteristic which leads to improve the efficiency of the solar cells. The improvement of the photon cycling effect upon the generation rate is shown more in direct semiconductors due to the higher absorbance. Thereby, showing the enhancement of photon recycling effect on silicon solar cells is a foundation which leads to study this effect for other semiconductor materials.

Accounting to the photon cycling effect analytically to the total of the generation rate leads to complicated expression due to the spatial dependency of the generation rate. Most the papers that have been reviewed tend to neglect the effect of photon cycling. Otherwise, it might be computed numerically through some computer software. The main obstacle of adding the photon cycling generation rate to the generation rate of the first pass is the spatial resolution since the nodes of the first pass differ than other cycles. Assuming all ray paths have the same length reduces the complexity of the analytical models for the photon cycling effect.

Furthermore, considering the incident angle always more significant than the critical angle. The first approach of the silicon junction design to determine the impact of three photon cycles is shown in figure 3.8, which is showing 144% increasing in the generation rate.

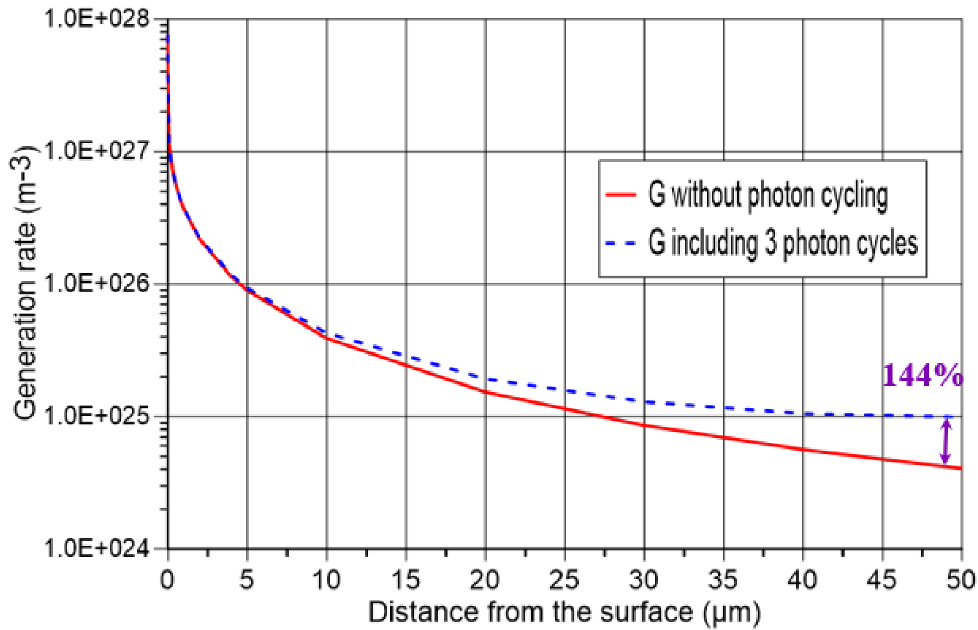

Figure 3.8 The enhancement of the photon cycling to the generation rate.

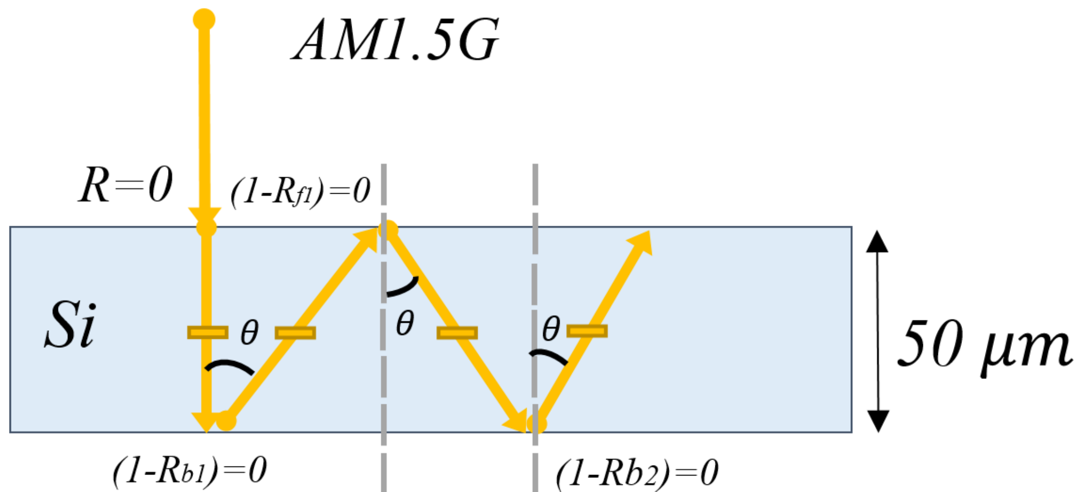

Figure 3.9 The initial approach of the silicon solar cell design to determine the photon cycling effect on generation rate.

To calculate the photon cycling effect, the schematic in figure 3.9 is applied assuming that all paths have the same length and the incident angle is larger than the critical angle. Furthermore, all internal reflections (R_b, R_f) and the external front surface reflection (R) have been set to zero temporally. The generation rate of the first pass, first cycle, second cycle, and third cycle is calculated based on the previous assumptions for the silicon solar cells. The curves of each generation rate are shown in figure 3.10. It shows that the contribution of generation rate decreases as the number of cycles increases. For the 50 μm silicon solar cells, it seems that the contribution of the generation rate decreases after the third cycle. However, as the thickness of the junction decreases the effect of photon cycling becomes more important such as in thin film solar cells. The effect of photon cycling on thin-film solar cells is discussed in section 2.8.

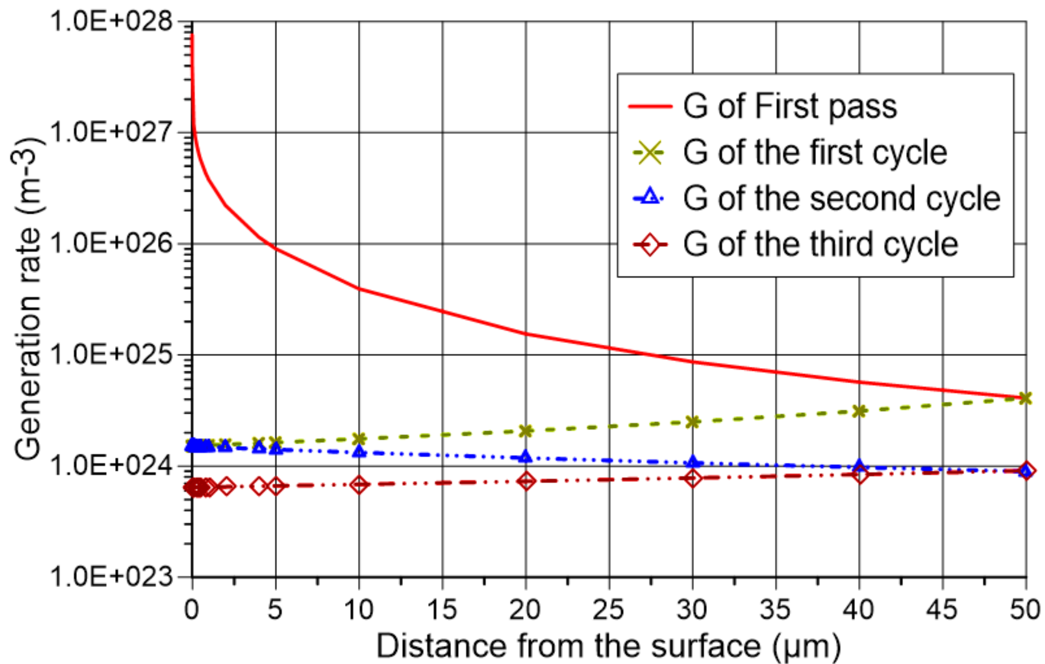

Figure 3.10 The generation rate of the first pass, first cycle, second cycle, and third cycle for 50 μm silicon solar cell.

Combining the contribution of the cycling generation rate to the generation rate of the first pass is not a simple process since the nodes of are not the same as the first pass nodes. However, Sarkar [98] proposed an expression to compute the generation rate including the photon cycling. For the first pass and first cycle, where the fist cycle reflects at the internal back surface, the generation rate is assumed to be

$$g_{total}(x) = g(x) + g(2t - x), \qquad \text{(1-cycle)} \quad (3.5)$$

where *t* is the thickness of the solar cell. For two cycles, where the second cycle reflects at the internal front surface, the expression of the generation rate is

$$g_{total}(x) = g(x) + g(2t - x) + g(2t + x). \qquad \text{(2-cycles)} \quad (3.6)$$

For multiple internal cycling the total generation rate

$$g_{total}(x) = g(x) + g(2t - x) + g(2t + x) + g(4t - x). \quad \text{(3-cycles)} \quad (3.7)$$

In this work the model (3.7) is implemented initially for the total electron-hole generation rate since Sarkar did not show the results of the proposed expression [98]. In this expression, the reflected incident rays assumed to be vertical to the surface and parallel to ray of the first pass. This assumption solves the challenges of summation the photon cycles generation rate contribution to the main one of the first pass to have a total generation rate. Another assumption to keep this expression valid is to set the critical angle to zero to avoid the escaping of the light ray, and the distance between the rays (ε) tends to be zero. Nevertheless, these are non-practical assumptions which cannot be applied in fact, but these analyses are led to the novel modelling in next section. To understand the criteria of this modelling an example is given in figure 3.11.

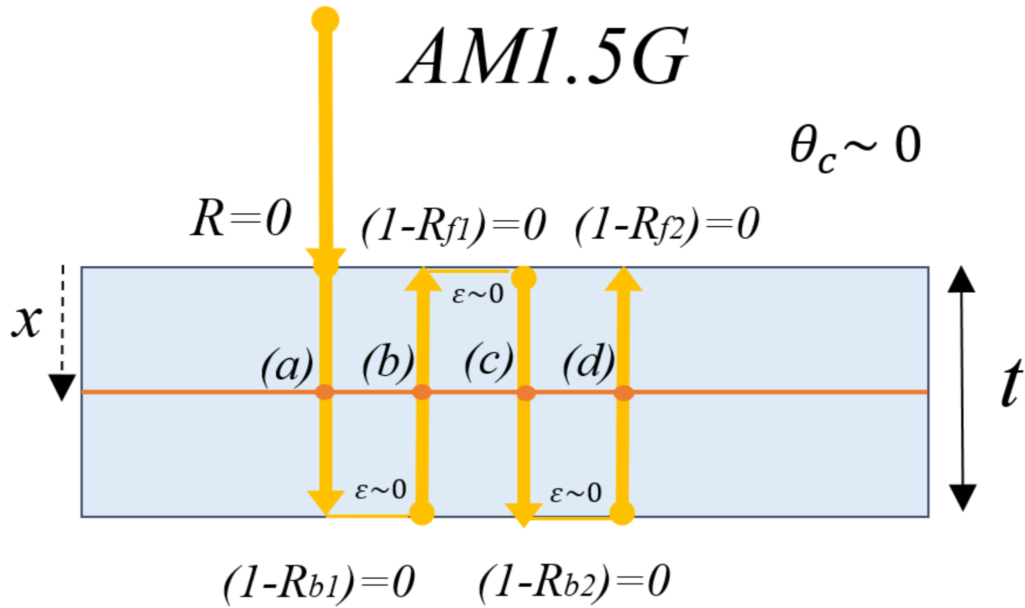

Figure 3.11 The design principle for the total generation rate of solar cells including the photon cycling effect where:
(a) generation rate of the first pass *g(x)*
(b) generation rate of the first cycle *g(2t - x)*
(c) generation rate of the second cycle *g(2t + x)*
(d) generation rate of the third cycle *g(4t - x)*.

At first, the loss of the light at front and back surface is presumed to be zero, but this assumption would be changed later. The result of this expression for a *50* μm silicon solar cell is shown in figure 3.8. An example of expression (3.7) is also given in figure 3.11 at depth *x=25* μm and *t=50* μm, so the expression could be rewritten to be,

$$g_{total}(25\mu m) = g(25\mu m) + g(75\mu m) + g(125\mu m) + g(175\mu m). \text{(3-cycles)} \quad (3.8)$$

The evaluation of the total generation rate based on the previous equation of Sarkar [98] requires extensive, time-consuming processes since the steps are repeated at each wavelength and for each *x* node. For instance, for silicon junction, to find the total generation rate at 25 μm including three photon cycles using equation (3.8), it requires 80 steps for each

term if $\Delta\lambda$ is considered to be 10 *nm*. As a result, it requires 320 steps to calculate the total generation rate at a certain depth with three cycles. Therefore, to calculate the total generation rate at ten different nodes of each pass, 3200 steps are involved. Thus, further simplifications are necessary to achieve reasonable time-consuming and steps for expression. The first modification is to set the position of the front surface to be zero always and the back surface to be 50 μm. The advantage of this adjustment to is to facilitate the process to establish a new approximation for the results. Subsequently, the expression (3.7) is adjusted to a new expression (3.9) and the pattern in figure 3.11 is changed to be as shown in figure 3.12.

$$g_{total}(x) = g(x) + g_{1st-cycle}(x) + g_{2nd-cycle}(x) + g_{3rd-cycle}(x). \text{(3-cycles)(3.9)}$$

The motivation of this alteration is to unify the term *x* in the brackets, thus, it becomes possible to create an approximation to calculate the total generation rate including all other cycles. For example, to compute the generation rate at depth $x=25\ \mu m$, the expression (3.9) is rewritten to be

$$g_{total}(25\mu m) = g(25\mu m) + g_{1st-cycle}(25\mu m)$$

(3-cycles) (3.10)

$$+g_{2nd-cycle}(25\mu m) + g_{3rd-cycle}(25\mu m).$$

The next step is to create an approximation for each term in expression (3.10) to avoid any time-consuming in the process of computing generation rate. Establishing new approximation of each term minimizes the number of steps to be four only at a particular depth. The purpose

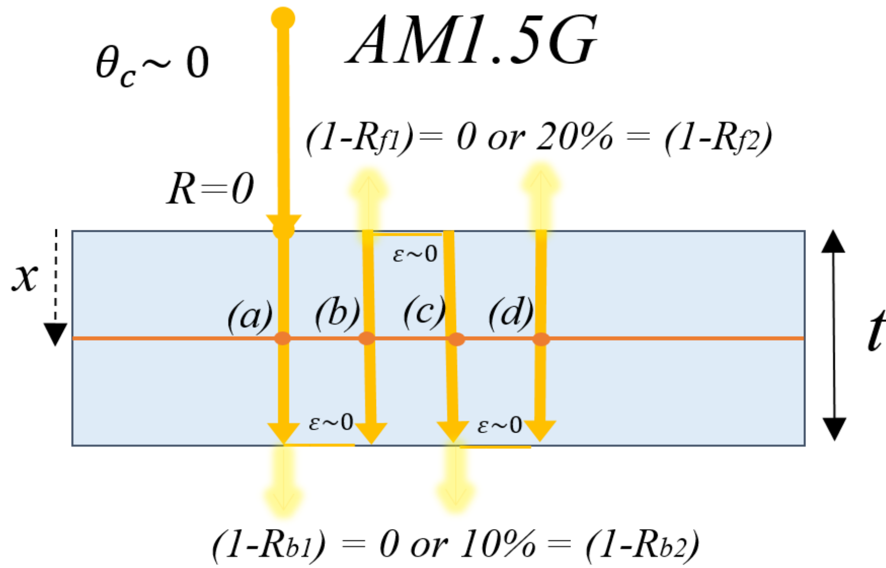

Figure 3.12 The modified pattern for the total generation rate of solar cells based on [98], including the photon cycling effect where:
(a) generation rate of the first pass *g(x)*
(b) generation rate of the first cycle $g_{1st-cycle}(x)$
(c) generation rate of the second cycle $g_{2nd-cycle}(x)$
(d) generation rate of the third cycle $g_{3rd-cycle}(x)$.

of creating an approximation for each term is to convey flexibility to the number of cycles in the expression. After that, an approximation for an overall $g_{total}(x)$ of expression (3.10) is created at the end of this section to reduce the number of steps to a single step. For the first pass, the schematic of the approximation is still considered the same as expression (3.4) and the coefficients are listed on table 3.5a or c. Since the decaying in the cycling generation rate is not extensive, a series of polynomial is used as a pattern for the approximation,

$$g_{m-cycle}(x) = \sum_{i=0}^{n} a_i x^i (\mu m) \quad \text{(m-cycles) (3.11)}$$

The coefficients of the new approximation of the first, second, third cycle are listed in table 3.5 for a *50 μm* silicon solar cell assuming no net light losses at back or front internal surface, or $(1\text{-}R_{b1,2})$=10% and $(1\text{-}R_{f1})$=20%. The results of these approximations show precise fitting comparing to the actual value of the cycling generation rate as shown in figure 3.13 for *R=0*. Finally, an approximation has been created using expression (3.4) which includes the first pass generation rate in addition to 3 cycles of generation rate. Initially the reflection and light losses set to zero, but then the external reflection set based on equation in (43), while $R_{b1,2}$ set to 90%, and R_{f1} fixes to 80%. The coefficients of this approximation are shown in table 3.6 for a for a *50 μm* silicon solar cell under AM1.5G.

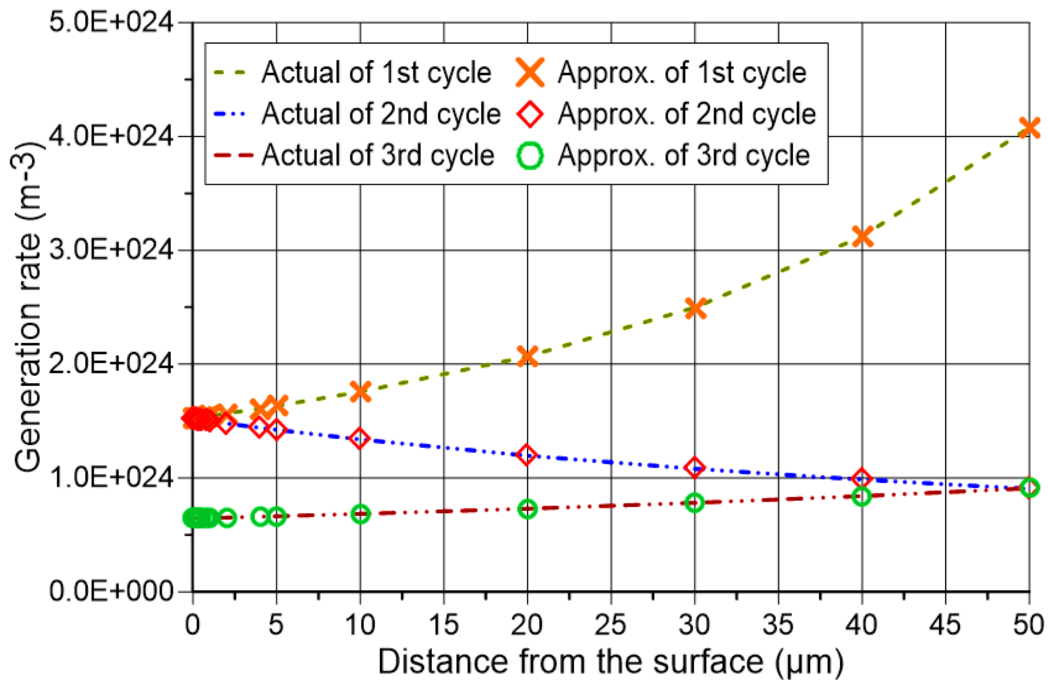

Figure 3.13 A comparison between the actual cycling carrier generation and the approximation cycling generation rate using (3.10) for a 50 *μm* Si junction assuming no light losses.

Table 3.5 Coefficients a_i and b_i for the silicon cycling carrier generation rate approximation of the 50 μm junction thickness under AM1.5G assuming no net light losses, 10% losses at back surface, and 20% losses at front surface, using model [98].

a) Generation rate of the first cycle [0, 50 μm]		
Percentage of light reflection	R_{b1}=100%	R_{b1}=90%
a_i	$\times 10^{20}$ m^{-3}	$\times 10^{20}$ m^{-3}
a_0	1.521×10^{4}	9.339×10^{3}
a_1	1.972×10^{2}	1.187×10^{2}
a_2	3.886	2.557
a_3	-4.473×10^{-2}	-3.278×10^{-2}
a_4	1.849×10^{-3}	1.175×10^{-3}
b) Generation rate of the second cycle [0, 50 μm]		
Percentage of light reflection	R_{f1}=100%	R_{f1}=80%
a_i	$\times 10^{20}$ m^{-3}	$\times 10^{20}$ m^{-3}
a_0	1.520×10^{4}	7.469×10^{3}
a_1	-2.026×10^{2}	-9.899×10^{1}
a_2	2.521	1.215
a_3	-2.464×10^{-2}	-1.158×10^{-2}
a_4	1.241×10^{-4}	5.671×10^{-5}
c) Generation rate of the third cycle [0, 50 μm]		
Percentage of light reflection	R_{b2}=100%	R_{b2}=100%
a_i	$\times 10^{20}$ m^{-3}	$\times 10^{20}$ m^{-3}
a_0	6.419×10^{3}	7.469×10^{3}
a_1	3.818×10^{1}	-9.905×10^{1}
a_2	2.163×10^{-1}	1.221
a_3	8.441×10^{-4}	1.175×10^{-2}
a_4	1.525×10^{-5}	5.825×10^{-5}

Table 3.6 Coefficients a_i and b_i for the silicon cycling carrier generation rate approximation of the 50 μm junction thickness under AM1.5G assuming no net light losses, 10% losses at back surface, and 20% losses at front surface, using model [98].

a) Generation rate of the first pass and all three cycles [0, 0.028 μm], R_{ext}=0%.			
Percentage of light reflection	$R_{b1,2}$=100%, R_{f1}=100%		
a_i	$\times 10^{27}$ m^{-3}	b_i	
a_0	1.702	b_0	1
a_1	5.879	b_1	1
b) Generation rate of the second cycle (0.028, 50 μm], R_{ext}=0%.			
Percentage of light reflection	$R_{b1,2}$=0%, R_{f1}=100%		
a_i	$\times 10^{27}$ m^{-3}	b_i	
a_0	5.185×10^{-2}	b_0	0
a_1	1.002	b_1	1
a_2	6.513	b_2	86.459
a_3	$1.559\times10^{1} * x\ \mu m$	b_3	17.891
a_4	$2.781\times10^{-1} * x^2 \mu m$	b_4	1
a_5	$-1.031\times10^{-3} * x\ \mu m$	b_5	0
a_6	$-3.983\times10^{-1} * x\ \mu m$	b_6	1
c) Generation rate of the first pass and all three cycles [0, 50 μm], R_{ext}= eq (43).			
Percentage of light reflection	$R_{b1,2}$=100%, R_{f1}=100%		
a_i	$\times 10^{27}$ m^{-3}	b_i	
a_0	1.611×10^{-2}	b_0	0
a_1	2.904	b_1	28.352
a_2	4.215×10^{-1}	b_2	1.386
a_3	1.522×10^{-1}	b_3	0.235
a_4	$2.202\times10^{-4} * x\ \mu m$	b_4	0

d) Generation rate of the first pass and all three cycles [0, 50 μm], R_{ext}= eq (43)			
Percentage of light losses	$R_{b1,2}$=90%, R_{f1}=80%		
a_i	$\times 10^{27}$ m^{-3}	b_i	
a_0	3.279×10^{-2}	b_0	0
a_1	$1.433\times 10^{-5} * x^2\ \mu m$	b_1	0
a_2	3.461	b_2	18.855
a_3	$1.728 * x\ \mu m$	b_3	1
a_4	$2.547\times 10^{-1} * x^3\ \mu m$	b_4	1
a_5	$-1.249\times 10^{-3} * x\ \mu m$	b_5	0
a_6	$-1.413 * x^2\ \mu m$	b_6	1

Eventually, although the previous analytics demonstrate appropriate outcomes, the scheme of the solar cells design stands on non-practical assumptions. The first assumption states that the ray reflects on the mirror of the back surface vertically, while the second assumption is to consider a zero critical angle with high optical confinement. While these assumptions are not valid in real-world manufacturers, but this concatenation led to expand the examination to figure out a valid pattern. Thus, further analyses based on practical artchitectures are investigated to obtain accurate data. In next section, a novel model for carrier generation rate including photon cycling effect is introduced.

3.5 A Novel Modelling of Carrier Generation Rate Including Photon Cycling Effect

In this section, a novel modelling for carrier generation rate includes the photon cycling effect which can be applied for all semiconductor materials is introduced. It has been demonstrated that expression (3.7) is no longer valid in practical designs of solar cells. Furthermore, as best

of my knowledge, there is no a clear analytical expression to dddetrmine the carrier generation rate, accounting the photon cycling effect. However, some software programs use numerical models to calculate the photon cycling generation rate by some different schemes such as ray tracing. Therefore, establishing a general expression to determine the exact generation rate including the photon cycling effect is necessary.

The Scheme of the expression is based on highly reflecting surface at the back and front interfaces to apply the photon cycling effect. Employing simple texturing, mirror Lambertian reflector, or Brag reflector effectively increase the light path length in the cell. In addition, since the reflection at the front surface is high for the air-semiconductors interface, adopting anti-reflection coating (ARC) is important to reduce the reflectivity. The ARC is usually a thin film layer of a dielectric material with a refractive index (n) which injects between two mediums to reduce the reflectivity. To minimize the reflection close to zero, the refractive index of the ARC (n_1) has to be

$$n_1 = \sqrt{n_o n_s}, \tag{3.12}$$

where n_o is the refractive index of the air and n_s is for the semiconductor. Moreover, improving the reflectivity can be achieved by applying more than one layer of ARC at the interface. For silicon, the external reflectivity of the front surface reaches to 30% without using any intermediate medium between silicon and air. Material such as silicon nitride (SiN, n=1.97), tantalum oxide (Ti_2O_5, n=2.10), and Indium Tin Oxide (ITO, n=1.92) are used as ARC for silicon solar cells where the ideal n of silicon ARC should be around 1.84. The central principle of the ARC is to reduce the alterations of the refractive index between two mediums at the

interface. The approach which is selected for this work is to apply ARC for the front surface to minimize the reflection, and texturing the back surface, assuming perfect reflectivity, to increase the incident ray path length in the cell as shown in figure 3.14. The thickness of the texturing of the back surface is considered to be too small comparing to the total thickness of the junction.

To understand the mechanism of light reflecting in figure 3.14, some necessary geometry analysis is required. First of all, the generation rate is computed regards to multiple nodes based on the depth of the cell (*x*), in addition to, considering the exact length of the ray at each reflection. For the first pass, the generation rate is readily determined using the regular process if the light penetrates the cell vertically ($\theta_o = 0$),

$$\mathrm{g}(x) = g\left(\frac{x}{cos\ \theta_o}\right), \tag{3.13}$$

and

$$t_o = \frac{t}{cos\ \theta_o}. \tag{3.14}$$

where *t* is the thickness of the cell. Whereas for the reflecting ray (cycles ray) the length of the light path depends on the reflection angle (θ_n). For the first cycle, determining the generation rate at specific depth *x* requires to find out the length of the reflected ray at the same *x* point, vector (*a*) in figure 3.14 which equals to

$$a = \frac{t - x}{\cos\theta_1}, \tag{3.15}$$

$$t_1 = \frac{t}{\cos\theta_1} \tag{3.16}$$

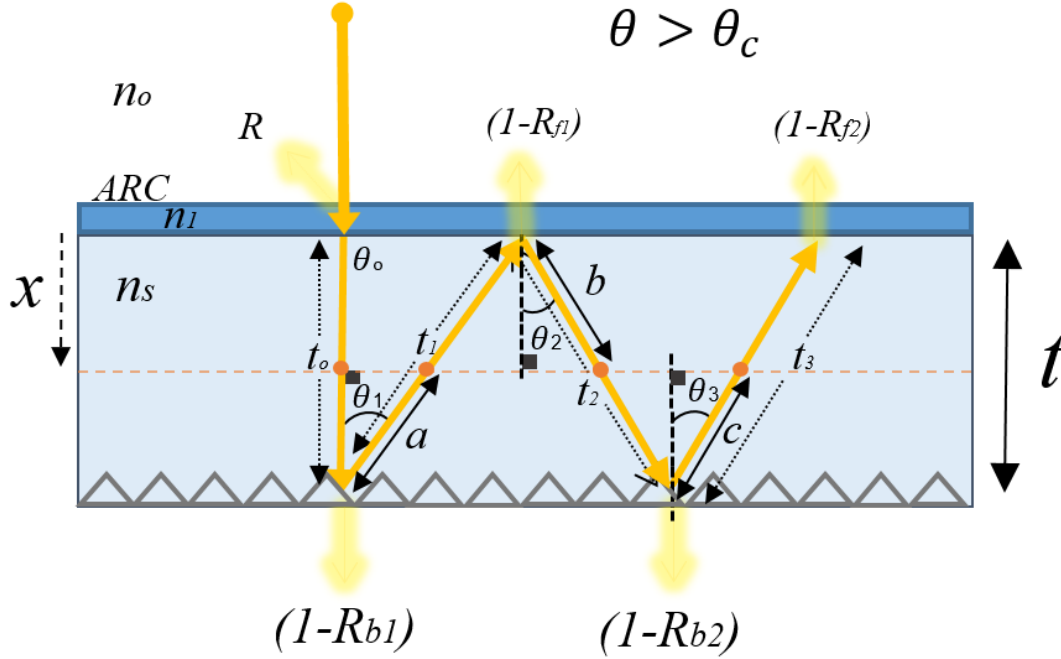

Figure 3.14 The final approach of the solar cell design which is selected to determine the total carrier generation rate including the photon cycling effect.

Therefore, the generation rate of the first cycle at depth x is

$$g_{1st-cycle}(x) = g(t_o + a) = g\left(\frac{t}{\cos\theta_o} + \frac{t-x}{\cos\theta_1}\right), \tag{3.17}$$

This equation is precisely applied to each node (x) of the first cycle. For the second cycle, this equation does not work since the length of the first cycle (t_1) is not equal to the length of first pass (t). Furthermore, since the ray reflects at the front surface, the length of b is

$$b = \frac{x}{\cos\theta_2}, \tag{3.18}$$

$$t_2 = \frac{t}{\cos\theta_1}, \tag{3.19}$$

and the carrier generation rate is equal to,

$$g_{2nd-cycle}(x) = g(t_o + t_1 + b) = g\left(\frac{t}{cos\ \theta_o} + \frac{t}{\cos\theta_1} + \frac{x}{\cos\theta_2}\right). \tag{3.20}$$

In the same context, the generation rate of the third cycle is

$$g_{3rd-cycle}(x) = g(t_o + t_1 + t_2 + c) = g\left(\frac{t}{cos\ \theta_o} + \frac{t}{\cos\theta_1} + \frac{t}{\cos\theta_2} + \frac{t-x}{\cos\theta_3}\right). \tag{3.21}$$

To combine all photon cycling equations in one general formula, it is necessary to differentiate between the ray cycle which reflects at the front surface or the back surface accounting the light losses,

$$g_{\ 3cycles}(x) = (1-R)\ (g_o(x) + (R_{b1})\ g_{1st-cycle}(x) + (R_{b1})(R_{f1})\ g_{2nd-cycle}(x)$$
$$+ (R_{b1})(R_{f1})(R_{b2})\ g_{3rd-cycle}(x)) \tag{3.22}$$

where $g_o(x)$ is the generation rate of the first pass, then

$$g_{total}(x) = (1-R)\begin{cases} g\left(\frac{x}{\cos\theta_o}\right), & first-pass \\ R_{fbn}\ g\left(\frac{t-x}{\cos\theta_n} + \sum_{i=0}^{n-1} t_i\right), & back\ surface\ cycles \\ R_{fbn}\ g\left(\frac{x}{\cos\theta_n} + \sum_{i=0}^{n-1} t_i\right), & front\ surface\ cycles \end{cases} \tag{3.23}$$

where n is the rank of the cycle, and

$$t_i = \frac{t}{\cos\theta_i}. \tag{3.24}$$

The R_{fb} is the total light of internal reflection is,

$$R_{fbn} = \begin{cases} (R_{b1}), & for\ the\ 1st\ cycle \\ (R_{b1})(R_{f1}), & for\ the\ 2nd\ cycle \\ (R_{b1})(R_{f1})(R_{b2}), & for\ the\ 3rd\ cycle \end{cases} \tag{3.25}$$

This model can be applied perfectly to any semiconductor materials of solar cells to extract the exact generation rate including reflecting effect. Moreover, it could work for any solar cells design patterns whether texturing, ARC, mirror, or specific reflector are injected at the back or front surface. The only condition that should be applied is to manipulate the reflection angle to be $-\frac{\pi}{2} < \theta_i < \frac{\pi}{2},\ where\ |\theta_i| > \theta_c$ while assuming all reflection occur at front or back surfaces only. . From here on, this model is considered as a standard model to determine the exact carrier generation rate including photon cycles effect.

For example, to calculate the total generation rate at depth 25 μm of a 50 μm junction, including three photon cycles and taking into account the exact length of the ray at $\theta_o = 0\,^{\circ} and\ \theta_{1,2,3} = 30\,^{\circ}$,

$$g_{total}(25\ \mu m) = g(25\ \mu m) + g_{1st-cycle}(25\ \mu m) + g_{2nd-cycle}(25\ \mu m) + g_{3rd-cycle}(25\ \mu m) \quad (3.26)$$

where,

$$g_{1st-cycle}(25\ \mu m) = g\left(\frac{50\mu m}{\cos 0°} + \frac{25\mu m}{\cos 30°}\right) = g\ (78.88\ \mu m) \quad (3.27)$$

$$g_{2nd-cycle}(25\ \mu m) = g\left(\frac{50\mu m}{\cos 0°} + \frac{50\mu m}{\cos 30°} + \frac{25\mu m}{\cos 30°}\right) = g\ (136.60\ \mu m) \quad (3.28)$$

$$g_{3rd-cycle}(25\ \mu m) = g\left(\frac{50\mu m}{\cos 0°} + \frac{50\mu m}{\cos 30°} + \frac{50\mu m}{\cos 30°} + \frac{25\mu m}{\cos 30°}\right) = g\ (194.34\ \mu m) \quad (3.29)$$

thus,

$$g_{total}(25\ \mu m) = g(25\ \mu m) + g(78.88\ \mu m) + g(136.60\ \mu m) + g(194.34\ \mu m). \quad (3.30)$$

Applying the same process for other various depth points as shown in figure 3.15 leads to obtain the entire spectrum of the generation rate of the junction (assuming all *R*=0) which is

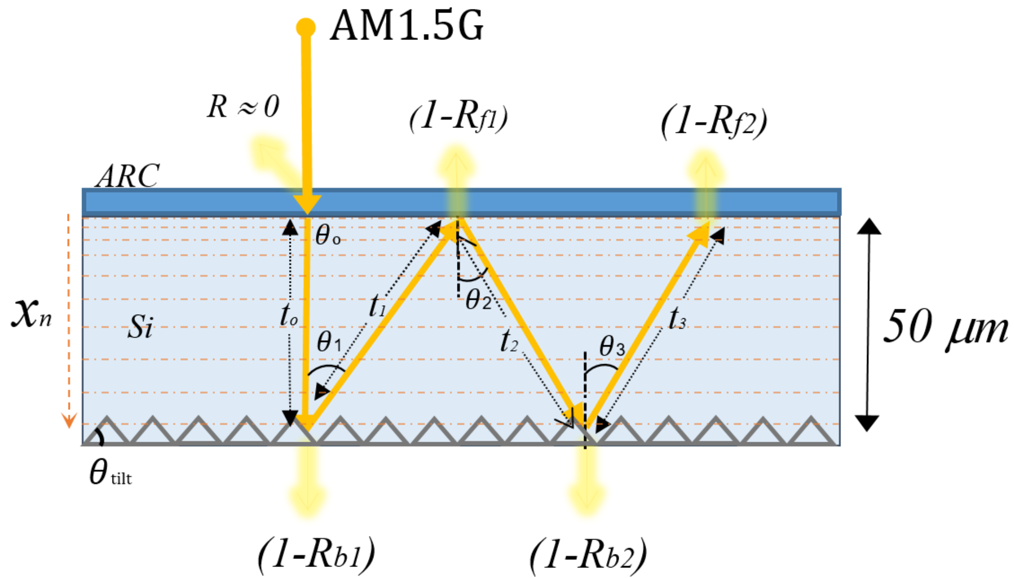

Figure 3.15 An example for the final approach of the solar cell design which is selected to determine the total carrier generation rate including the photon cycling effect, assuming all *R=0%.*

presented in figure 3.16. It is important to minimize the segment of the depth (x) near to the front surface due to the exponentially decaying of the generation rate. The θ_{tilt} of the texturing at the back surface should be greater than $(\frac{1}{2}\theta_c)$ to allow the incident ray to be reflected at an angle greater than θ_c. Furthermore, when the positive and negative tilt angle are equal, the incident ray reflects three time across the cell. The overall path length of the reflected ray depends on the size and the tilt angle of the texture which is considered neglecting here.

Comparing the current model to the previous one [98] for the cycling generation rate reveals the imprecision of the latter model with error reaches to 20% for the previous example. The percentage of the error increases for a wider angle and as the rank of the cycle increases. However, for the total generation rate, including three photon cycles, Sarkar's model [98] shows a good agreement with less than 5% for the same example as shown in figure 3.16. The reason for this congruence is the similarity of the first-pass path which contributes the most for

the junction. Using different first-pass path and manipulating θ_o leads to increase the distinction between the models. Assuming $\theta_{1,2,3} = 30\,°$, a comparison of photocarrier cycling generation rate between the two models are shown in figure 3.17, 3.18 and 3.19 for the first, second and third cycle, respectively.

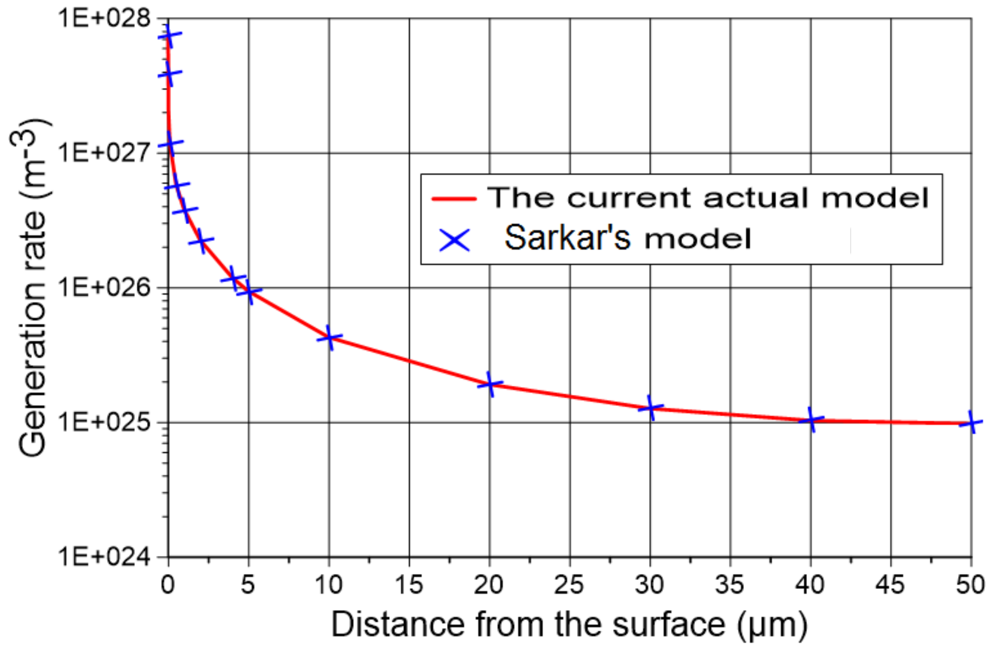

Figure 3.16 The outcome of the current actual model for the carrier generation rate, including three photon cycles and comparing the results with the previous model [98].

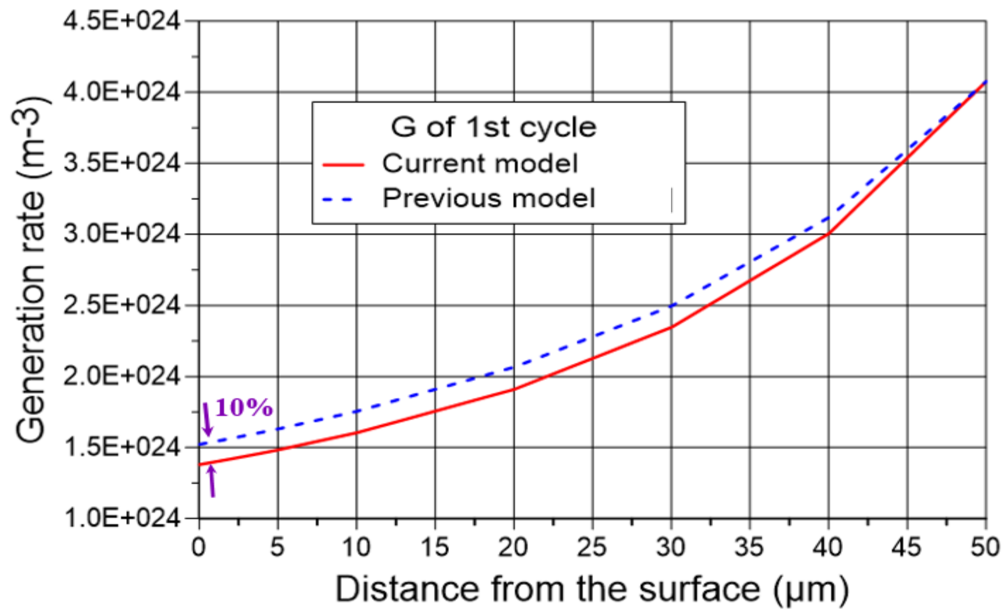

Figure 3.17 A comparison between the current model and Sarkar's model [98] for the generation rate of the first cycle.

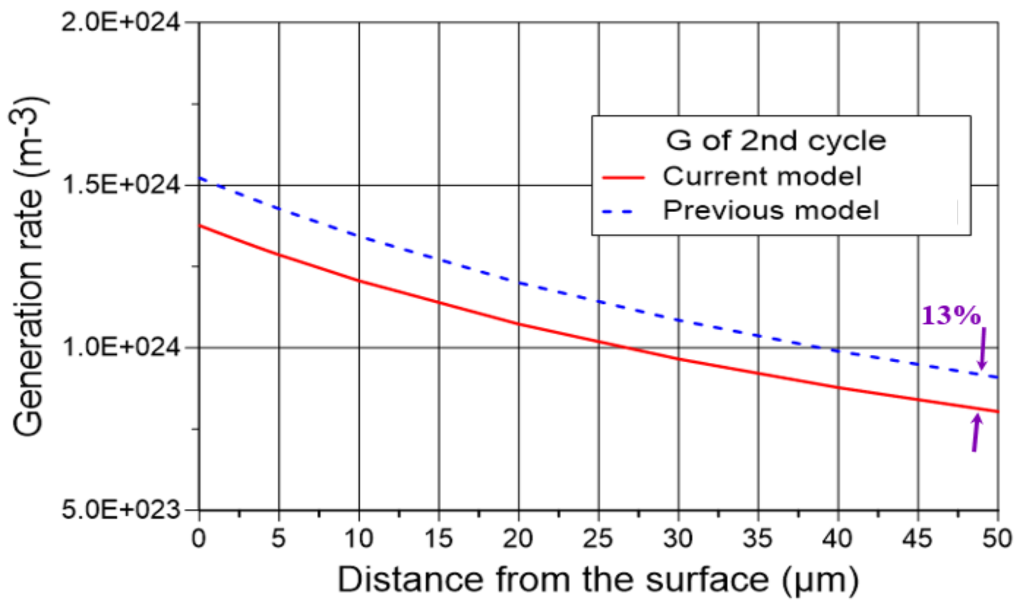

Figure 3.18 A comparison between the current model and Sarkar's model [98] for the generation rate of the second cycle

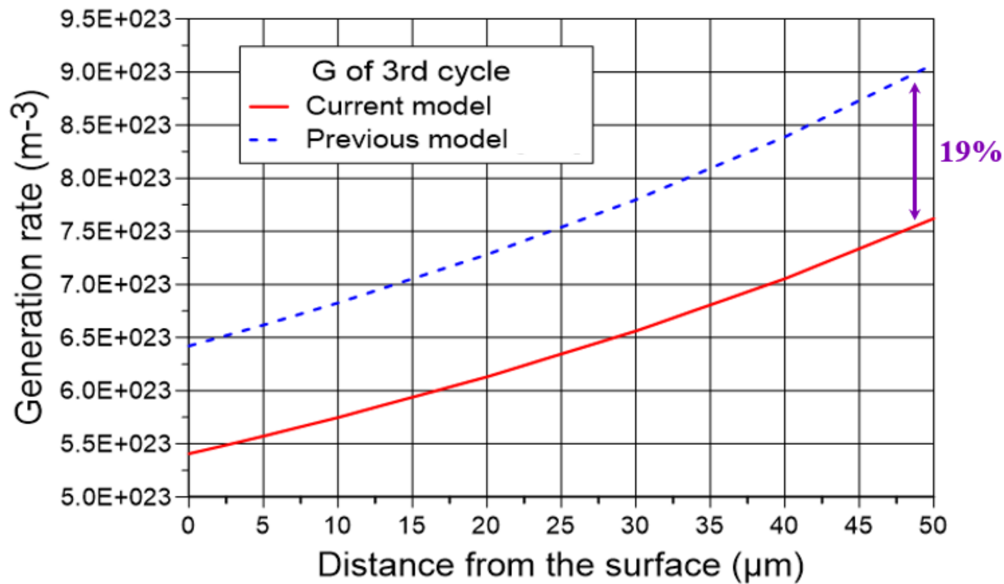

Figure 3.19 A comparison between the current model and Sarkar's model [98] for the generation rate of the third cycle

The contribution of the photon cycling generation rate to the total carrier generation rate depends on the thickness of the junction in addition to the light losses and the reflection angle of the incident ray. Photon cycling generation rate inversely proportional to the thickness of the junction. Therefore, the effect of photon recycling is remarkably significant and should be considered in thin film solar cells. Figure 3.20 shows the contribution percentage of the cycling generation rate for the previous example comparing to the total generation rate based on the number of the cycle. It shows that the contribution of the cycle generation rate is high near to the back surface comparing to the front surface. The reason for this is that the solar cell attains the highest generation rate near to the front surface which is normally two to three magnitude larger than the bottom generation rate. Therefore, the photon cycling generation rate, in general, enhance the carrier densities near to the bottom of the junction for bulk solar cells. Also, it demonstrates that the contribution of the cycle generation rate tends to be

insignificant after two or three cycles for the 50 μm silicon junction. Typically, increasing the angle of the internal reflection enhances the length of the light path. However, increasing the light path leads to more attenuation to the ray before reaching to the certain depth where the generation rate is calculated. Thereby, increasing the light path is not recommended for this model, while tightening the internal reflection angle leads to enhancing the magnitude of the cycle generation rate. Thus, the photon cycling generation rate reaches the maximum when the incident ray reflects at the critical angle θ_c. The effect of the internal reflection angle is showing in figure 3.21 by changing $\theta_{1,2,3}$ of the cycle rays.

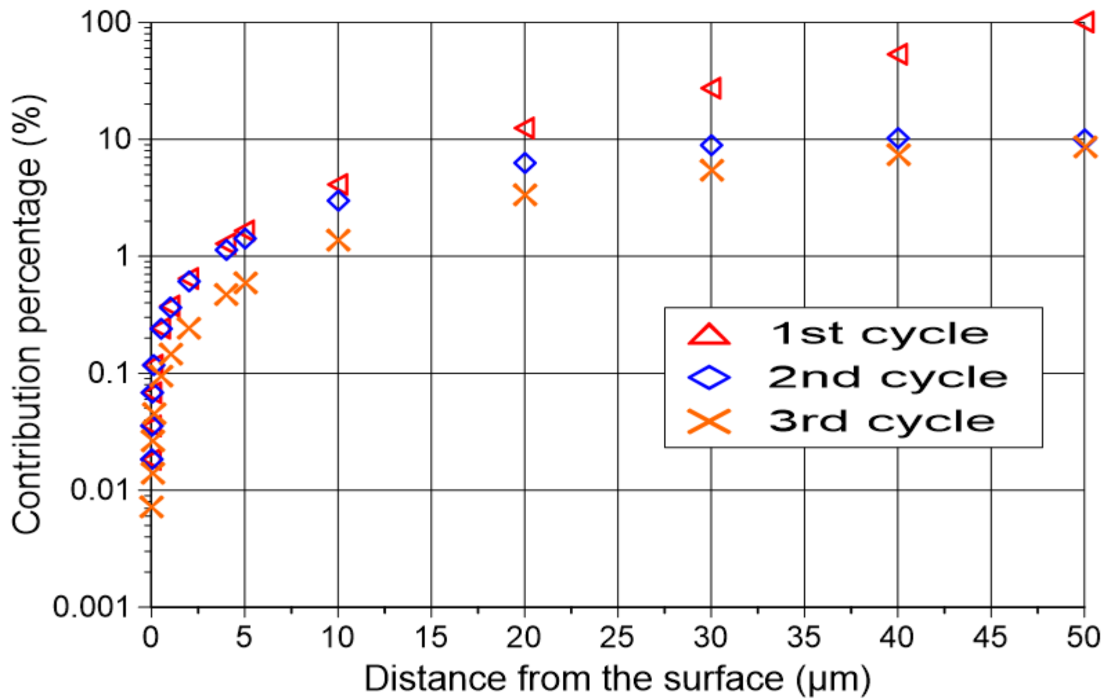

Figure 3.20 The contribution percentage of the photon cycling generation rate to the total generation rate based on the number of the cycle for $\theta_o = 0^\circ and\ \theta_{1,2,3} = 30^\circ$.

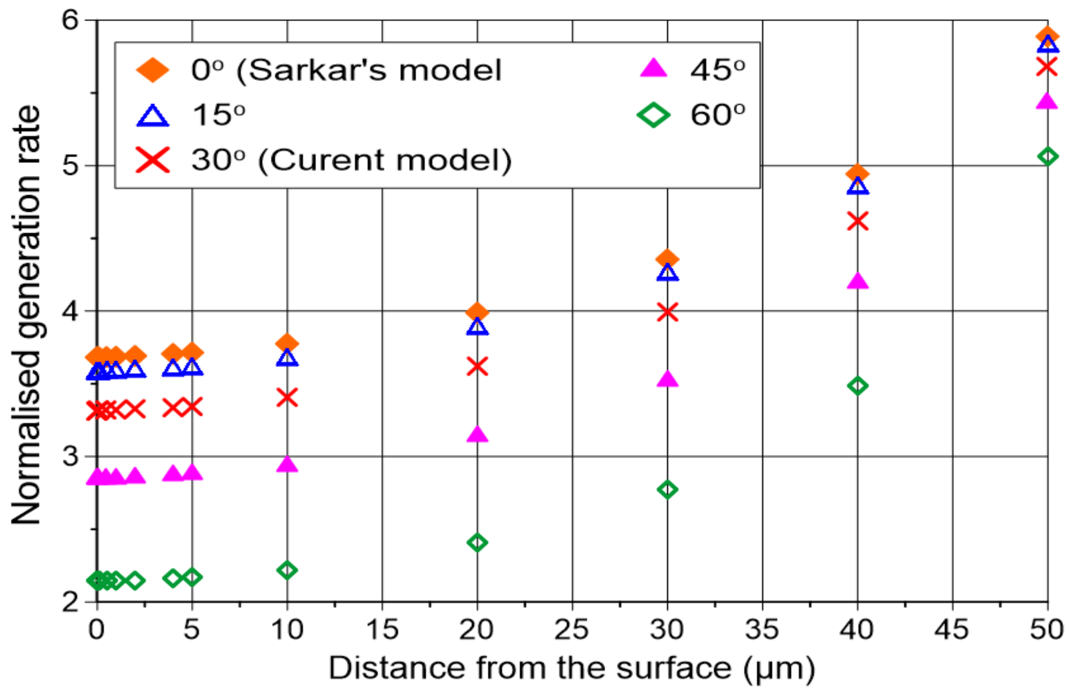

Figure 3.21 The effect of the reflection angle on the generation rate of the cycle incident rays.

After investigating the effect of the reflecting angle on the generation rate of solar cells, it is essential to examine the effect of junction thickness on the photon cycling generation rate. It is evident that decreasing the thickness of the junction improves the rate of generating carriers of the cycle rays, but choosing the optimum thickness necessitates further analysis. Moreover, it is clear that minimizing solar cells thickness is associated with reducing the cost of manufacturing and increasing the efficiency of the collection probability. However, reducing the thickness is also associated with some undesirable issues such as increasing the series resistance. Figure 3.22 and figure 3.23 demonstrate the effect of altering the thickness on the carrier generation rate. In figure 3.22, it shows the total generation rate up to 30 μm for different junction thicknesses, while figure 3.23 shows the effect of the thickness parameter

on the photon cycling generation rate only. The reduction of generation rate due to increasing the thickness of the junction is attributed to the attenuating of the photon flux inside the cell. Therefore, minimizing the thickness of the junction enhances the effect of the generation rate which is resulted from the photon cycling effect.

The criteria which has been implemented to calculate the generation rate is to assume the solar cell is exposed to unpolarised light and each photon is responsible to create one electron-hole pair only. Therefore, the multi-photon transition is not considered here since it has much smaller probability. Moreover, the photon recycling effect is not yet considered as it is found to be neglected when the radiative recombination is not dominated [90]. After showing the validity of the current model, it is important to generate an approximation to simplify and minimize the steps and time-consuming of the calculation.

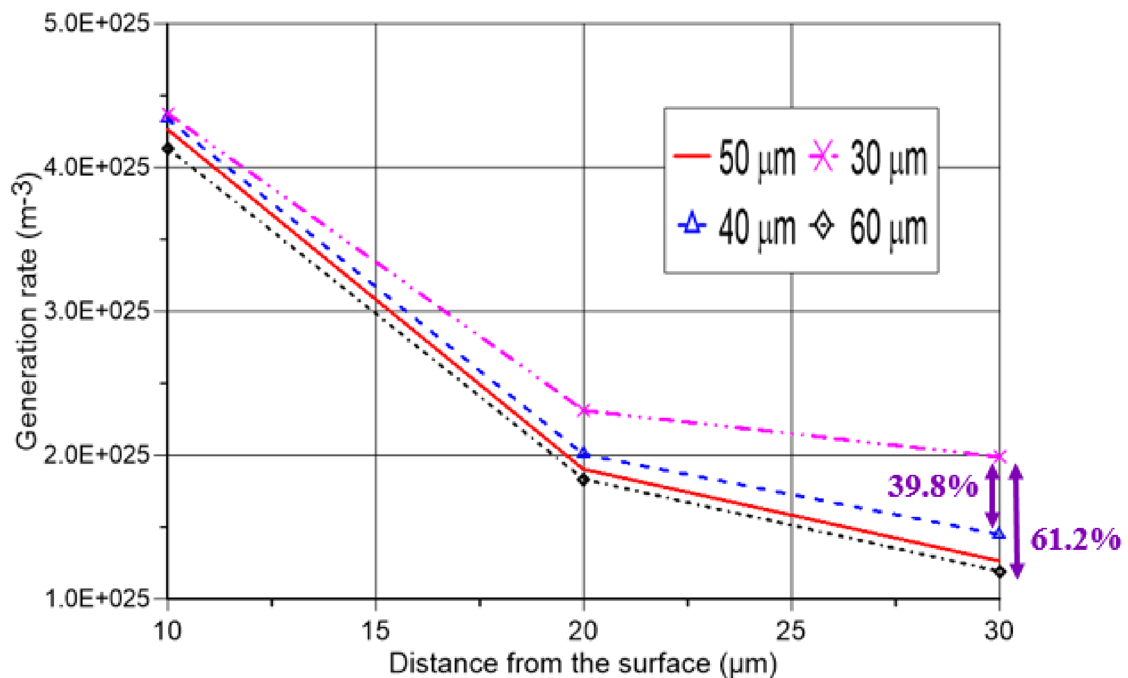

Figure 3.22 The effect of thickness on the total generation rate of a solar cell. The generation rate is showed up to 30 μm.

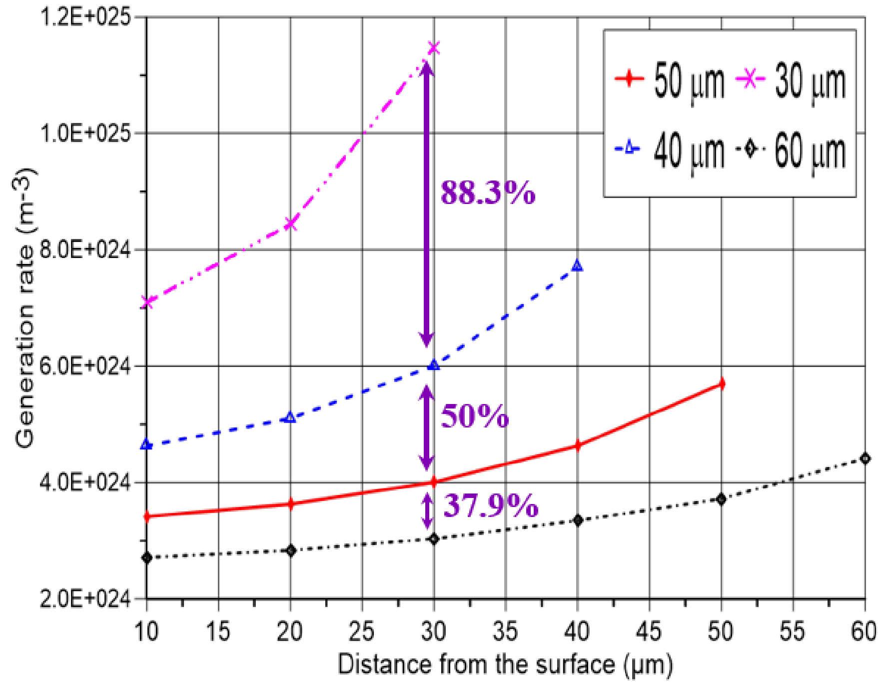

Figure 3.23 The effect of thickness on the generation rate of the cycle rays only.

The approximation (3.4) of the first pass generation rate is still valid here for the 50 µm junction since $\theta_o = 0\,°$. While the approximation of the photon cycling generation rate in appendix B is no longer valid due to the differences in $\theta_{1,2,3}$. Hence, establishing new approximations for the cycling generation rate, taking into account the impact of the reflection angle, is required. The model (3.11) is still considered for the approximation since it shows high fitting to the actual data of the cycling generation rate. The approximations have been established for different reflection angles $\theta_{1,2,3}$ and three cycle rays, assuming initially zero light losses at the front or back surfaces for a 50 µm silicon intrinsic junction. The coefficients of the approximation are listed in table 3.7 at $\theta_{1,2,3} = 15°, 30°, 45°, and\ 60°$. The approximations provide high accurate results comparing to the actual one with error less than 1% along the different depth points. The reason for creating approximations at different

reflection angle is to provide flexibility to the expression. The results of the approximation comparing to the actual generation rate of the of the photon cycling are shown in figure 3.24, 3.25, and 3.26 based on the cycle rank for different reflection angle. Considering the external reflections at the front surface tend to be zero, constituting simplicity in the evaluation of the light losses in the cycling generation rate when the internal light losses are uniform for the whole range of the wavelength. Hence, the approximation equation becomes

$$g_{n-cycle}(x) = R_{fbn} \sum_{i=0}^{n} a_i x^i (\mu m) \tag{3.31}$$

where n is the rank of the cycle and R_{fbn} is found by computing or assuming $R_{b1,2}$ and R_{f1} in equation model (3.23). According to the external reflectance *R*, to simplify its impact in the computing of the generation rate, a comparison between the generation rate with and without R for air-silicon interface is led to

$$R \approx \begin{cases} 0.525, & x \leq 0.028 \\ 0.343, & x > 0.028. \end{cases} \tag{3.32}$$

Further investigation is required to analytically study and simplify the effect of reflection in photocarrier generation rate calculation.

Establishing new approximations to calculate the carrier generation rate of solar cells including the photon cycling effect minimizes the stages and the time-consuming of the calculations. Furthermore, these simple approximation demonstrates high fitting comparing to the actual data of the generation rate. Although the approximations which have been developed are only restricted to the exact parameters assumption, the new model (3.23) is flexible and can be fitted to compute the generation rate of any semiconductor materials.

Table 3.7 Coefficients a_i for the silicon cycling carrier generation rate approximations for a 50 μm Si junction thickness under AM1.5G assuming no net light losses at the front surface or back surface, using the new model. The approximation form is $g_{n-cycle}(x) = \sum_{i=0}^{n} a_i x^i (\mu m)$.

a) Generation rate of the first cycle [0, 50 μm]				
angle	15°	30°	45°	60°
$a_0 \times 10^{24}$ m^{-3}	1.486	1.378	1.189	0.907
$a_1 \times 10^{22}$ m^{-3}	1.949	1.917	1.704	1.445
$a_2 \times 10^{20}$ m^{-3}	3.906	2.996	3.731	3.151
$a_3 \times 10^{18}$ m^{-3}	4.758	2.409	0	0
$a_4 \times 10^{17}$ m^{-3}	1.9717	0	0	0
$a_5 \times 10^{15}$ m^{-3}	0	2.202	3.521	5.303
b) Generation rate of the second cycle [0, 50 μm]				
angle	15°	30°	45°	60°
$a_0 \times 10^{24}$ m^{-3}	1.485	1.378	1.189	0.907
$a_1 \times 10^{22}$ m^{-3}	2.005	1.932	1.772	1.471
$a_2 \times 10^{20}$ m^{-3}	2.527	2.538	2.468	2.186
$a_3 \times 10^{18}$ m^{-3}	2.499	2.608	2.676	2.525
$a_4 \times 10^{16}$ m^{-3}	1.271	1.360	1.447	1.431
c) Generation rate of the third cycle [0, 50 μm]				
angle	15°	30°	45°	60°
$a_0 \times 10^{23}$ m^{-3}	6.223	5.409	4.468	3.267
$a_1 \times 10^{21}$ m^{-3}	3.713	3.25	3.000	2.296
$a_2 \times 10^{19}$ m^{-3}	2.361	1.774	1.959	1.597
$a_3 \times 10^{16}$ m^{-3}	0	6.762	0	0
$a_4 \times 10^{15}$ m^{-3}	2.355	1.161	2.0225	1.685

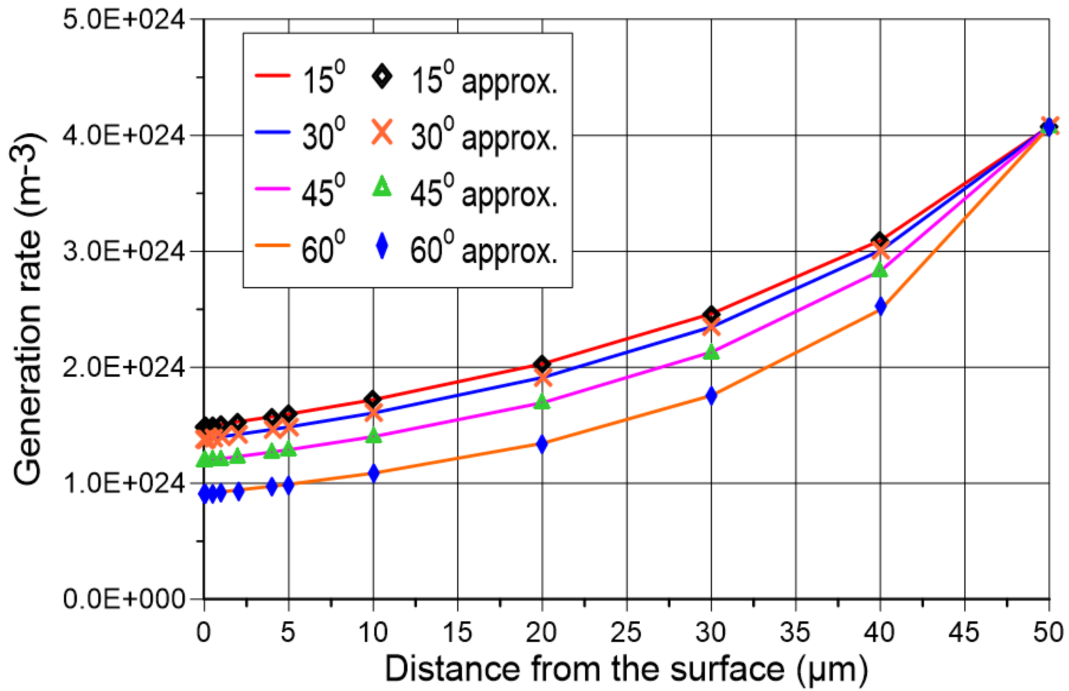

Figure 3.24 The actual data of the first cycle generation rate comparing to the results of the approximation using equation (3.31).

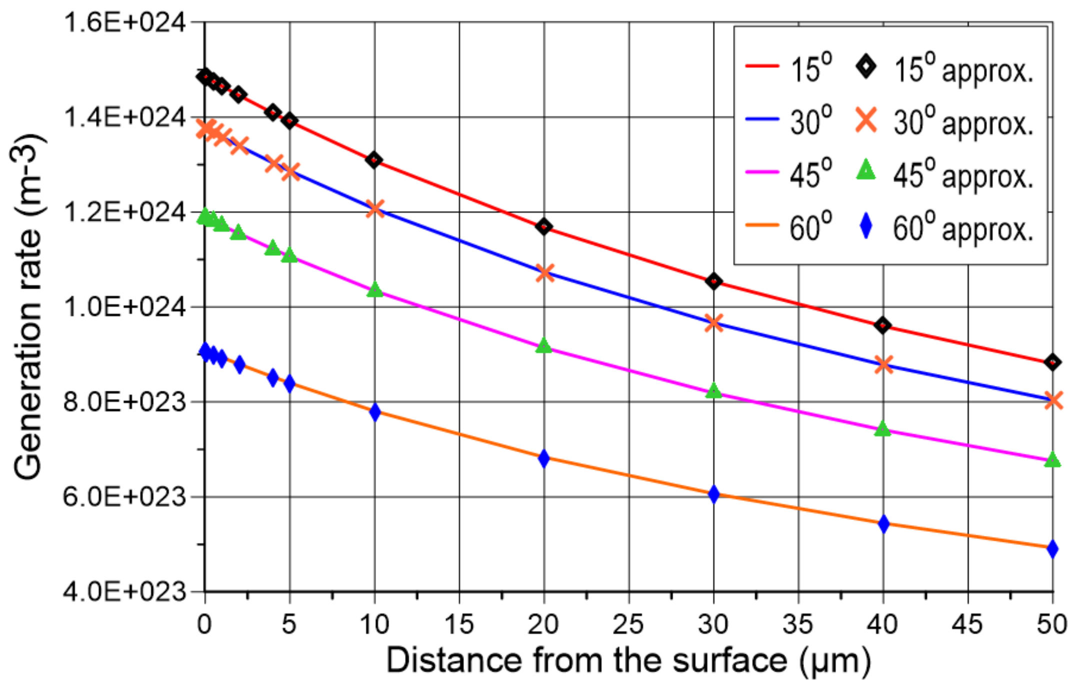

Figure 3.25 The actual data of the second cycle generation rate comparing to the results of the approximation using equation (3.31).

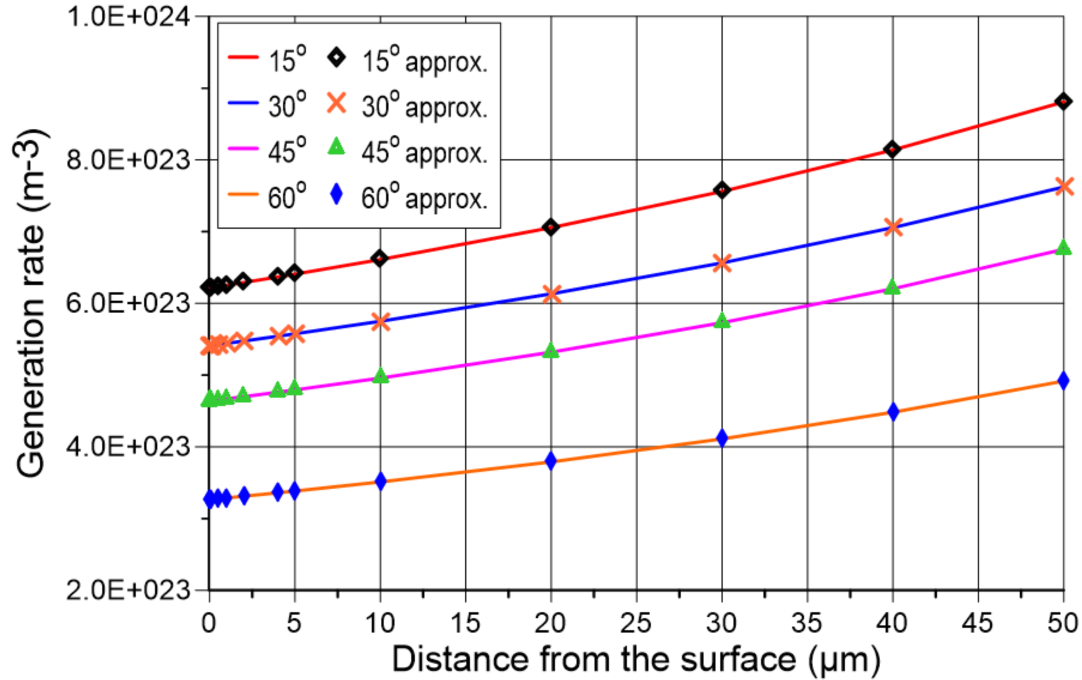

Figure 3.26 The actual data of the third cycle generation rate comparing to the results of the approximation using equation (3.31).

The previous approximations are proposed to calculate the carrier generation rate of silicon solar cell where the photon cycling and the doping effects are assumed to be omitted [90]. Therefore, the photon recycling and the doping effect were not considered in the calculation. In the next sections, the photon cycling effect is evaluated for GaAs solar cells where the radiative recombination is dominated. In addition, the luminescent coupling for the multi-junction solar cell is computed. Finally, the results of the generation rate including the photon cycling, photon recycling, luminescent coupling effect are combined in comprehensive approximations.

3.6 The Effect of Doping Concentration on Carriers Generation Rate

The effect of introducing different impurities to the silicon absorption coefficient have been examined by Jellison *et al.* [57]. The impact is being noticed by increasing the magnitude of the dopant concentration especially when approaching the degenerated level where ($n > N_c$) or ($p > N_v$) and the Fermi-Dirac statistics has to be considered. In heavy doping, the impurities atoms become closer to each other and interact with the conduction or valance band of the substance. Hence, the band structure of the material starts altering to form a narrow energy band and slightly shifts the bandgap energy down. Increasing the dopant concentration increases the narrowing of the band gap until reaching to the tunnelling effect where the Fermi level is shifted above the conduction band (n-type) or below the valance band (p-type). In silicon, at high dopant concentration, direct transitions of electrons are possible which in result increases the carrier generation rate of the junction. Moreover, increasing the dopant level to some limits improves the mobility of the carriers which enhances the conductivity of the junction and reduces the resistivity. However, increasing the dopant level is associated with some drawbacks such as increasing the recombination rate and forming inconsistency of the structures.

Jellison *et al.* [57] illustrate the impact of doping on the silicon absorption coefficient in equation (2.40). It shows that the absorbance of semiconductors is enhanced by increasing the dopant concentration. Indeed, increasing the dopant level improves the free carrier absorption. In this work, the Jellison *et al.* model [57] is adopted to show the effect of doping concentration on the silicon generation rate. Before illustrating the doping effect on the generation rate, it should be stated that increasing the absorption is not always improve the

generation rate. In fact, improving the absorption coefficient may enhance or degrade the generation rate based on the junction depth. Figure 3.27 shows the effect of increasing the absorption coefficient on the generation rate of semiconductor junction based on at different depths. The results of applying Jellison *et al.* [57] model for n-type silicon absorption coefficient at various GaAs doping level is shown in figure 3.28.

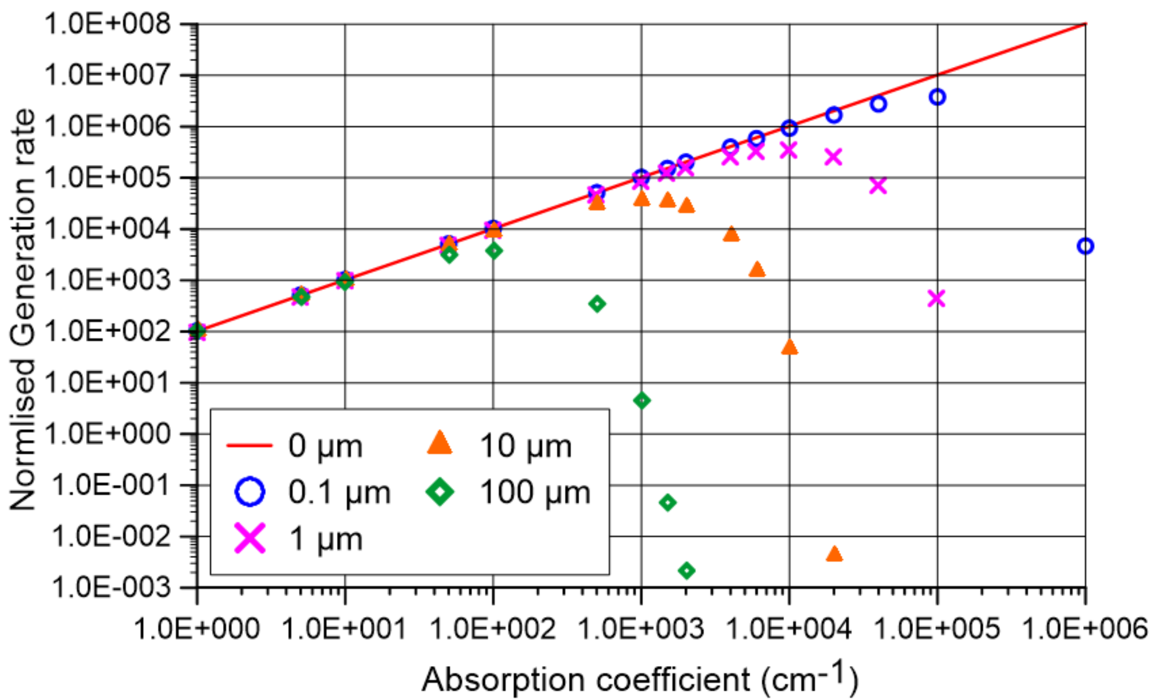

Figure 3.27 The effect of increasing the absorption coefficient on the normalized generation rate.

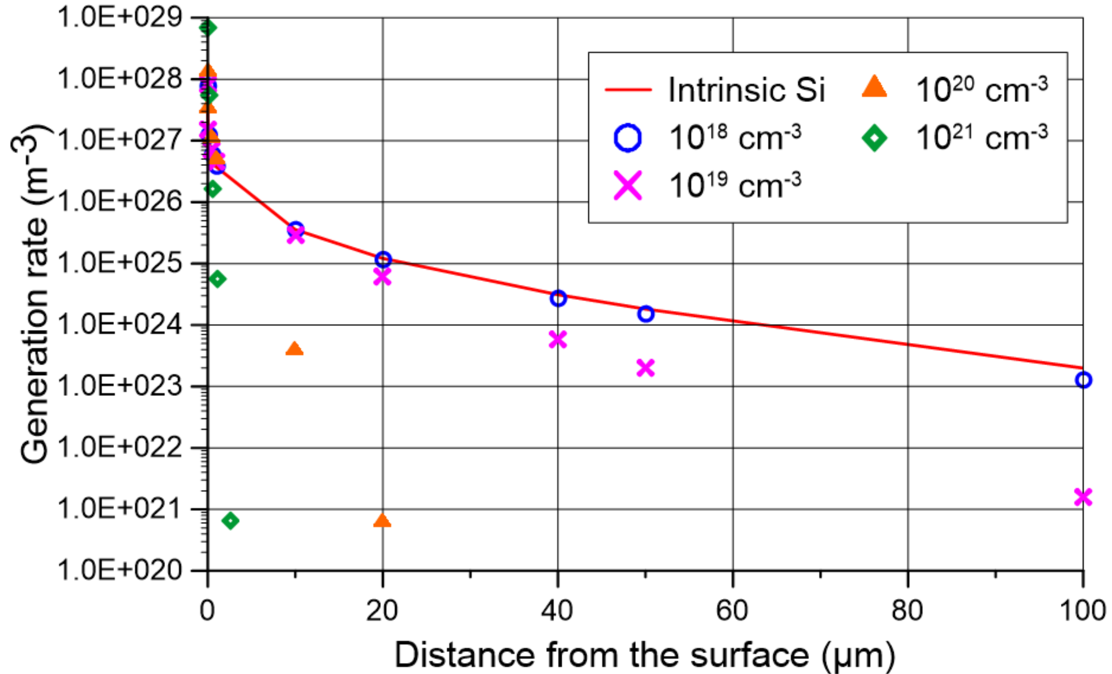

Figure 3.28 The effect of the doping concentration on the n-type silicon generation rate using Jellison *et al.* [57] data.

3.7 Optimizing a GaAs/Si tandem solar cell by introducing Photon cycling, Photon Recycling, and Luminescent Coupling Effects.

The photon recycling effect has been addressed and reviewed in chapter 2 of this work. It is the effect reabsorbing the photon which is emitted from the radiative recombination process. This effect is intensely important in the direct semiconductors where the radiative recombination is dominated such as in GaAs (1.434 eV), while it is assumed neglected if the SRH or auger recombination are dominated. The Shockley and Queisser [69] did not consider the photon recycling effect when they determined the detailed balance limit of efficiency of pn junction solar cells which led to underestimation for the III-V solar cells theoretical efficiency. Another important effect which relates to the multi-junction or tandem solar cells is the luminescent coupling effect. This effect is resulted when the photon which has been emitted in

the radiative recombination is being absorbed in another junction, usually junction with a lower bandgap as seen in figure 3.29. Both effects enhance the generation rate of solar cells which eventually could improve the efficiency of PV.

In this section, the work of Ren *et al.* [90], 2015, has been optimized by introducing the photon cycling effect in addition to the photon recycling and luminescent coupling of GaAs/Si solar cell. Although GaAs and Si tandem solar cells have attracted considerable attention recently [99, 100], their bandgaps combination (1.43/1.12 eV) do not attain the ideal double-junction of tandem solar cells combination (1.87/0.98 eV) [101]. One more issue is mismatched in the lattice constant (5.65/5.43 A) which can be partially solved by using different techniques such as using different growth mechanism or implanting a buffer between the two junctions, for example SiGe [102]. However, GaAs and Si are well-understood materials which have been highly recognized in current PV applications. In addition, the Shockley and Queisser efficiency for the double junction tandem of GaAs/Si is 39.2% ideally and drops to 31% by considering the resistance and recombination losses. Figure 3.30 shows the GaAs/Si tandem device architecture of Ren *et al.* [90]. What related to this thesis is the

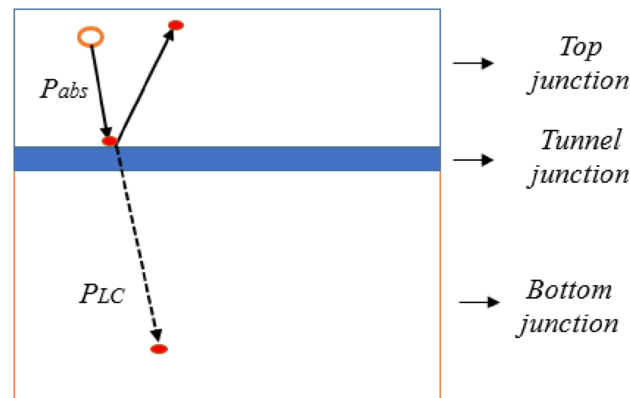

Figure 3.29 The luminescent coupling effect in tandem solar cells.

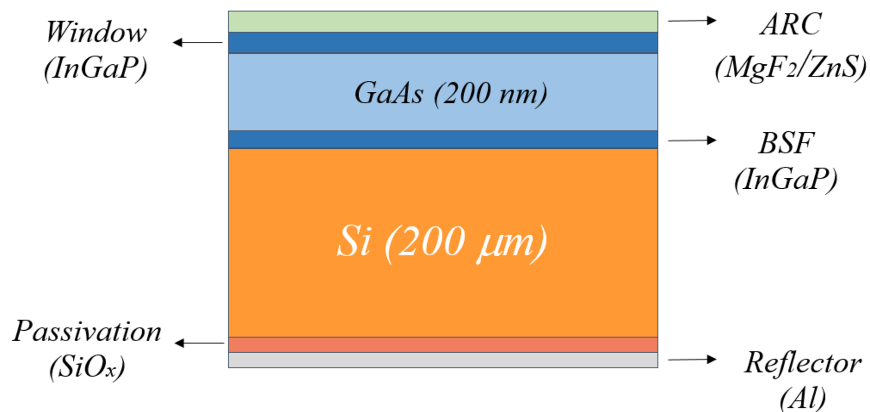

Figure 3.30 The tandem solar cell structure of Ren *et al.* [90] for the GaAs/Si double-junction.

active layers of the tandem, assuming perfect tunnel junction, ARC, window, and rear reflector. First, to optimize the device design, the first suggestion approach is to introduce the photon cycling effect by implanting texturing at the rear surface of silicon. The photon cycling effect leads to increase the path length of the incident ray inside the cell which results in enhancing the generation rate. Therefore, the 200 μm path length of light could be achieved by 50 μm silicon with three photon cycles. As a result, the cost of the substrate reduces by 75%. Due to the convergence between the Si refractive index and the Indium Gallium Phosphide (InGaP) [103] ($\theta_c > 50°$), it is important to implant sharper texturing to achieve higher reflecting angle to avoid light escaping from the top surface of Si. The proposed structure for the new GaAs/Si tandem solar cell, applying the photon cycling effect, is illustrated in figure 3.31. Furthermore, another suggestion to improve the cost of the structure is to reduce the thickness of the reflector since texturing is implanted to reflect the incident ray. Now, by applying the model (3.23) which has been established in section 3.5, the generation rate of the bottom cell (Si) in figure 3.31 is obtained in figured 3.32. The reflectance angle and the exact ray lengths are counted

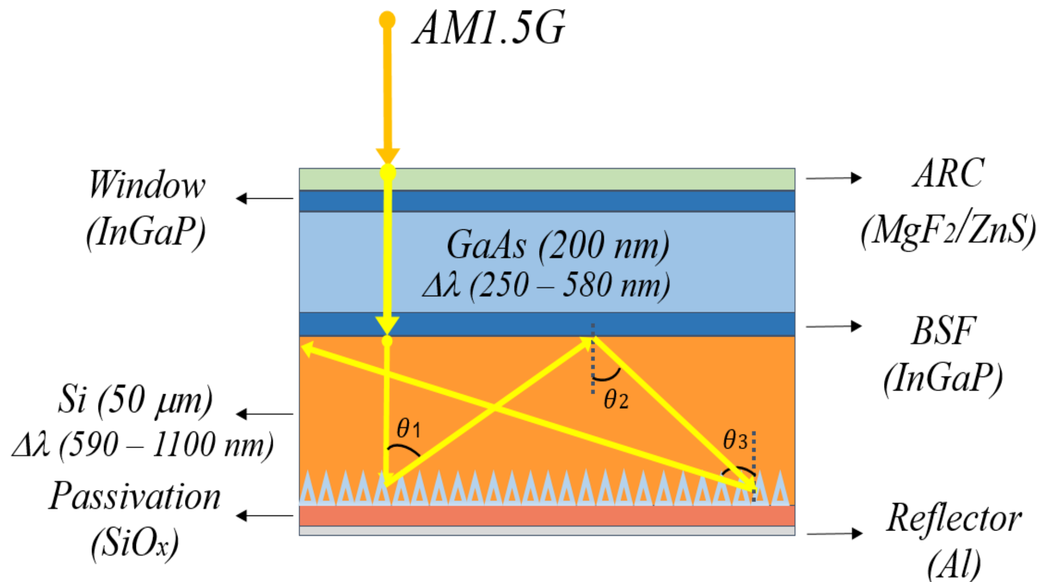

Figure 3.31 The optimized tandem solar cell structure of Ren *et al.* [90] for the GaAs/Si double-junction, applying the photon cycling effect on the rear texturing surface.

into the calculation, while the texturing thickness is assumed to be too small comparing to the junction thickness. The angles for the rear and front reflections are assumed to be 60° for the first two reflection angle and 75° for the last reflection angle, where $\theta_{1,2,3} > \theta_c$. Indeed, the attenuation of the incident ray through the top multiple interface layers have been measured assuming zero reflection. The bandwidth of the wavelength of the silicon generation rate starts from 590 *nm* instead of 300 *nm* since the preceding wavelength range is absorbed by the top junction (GaAs) for the AM1.5G. The thickness of the GaAs has been chosen by Ren *et al.* [90] which is adjustable, however, this thickness is corresponding to the absorption depth $(1/\alpha)$ of the 580 *nm* wavelength absorption. Furthermore, the generation rate of the GaAs junction is obtained for the AM1.5G with and without the photon recycling effect as shown in figure 3.33. It shows that the photon recycling generation rate improves up to 65% at the bottom of the GaAs for the photon emitted at the surface. The contribution of the photon

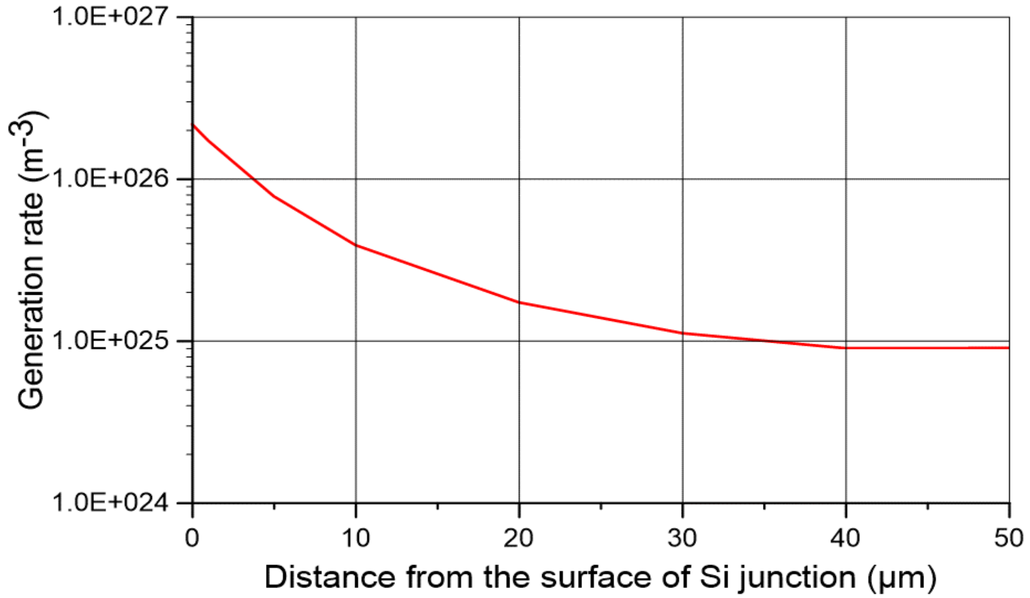

Figure 3.32 The generation rate of the bottom junction (Si) of optimized tandem solar cell structure of Ren *et al.* [90] for the GaAs/Si double-junction, including three photon cycles.

recycling generation to the total generation rate, which reaches to 65% at the back of the junction, is shown in figure 3.34. The radiative emission of GaAs has been calculated using van Roosbroeck–Shockley [89] equation, assuming Δμ is too small. The reabsorption probability of the emitted photons can be calculated by [83]

$$P_{abs} = \left(1 - e^{\frac{-\alpha x}{cos\theta}}\right) + \frac{e^{\frac{-\alpha x}{cos\theta}} R_f \left(1 + e^{\frac{-\alpha t}{cos\theta}} R_b\right)}{1 - e^{\frac{-2\alpha t}{cos\theta}} R_f R_b} + \left(1 - e^{\frac{-\alpha(t-x)}{cos\theta}}\right) \frac{e^{\frac{-\alpha(t-x)}{cos\theta}} R_b \left(1 + e^{\frac{-\alpha t}{cos\theta}} R_f\right)}{1 - e^{\frac{-2\alpha t}{cos\theta}} R_f R_b}. \quad (3.33)$$

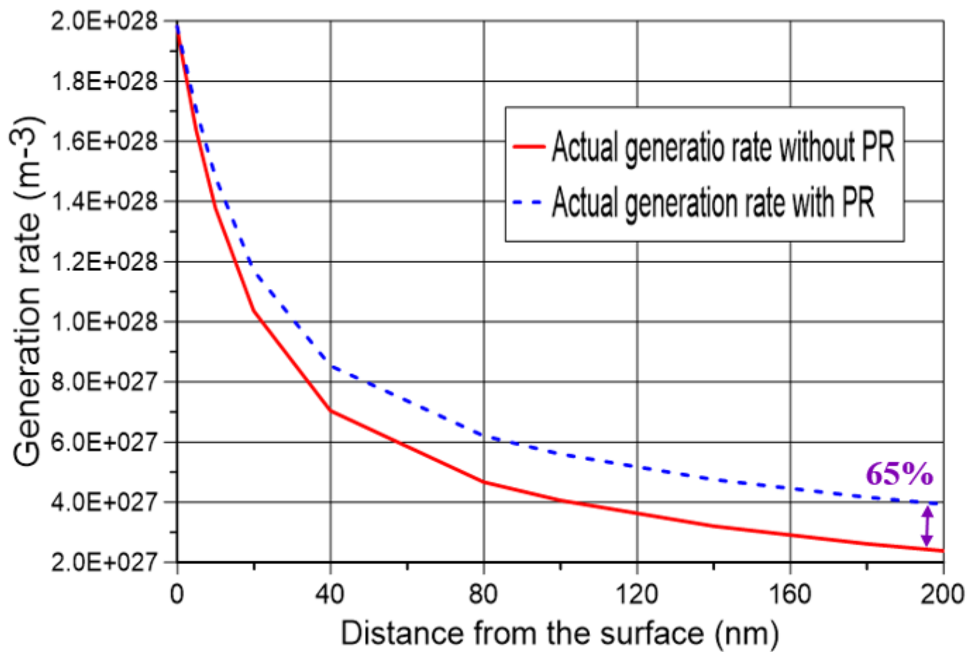

Figure 3.33 The generation rate of the top junction (GaAs) of tandem solar cell structure of Ren *et al.* [90] for the GaAs/Si double-junction with and without the photon recycling effect.

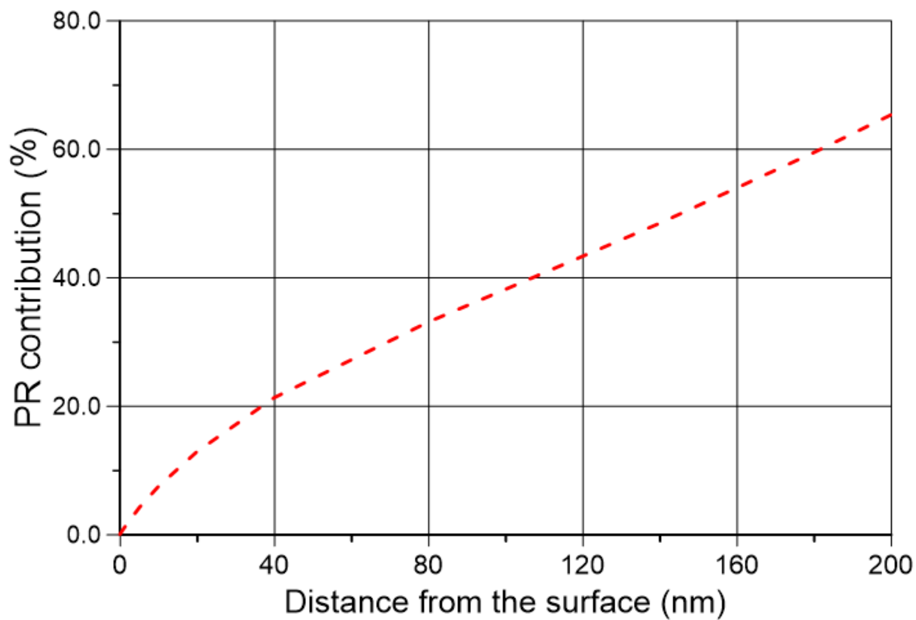

Figure 3.34 The contribution of the photon recycling generation rate to the total generation rate in the GaAs junction.

The reabsorption probability of an emitted photon at the surface and travelled at distance x can be reduced to [88],

$$P_{abs}(x) = 1 - e^{-\alpha x}. \quad (3.34)$$

Then the $P_{abs}(x)$ can be integrated over the spectrum of the wavelength to provide $P_{abs}(x, E)$ Finally, the photon recycling generation rate is calculated by [83]

$$G_{PR}(x) = R_{emit}(E, \Delta\mu) \cdot P_{abs}(x, E). \quad (3.35)$$

Then, the total generation rate in the GaAs junction is,

$$G_{total}(x) = G(x) + G_{PR}(x). \quad (3.36)$$

Ren *et al.* [90] show that considering the photon recycling effect improves the voltage by 1.3% and 0.5% for the current. However, the results of the generation rate calculations including the photon recycling effect are not illustrated in the paper [90].

Another effect that could improve the generation rate of tandem solar cells is the luminescent coupling effect. Applying the tandem solar cell structure of figure 3.31 again, when a photon is emitted from radiative recombination in the GaAs junction, this photon might be absorbed in the same junction based on the reabsorption probability. If the photon has not been absorbed in the GaAs cell, it has a chance to transport to the lower junction which has smaller bandgap by a coupling factor η_{LC} (radiative coupling efficiency) which is equal one in the ideal case. This parameter depends on the light losses or the parasitic absorption while travelling through different layers such as tunnel junction, window, and passivation. Also, it depends on material quality for the luminescing junction. The radiative coupling efficiency can be defined by [104],

$$\eta_{LC} = \frac{\eta_{int} P_{LC}}{1 - \eta_{int} P_{abs}} \tag{3.37}$$

where η_{int} is the internal luminescent efficiency and P_{LC} is the absorption probability of the luminescent coupling. The factor η_{int} is related to the ratio of the radiative recombination to the total recombination. The P_{LC} can be obtained by using the same approach of P_{abs} using a complicated equation, further details is provided in [86]. However, from another prospective the P_{LC} can be determined using simple and rational method. The P_{abs} reaches its maximum value at the rear surface of the top cell (GaAs here); thus, P_{LC}, as shown in figure 3.35, can be computed by taking into account the effect of the back reflection at the GaAs back surface as follows,

$$P_{LC} = (1 - R_b)(1 - P_{abs_\mathrm{max}}) \tag{3.38}$$

Hence, the generation rate of the luminescent coupling can be defined by,

$$G_{LC} = \eta_{LC} \cdot P_{LC} \cdot R_{emit}(E, \Delta\mu) \cdot \exp(-\alpha x). \tag{3.39}$$

Most of the luminescent coupling model, including Ren *et al.* [90], of the generation rate do not consider the attenuation of the light in the bottom cell, which may lead to an error in the calculation. Here, the attenuation of the light is taken into account by the factor $\exp(-\alpha x)$ as shown in equation (3.39). Thus, the total generation rate of the bottom cell is,

$$G_{total}(x) = G(x) + G_{LC}(x). \tag{3.40}$$

By applying the two above equations, the generation rate of the luminescent coupling effect for different coupling factors is shown in figure 3.36. It shows that the $G_{LC}(x)$ is much smaller than the $G(x)$ of the silicon and error of not considering the $G_{LC}(x)$ in the $G_{total}(x)$ is less than 1.5%.

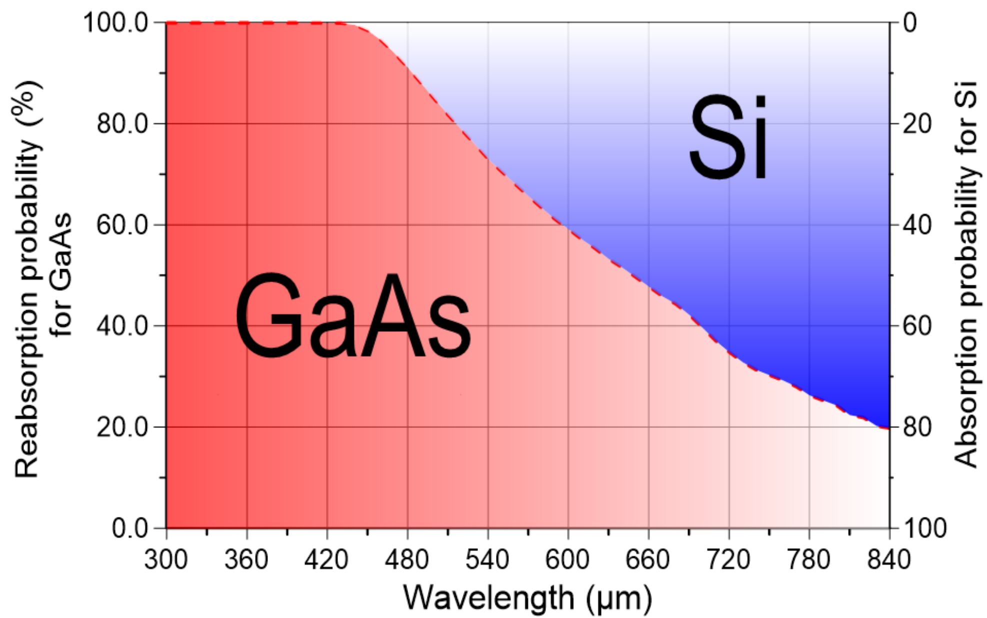

Figure 3.35 The reabsorption and absorption probability in the GaAs and Si, for the radiative emission of the GaAs at R_b=0.

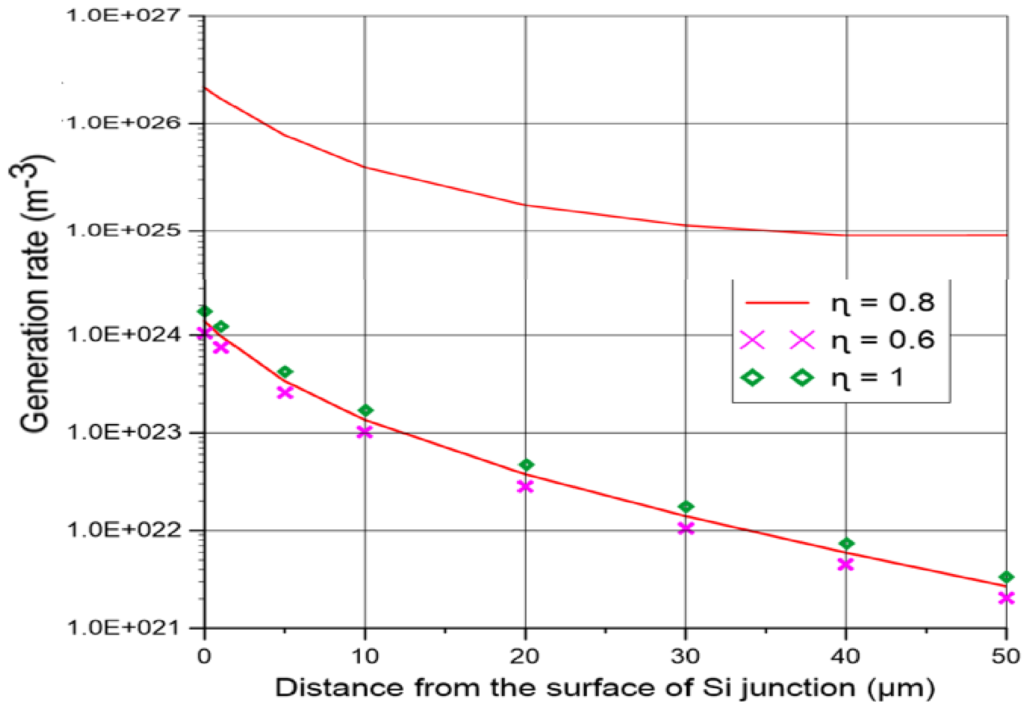

Figure 3.36 The generation rate of Silicon without LC and the generation rate of the LC effect of the Si junction for different coupling factors at R_b=0.

In summary, an optimized junction design for the Ren *et al.* [90] has been introduced using texturing at the back of the Si junction. Thereby, enhanceing the optical confinement and the incident ray path length in the bottom junction. Moreover, the thickness of the junction can be reduced 75% by introducing three photon cycles in the cell to maintain the light path at the same level. Then, the effect of photon recycling on GaAs generation has been assessed which results in increasing the generation rate by 65% at maximum. Finally, the luminescent coupling effect on the Si junction has been calculated using new approach which indicates the low impact of G_{LC} on G_{total} in this tandem junction.

Chapter 4

Conclusion and Future Work

This work represents a comprehensive analyses for photocarrier generation rate in the photovoltaic devices, which plays a key role in determining and constraining the efficiency of the semiconductor devices. One of the objective of this thesis is to optimize the generation rate by introducing different effects such as photon cycling, photon recycling, and luminescent coupling. The generation rate mainly depends on the absorption coefficient of the material, which depends on the optical properties of the material and several other parameters such as doping concentration and temperature. Thus, reviewing the optical properties of semiconductors in-depth is important to understand and investigate the generation rate. Since silicon solar cells are dominated in the PV manufacturing [2], it has been selected to show practical illustrations. After assessing the Si absorption coefficient based on several current reviewed publications, it shows that there is a demand to establish a new approximation to relate the wavelength of the light directly to the absorption coefficient. Thus, a new approximation has been created and examined to provide highly fitting results with point-to-point error of less than 2%. Then, the approximations of the previous generation rate have been updated, taking the reflection effect into account, using recent data for the absorption coefficient and solar irradiance. The updated approximations demonstrate higher accuracy with mean absolute error of less than 1.5%.

A novel model for the total generation rate including the photon cycling effect for multiple reflections at the back and front surface of the junction is established in section 3.5.

The validation of the model has been examined using practical example on Si junction with three photon cycles. It shows that including the cycling generation rate enhances the total generation rate of the junction and leads to reduce the thickness of the substrate. Furthermore, the impact of the internal reflection angle and junction thickness on the cycling generation rate are measured. Finally, an optimized proposed design for an exist GaAs/Si tandem solar cell of [90] has been developed by introducing the photon cycling effect, in addition to the photon recycling and luminescent coupling effects.

The new established model of the photon cycling generation rate is applicable for any semiconductor devices. However, due to the time-limiting for this work, it was not extended to other materials than silicon solar cells. Furthermore, there is no recent data for the effect of the BGN of the absorption coefficient of the Si, so a new experimental measurement is required. The computing of the generation rate is the first step to short circuit current in a junction, thus, further calculations are requires to obtain the I-V characterization. For the light absorption, it is only considered one photon creates one electron-hole pair, which means effects such as hot carriers, the photonic up and down conversion, optical filter, and concentration have not been discussed here [105, 106, 107, 108, 109, 110, 111]. Lastly, the luminescent coupling generation rate requires more investigation to achieve accurate results to enhance total generation rate.

The Future of the of the solar cells progresses toward the quantum dot devices, because of their extraordinary properties. The quantum dot effectively reduces the cost of the semiconductor devices due to its Nano size. Furthermore, the quantum dot has the feature of

tuning the bandgap based on the radius of the dot, which results in harvesting more energy from the solar spectrum.

References

[1] R. S. Ohl, "Light-sensitive electric device". US Patent 2402662A, 27 5 1941.

[2] "REN21," [Online]. Available: http://www.ren21.net. [Accessed 10 November 2017].

[3] N. Yastrebova, "High-efficiency multi-junction solar cells: Current status and future potential.," Centre for Research in Photonics, University of Ottawa, 2007.

[4] T. Tiedje, E. Yablonovitch, G. D. Cody and B. G. Brooks, "Limiting Efficiency of Silicon Solar Cells," *IEEE Transactions on Electron Devices,* vol. 31, pp. 711-716, 1984.

[5] H. Yan, F. Xia, W. Zhu, M. Freitag, C. Dimitrakopoulos, A. A. Bol, G. Tulevski and P. Avouris, "Infrared spectroscopy of wafer-scale graphene," *Acs Nano,* vol. 5, pp. 9854-9860, 2011.

[6] A. Goetzberger, C. Hebling and a. H. Schock, "Photovoltaic materials, history, status and outlook," *Materials Science and Engineering: R: Reports,* Vols. 40, no. 1, pp. 1- 46, 2003.

[7] "Standard Solar Constant and Zero Air Mass Solar Spectral Irradiance," ASTM International, West Conshohocken, PA, 2014.

[8] "ASTM E617-13 Standard Specification for Laboratory Weights and Precision Mass Standards,," ASTM International, West Conshohocken, PA, 2013.

[9] M. Levinštejn, S. Rumyantsev and M. Shur, Handbook series on semiconductor parameters, vol. 1, Singapore: World Scientific., 1996.

[10] D. E. Aspnes and J. B. Theeten, "Spectroscopic Analysis of the Interface Between Si and Its Thermally Grown Oxide," *J. Electrochem. Soc,* vol. 127, no. 6, pp. 1359-1365, 1980.

[11] C. Sah, R. Noyce and W. Shockley, "Carrier generation and recombination in pn junctions and pn junction characteristics," *Proceedings of the IRE 45,* vol. 9, pp. 1228-1243, 1957.

[12] P. A. M. Dirac, "The Quantum Theory of the Emission and Absorption of Radiation," *The Royal Society ,* vol. 114, pp. 243-265, 1927.

[13] P. A. M. Dirac, "The Quantum Theory of the Emission and Absorption of Radiation," *Special Relativity and Quantum Theory,* pp. 157-179, 1988.

[14] J. M. Zhang and Y. Liu, "Fermi's golden rule: its derivation and breakdown by an ideal model," *European Journal of Physics,,* vol. 37, no. 6, p. 065406, 2016.

[15] R. M. Swanson and R. A. Sinton, in *High efficiency silicon solar cells* , 1990, pp. 427-484.

[16] J. Nelson, The physics of solar cells., London: Imperial College Press, 2003.

[17] R. A. Smith, Semiconductors, Cambridge: Cambridge Univ. Press, 1987.

[18] C. Schinke, P. C. Peest, J. Schmidt, R. Brendel, K. Bothe, M. R. Vogt, I. Kröger, S. Winter, A. Schirmacher, S. Lim, H. T. Nguyen and D. Macdonald, "Uncertainty analysis for the coefficient of band-to-band absorption of crystalline silicon," *AIP Advances,* vol. 5, no. 6, p. 067168, 2015.

[19] R. S. Sirohi, "Ellipsometric Determination of Optical Constants: A New Method," *Applied Optics,* vol. 10, no. 10, pp. 23-69, 1971.

[20] C. M. Herzinger, B. Johs, W. A.Mcgahan, J. A. Woollam and W. Paulson, "Ellipsometric determination of optical constants for silicon and thermally grown silicon dioxide via a multi-sample, multi-wavelength, multi-angle investigation," *Journal of Applied Physics,* vol. 83, no. 6, pp. 3323-2336, 1998.

[21] H. G. Tompkins, Handbook of ellipsometry, Norwich, NY: Andrew, 2010.

[22] P. Kubelka and F. Munk, "An article on optics of paint layers," *Z. Tech. Phys,* vol. 12, pp. 593-601, 1931.

[23] U. Rau, "Reciprocity relation between photovoltaic quantum efficiency and electroluminescent emission of solar cells," *Phys. Rev. B,* vol. 76, no. 8, 2007.

[24] P. Würfel, T. Trupke, T. Puzzer, E. Schäffer, W. Warta and G. S, "Diffusion lenghts of silicon solar cells from luminescence images," *J. Appl. Phys,* vol. 101, no. 12, 2007.

[25] D. Hinken, K. Bothe, K. Ramspeck, S. Herlufsen and R. Brendel, "Determination of the effective diffusion length of silicon," *Journal of Applied Physics,* vol. 105, no. 10, p. 104516, 2009.

[26] C. Schinke, D. Hinken, J. Schmidt, K. Bothe and R. Brendel, "Modeling the spectral luminescence emission of silicon solar cells and wafers," *IEEE J. Photovoltaice,* vol. 3, no. 3, pp. 1038-1052, 2013.

[27] P. Würfel, "Generalized planck's radiation law for luminescence via indirect transitions," *Appl. Phys. A,* vol. 60, pp. 67-70, 1995.

[28] W. Dash and R. Newman, "Intrinsic Optical Absorption in Single-Crystal Germanium and Silicon at 77°K and 300°K," *Physical Review,* vol. 99, no. 4, pp. 1151-1155, 1955.

[29] H. R. Philipp and E. A. Taft, " Optical constants of silicon in the region 1 to 10 eV," *Physical Review,* vol. 120, no. 1, p. 37, 1960.

[30] G. G. Macfarlane, T. P. Mclean, J. E. Quarrington and V. Roberts, "Fine Structure in the Absorption-Edge Spectrum of Si," *Physical Review,* vol. 111, no. 5, pp. 1245-1254, 1958.

[31] G. G. Macfarlane and V. Roberts, "Infrared Absorption of Silicon Near the Lattice Edge," *Physical Review,* vol. 98, no. 6, pp. 1865-1866, 1955.

[32] H. A. Weakliem and D. Redfield, "Temperature dependence of the optical properties of silicon," *Journal of Applied Physics,* vol. 50, no. 3, pp. 1491-1493, 1979.

[33] G. E. Jellison, "Optical functions of silicon determined by two-channel polarization modulation ellipsometry," *Optical Materials,* vol. 1, no. 1, pp. 41-47, 1992.

[34] G. G. Macfarlane, T. P. McLean, J. E. Quarrington and V. Roberts, " Exciton and phonon effects in the absorption spectra of germanium and silicon," *Journal of Physics and Chemistry of Solids,* vol. 8, pp. 388-392, 1959.

[35] R. Hulthén, "Optical constants of epitaxial silicon in the region 1-3.3 eV," *Phys. Scr. ,* vol. 12, no. 6, p. 342–344, 1975.

[36] D. E. Aspnes and A. A. Studna, "Dielectric functions and optical parameters of Si, Ge, GaP, GaAs, GaSb, InP, InAs, and InSb from 1.5 to 6.0 eV," *Phys. Rev. B,* vol. 27, no. 2, p. 985–1009 , 1983.

[37] E. Daub and P. Würfel, "Ultralow values of the absorption coefficient of Si obtained from luminescence," *Phys. Rev. Letters,* vol. 74, no. 6, pp. 1020-1023, 1995.

[38] M. A. Green and M. J. Keevers, "Optical properties of intrinsic silicon at 300 K," *Progress in Photovoltaics: Research and Applications,* vol. 3, no. 3, pp. 189-192, 1995.

[39] M. A. Green, "Self-consistent optical parameters of intrinsic silicon at 300K including temperature coefficients," *Solar Energy Materials and Solar Cells,* vol. 92, no. 11, p. 1305–1310, 2008.

[40] H. Fan and M. Becker, "Semiconducting materials," *Butterworth's,* p. 132, 1951.

[41] K. Rajkanan, R. Singh and J. Shewchun, "Absorption coefficient of silicon for solar cell calculations,”," *Solid-State Electronics,* vol. 22, no. 9, pp. 793-795, 1979.

[42] H. A. Weakliem and D. Redfield, "Temperature dependence of the optical properties of silicon," *Journal of Applied Physics,* vol. 50, no. 3, pp. 1491-1493, 1979.

[43] G. E. Jellison and F. A. Modine, "Optical absorption of silicon between 1.6 and 4.7 eV at elevated temperatures," *Applied Physics Letters,* vol. 40, no. 2, p. 180–182, 1982.

[44] H. Rogne, P. J. Timans and H. Ahmed, "Infrared absorption in silicon at elevated temperatures," *Applied Physics Letters,* vol. 69, no. 15, p. 2190–2192, 1996.

[45] G. E. Jellison and F. A. Modine, "Optical functions of silicon at elevated temperatures," *Journal of Applied Physics,* vol. 76, no. 6, p. 3758–3761, 1994.

[46] C. Schinke, P. C. Peest, K. Bothe, J. Schmidt, R. Brendel, M. R. Vogt, I. Kröger, S. Winter, A. Schirmacher, S. Lim, H. T. Nguyen and D. Macdonald, "C. Schinke, P. C. Peest, K. Bothe, J. Schmidt, R. Brendel, M. R. Vogt, I. Kröger, S. Winter, A. Schirmacher, S. Lim, H. T. Nguyen, and D. Macdonald, “Experimental Determination of the Uncertainty of the Absorption Coefficient of Crystalline Silicon," *Energy Procedia, vol. 77, pp. 170–178, 2015.,* vol. 77, pp. 170-178, 2015.

[47] C. Schinke, P. C. Peest, J. Schmidt, R. Brendel, K. Bothe, M. R. Vogt, I. Kröger, S. Winter, A. Schirmacher, S. Lim, H. T. Nguyen and D. MacDonald, "Uncertainty analysis for the coefficient of band-to-band absorption of crystalline silicon," *AIP Advances,* vol. 5, no. 6, p. 067168, 2015.

[48] B. Bhaumik and R. Sharan, "Temperature effects in Schottky-barrier solar cells," *Applied Physics Letters ,* vol. 29, no. 4, p. 257–259, 1976.

[49] L. H. Hall, J. Bardeen and F. J. Blatt, "Infrared Absorption Spectrum of Germanium," *Physical Review,* vol. 95, no. 2, p. 559–560, 1954.

[50] J. M. Palmer, "Near-Infrared Limitations To Silicon Photodetector Self-Calibration," *Optical Radiation Measurements,* vol. 499, pp. 7-14, 1985.

[51] J. Geist, A. Migdall and H. P. Baltes, "Analytic representation of the silicon absorption coefficient in the indirect transition region," *Applied Optics,* vol. 27, no. 18, p. 3777–3779, 1988.

[52] D. Yan and A. Cuevas, "Empirical determination of the energy band gap narrowing in highly doped n+ silicon," *Journal of Applied Physics ,* vol. 114, no. 4, p. 044508, 2013.

[53] D. Yan and A. Cuevas, "Empirical determination of the energy band gap narrowing in p+ silicon heavily doped with boron," *Journal of Applied Physics ,* vol. 116, no. 19, p. 194505, 2014.

[54] A. Kimmerle, J. Greulich, H. Haug and A. Wolf, "Application and comparison of band gap narrowing models for passivated phosphorus doped silicon surfaces," *Journal of Applied Physics,* vol. 119, no. 2, p. 025708, 2016.

[55] W. Spitzer and H. Y. Fan, "Infrared Absorption in n-Type Silicon," *Physical Review,* vol. 108, no. 2, pp. 268-271, 1957.

[56] M. Balkanski, A. Aziza and E. Amzallag, "Infrared Absorption in Heavily Doped n-Type Si," *physica status solidi (b) 31.1 (1969): 323-330.,* vol. 31, no. 1, pp. 323-330, 1969.

[57] G. E. Jellison, F. A. Modine, C. W. White, R. F. Wood and R. T. Young, "Optical Properties of Heavily Doped Silicon between 1.5 and 4.1 eV," *Physical Review Letters,* vol. 46, no. 21, p. 1414–1417, 1981.

[58] H. C. Hsieh, C. Hu and C. I. Drowley, "A New Method of Analyzing the Short-circuit Current of Silicon Solar Cells," *IEEE Transactions On Electron Devices ,* vol. 27, no. 4, pp. 883-885, 1980.

[59] J. G. Fossum, "Computer-aided numerical analysis of silicon solar cells," *Solid-state Electron,* vol. 19, pp. 269-277, 1976.

[60] P. M. Dunbar and J. R. Hauser, "A study of efficiency in low resistivity silicon solar cells," *Solid State Electron,* vol. 19, pp. 95-102, 1976.

[61] J. Furlan and S. Amon, "Approximation of the carrier generation rate in illuminated silicon," *Solid-state electronics,* vol. 28, no. 12, pp. 1241-1243, 1985.

[62] S. N. Mohammad, "An alternative method for the performance analysis of silicon solar cells," *Journal of Applied Physics,* vol. 61, no. 2, p. 767–772, 1987.

[63] A. Anvar, C. R. Selvakumar and S. Karmalkar, "Novel Solution to Minority Continuity Equation in PN Junction Solar Cells Under Arbitrary Optical Generation," 2014.

[64] M. M. Chowdhury and B. Debnath, "Approximation of Carrier Generation Rate in Common Solar Cells and Studies for Optimization of n+p Silicon Solar Cell for AM1.5G and AM1.5D," in *7th International Conference on Electrical and Computer Engineering*, Bangladesh, 2012.

[65] P. A. Basore and D. A. Clugston, "PC1D for Windows: from analysis to design," in *Proc. 25th IEEE PhotovoltaicSpecialists Conference*, Washington, DC, USA, 1996.

[66] W. P. Dumke, "Spontaneous Radiative Recombination in Semiconductors*," *PHYSICAL REVIEW,* vol. 105, no. 1, pp. 139-144, 1957.

[67] W. Shockley, "The Theory of p-n Junctions in Semiconductors and p-n Junction Transistors," *Bell System Technical Journal,* vol. 28, pp. 435-489, 1949.

[68] A. Martı, J. Balenzategui and R. Reyna, "Photon recycling and Shockley's diode equation," *Journal of applied physics,* vol. 82, pp. 4067-4075, 1997.

[69] W. Shockley and H. Queisser, "Detailed balance limit of efficiency of p-n junction solar cells," *Journal of applied physics,* vol. 32, pp. 510-519, 1961.

[70] P. Campbell and M. A. Green, "The limiting efficiency of silicon solar cells under concentrated sunlight," *IEEE Trans. Electron Devices,* vol. 33, pp. 234 - 239, 1986.

[71] F. Stern and J. M. Woodall, "Photon recycling in semiconductor lasers," *Journal of Applied Physics,* vol. 45, no. 9, p. 3904–3906, 1974.

[72] E. Velmre, "Numerical modelling of semiconductor structures including electron-hole scattering and recombination radiation recycling effect," *Periodica Polytechnica Electrical Engineering ,* vol. 33, no. 3, pp. 141-150, 1989.

[73] R. K. Ahrenkiel, D. J. Dunlavy, B. Keyes, S. M. Vernon, T. M. Dixon, S. P. Tobin, K. L. Miller and R. E. Hayes, "Ultralong minority-carrier lifetime epitaxial GaAs by photon recycling," *Applied Physics Letters,* vol. 55, no. 11, p. 1088–1090, 1989.

[74] J. Parrott, "Radiative recombination and photon recycling in photovoltaic solar cells," *Solar Energy Materials and Solar Cells,* vol. 30, no. 3, p. 221–231, 1993.

[75] V. Badescu and P. T. Landsberg, "Theory of some effects of photon recycling in semiconductors," *Semiconductor Science and Technology,* vol. 8, no. 7, pp. 1267-276, 1993.

[76] R. K. Ahrenkiel, B. M. Keyes, G. B. Lush, M. R. Melloch, M. S. Lundstrom and H. F. MacMillan, "Minority-carrier lifetime and photon recycling in n-GaAs," *Journal of Vacuum Science & Technology A: Vacuum, Surfaces, and Films,* vol. 10, no. 4, pp. 990-995, 1992.

[77] P. Renaud, F. Raymond, B. Bensaïd and C. Vèrié, "Influence of photon recycling on lifetime and diffusion coefficient in GaAs," *Journal of Applied Physics,* vol. 71, no. 4, p. 1907–1913, 1992.

[78] W. P. Joseph, K. Brennan and A. W. Smith, "Numerical Examination of Photon Recycling as an Explanation of Observed Carrier Lifetime in Direct Bandgap Materials," *VLSI Design, vol. 8, no. 1-4, pp.,* vol. 8, no. 1-4, pp. 153-157, 1998.

[79] V. Badescu and P. T. Landsberg, "Influence of photon recycling on solar cell efficiencies," *Semiconductor Science and Technology,* vol. 12, no. 11, p. 1997, 1491–1497.

[80] J. Balenzategui and A. Martí, "Detailed modelling of photon recycling: application to GaAs solar cells," *Solar Energy Materials and Solar Cells,* vol. 90, no. 7-8, p. 1068–1088, 2006.

[81] M. Rüdiger, T. Trupke, P. Würfel, T. Roth and S. W. Glunz, "Influence of photon reabsorption on temperature dependent quasi-steady-state photoluminescence lifetime measurements on crystalline silicon," *Applied Physics Letters,* vol. 92, no. 22, p. 222112, 2008.

[82] A. W. Walker, O. Hohn, D. N. Micha, B. Blasi, A. W. Bett and F. Dimroth, "Impact of Photon Recycling on GaAs Solar Cell Designs," *IEEE Journal of Photovoltaics,* vol. 5, no. 6, p. 1636–1645, 2015.

[83] G. L´etay, M. Hermle and n. A. W. Bett, "Simulating single-junction GaAs solar cells including photon recycling," *Prog. Photovoltaics,* vol. 14, pp. 683-696, 2006.

[84] D. J. Friedman, J. F. Geisz and M. A. Steiner, "Analysis of multijunction solar cell current-voltage characteristics in the presence of luminescent coupling," *IEEE J. Photovoltaics,* vol. 3, no. 4, p. 1429–1436, 2013.

[85] M. A. Steiner, J. F. Geisz, I. Garcia, D. J. Friedman, A. Duda and S. R. Kurtz, "Optical enhancement of the open-circuit voltage in high quality GaAs solar cells," *J. Appl. Phys.,* vol. 113, pp. 123109-1–123109-11, 2013.

[86] M. A. Steiner, J. F. Geisz, I. Garc´ıa, D. J. Friedman, A. Duda, W. J. Olavarria, M. Young and S. R. Kurtz, "Effects of internal luminescenceand internal optics on the Voc and Jsc of III–V solar cells," *IEEE J. Photovoltaics,* vol. 3, no. 4, p. 1437–1442, 2013.

[87] M. A. Steiner and J. F. Geisz, "Non-linear luminescent coupling in series-connected multijunction solar cells," *Appl. Phys. Lett.,* vol. 100, pp. 251106-1–251106-5, 2012.

[88] R. Ahrenkiel and M. Lundetorm, Minority Carriers in III-V Semiconductors: Physics and Applications, London: Academic Press , 1993.

[89] W. V. Roosbroeck and W. Shockley, "Photon-radiative recombination of electrons and holes in germanium," *Phys. Rev.,* vol. 94, p. 1558–1560, 1954.

[90] Z. Ren, J. P. Mailoa, Z. Liu, H. Liu, S. C. Siah, T. Buonassisi and I. M. Peters, "Numerical Analysis of Radiative Recombination and Reabsorption in GaAs/Si Tandem," *IEEE Journal of Photovoltaics,* vol. 5, no. 4, pp. 1079-1085, 2015.

[91] Z. Ren, J. P. Mailoa, Z. Liu, H. Liu, S. E. Sofia, N. Sahraei, S. C. Siah, F. Lin, T. Buonassisi and I. M. Peters, "Device impact of photon recycling and luminescent coupling on InGaP/Si tandems," in *2015 IEEE 42nd Photovoltaic Specialist Conference (PVSC)*, New Orleans, LA, USA, 2015.

[92] M. Yuan, Z. Lyu, J. Jia, Y. Chen, Y. Liu, Y. Huo, Y. Miao and J. Harris, "Numerical modeling of photon recycling and luminescence coupling in non-ideal multijunction solar cell," *Physics, Simulation, and Photonic Engineering of Photovoltaic Devices V,* vol. 9743, p. 974306, 2016.

[93] J. M. Gee and G. F. Virshup, "A 31%-efficient GaAs/silicon mechanically stacked, multijunction concentrator solar cell," in *The 20th IEEE Photovoltaic Spec. Conf.* , Las Vegas, NV, USA, 1988.

[94] M. Yamaguch, Y. Ohmachi, T. Oh'hara, Y. Kadota, M. Imaizumi and S. Matsuda, "GaAs solar cells grown on Si substrates for space use," *Prog. Photovoltaic,* vol. 9, pp. 191-201, 2001.

[95] T. Mishima, M. Taguchi, H. Sakata and E. Maruyama, "Development status of high-efficiency efficiency HIT solar cells,," *Solar Energy Materials and Solar Cells,* vol. 95, pp. 18-21, 2011.

[96] M. Zeman, "THIN–FILM SILICON PV TECHNOLOGY," *Journal of ELECTRICAL ENGINEERING,* vol. 61, no. 5, pp. 271-276, 2010.

[97] C. Petti, B. Newman, R. Brainard and J. Li, "Optimal thickness for crystalline silicon solar cells," *Twin Creek Technologies,* vol. 2, pp. 1-5, 2011.

[98] D. Sarkar, "Design Optimization of Thin Crystalline-Silicon Solar Cells," 2012.

[99] Y. Shimizu and Y. Okada, "Growth of high-quality GaAs/Si films for," *J. Crystal Growth,* vol. 265, pp. 99-106, 2004.

[100] M. Yamaguch, T. Ohmachi, Oh'hara, Y. Kadota, M. Imaizumi and S. Matsuda, "GaAs solar cells grown on Si substrates for space use," *Prog. Photovoltaic ,* vol. 9, pp. 191-201, 2001.

[101] A. Martí and G. L. Araújo, "Limiting efficiencies for photovoltaic energy conversion in multigap systems," *Sol. Energy Mater. Sol. Cells,* vol. 43, pp. 203-222, 1996.

[102] S. Ringel, J. Carlin, C. Andre, M. Hudait, M. Gonzalez, D. Wilt, E. Clark, P. Jenkins, D. Scheiman, A. Allerman, E. Fitzgerald and C. Leitz, "Single-junction InGaP/GaAs solar cells grown on Si substrates with SiGe buffer layers," *Prog. Photovoltaics,* vol. 10, pp. 417-426, 2002.

[103] R. Ferrini, G. Guizzetti, M. Patrini, A. Parisini, L. Tarricone and B. Valenti, "Optical functions of InGaP/GaAs epitaxial layers from 0.01 to 5.5 eV," *The European Physical Journal B ,* vol. 27, pp. 449-458, 2002.

[104] M. Steiner, J. Geisz, I. Garcı`a, D. Friedman, A. Duda, W. Olavarria, M. Young, D. Kuciauskas and S. Kurtz, "Effects of Internal Luminescence and Internal Optics on Voc and Jsc of III–V Solar Cells," *IEEE Journal of Photovoltaics,* vol. 3, no. 4, pp. 1437-1442, 2013.

[105] M. A. Green and S. P. Bremner, "Energy conversion approaches and materials for high-efficiency photovoltaics," *Nature Materials,* vol. 16, no. 1, pp. 23-34, 2016.

[106] R. F. Pierret, Semiconductor Device Fundamentals, New Delhi (Indai): Pearson/Education Print., 2008.

[107] H. Lanyon, " The physics of heavily doped n+-p junction solar cells," *Solar Cells,* vol. 3, no. 4, pp. 289-311, 1981.

[108] R. V. Overstraeten and R. P. Mertens, "Heavy doping effects in silicon," *Solid-State Electronics,* vol. 30, no. 11, p. 1077–1087, 1987.

[109] C. R. Selvakumar, "Simple general analytical solution to the minority carrier transport in heavily doped semiconductors," *Journal of applied physics ,* vol. 56, no. 12, pp. 3476-3478, 1984.

[110] T. T. Mnatsakano, M. E. Levinshtein, V. B. Shuman and B. M. Seredin, "On the limit of the injection ability of silicon p+–n junctions as a result of fundamental physical effects," *Semiconductors,* vol. 51, no. 6, pp. 798-802, 2017.

[111] M. Dahlinger and K. Carstens, "Band gap narrowing models tested on low recombination phosphorus laser doped silicon," *Journal of Applied Physics,* vol. 120, no. 5, p. 155701, 2016.

Appendix A

Generation Rate Calculation

wavelength (nm)	spectral irrd Global tilt W*m-2*nm-1	photon flux (#ph/m^2.sec)	absorp coeff. (/cm)	Reflection	generation rate at x=0
280	4.73E-23	1.87E-02	2.36E+06	7.23E-01	1.22E+06
290	6.02E-09	2.55E+12	2.24E+06	6.84E-01	1.80E+20
300	1.02E-03	4.62E+17	1.73E+06	6.23E-01	3.01E+25
310	5.0939E-02	2.46E+19	1.44E+06	5.90E-01	1.45E+27
320	2.05E-01	1.06E+20	1.28E+06	5.74E-01	5.76E+27
330	4.71E-01	2.58E+20	1.17E+06	5.66E-01	1.31E+28
340	5.02E-01	2.92E+20	1.09E+06	5.62E-01	1.39E+28
350	5.28E-01	3.25E+20	1.04E+06	5.65E-01	1.47E+28
360	5.98E-01	3.90E+20	1.02E+06	5.83E-01	1.66E+28
370	7.55E-01	5.20E+20	6.97E+05	5.84E-01	1.51E+28
380	7.01E-01	5.09E+20	2.93E+05	5.47E-01	6.76E+27
390	7.97E-01	6.10E+20	1.50E+05	5.11E-01	4.47E+27
400	1.11E+00	8.97E+20	9.52E+04	4.86E-01	4.39E+27
410	1.05E+00	8.87E+20	6.74E+04	4.67E-01	3.19E+27
420	1.12E+00	9.97E+20	5.00E+04	4.52E-01	2.73E+27
430	8.75E-01	8.14E+20	3.92E+04	4.39E-01	1.79E+27
440	1.35E+00	1.31E+21	3.11E+04	4.29E-01	2.34E+27
450	1.56E+00	1.59E+21	2.55E+04	4.20E-01	2.35E+27
460	1.53E+00	1.63E+21	2.10E+04	4.11E-01	2.01E+27
470	1.51E+00	1.68E+21	1.72E+04	4.04E-01	1.72E+27
480	1.62E+00	1.88E+21	1.48E+04	3.98E-01	1.67E+27
490	1.62E+00	1.96E+21	1.27E+04	3.92E-01	1.51E+27
500	1.55E+00	1.94E+21	1.11E+04	3.87E-01	1.32E+27
510	1.55E+00	2.03E+21	9.70E+03	3.82E-01	1.21E+27
520	1.52E+00	2.07E+21	8.80E+03	3.78E-01	1.13E+27
530	1.54E+00	2.18E+21	7.85E+03	3.74E-01	1.07E+27
540	1.48E+00	2.17E+21	7.05E+03	3.70E-01	9.65E+26
550	1.54E+00	2.34E+21	6.39E+03	3.67E-01	9.47E+26
560	1.47E+00	2.33E+21	5.78E+03	3.64E-01	8.55E+26
570	1.48E+00	2.42E+21	5.32E+03	3.61E-01	8.23E+26
580	1.50E+00	2.54E+21	4.88E+03	3.59E-01	7.96E+26
590	1.37E+00	2.40E+21	4.49E+03	3.56E-01	6.94E+26
600	1.48E+00	2.67E+21	4.14E+03	3.54E-01	7.14E+26
610	1.47E+00	2.75E+21	3.81E+03	3.52E-01	6.79E+26
620	1.47E+00	2.85E+21	3.52E+03	3.50E-01	6.52E+26
630	1.39E+00	2.78E+21	3.27E+03	3.48E-01	5.93E+26
640	1.43E+00	2.95E+21	3.04E+03	3.46E-01	5.87E+26
650	1.36E+00	2.89E+21	2.81E+03	3.45E-01	5.32E+26
660	1.40E+00	3.07E+21	2.58E+03	3.43E-01	5.19E+26
670	1.42E+00	3.21E+21	2.38E+03	3.42E-01	5.02E+26
680	1.40E+00	3.25E+21	2.21E+03	3.40E-01	4.74E+26
690	1.18E+00	2.83E+21	2.05E+03	3.39E-01	3.84E+26
700	1.28E+00	3.16E+21	1.90E+03	3.38E-01	3.98E+26
710	1.32E+00	3.34E+21	1.77E+03	3.36E-01	3.92E+26